1.0

1.1

1.25

4.5
5.0
5.6
6.3

2.8

3.2

3.6

4.0

1.4

2.5

2.2

2.0

1.8

1.6

MICROCOPY RESOLUTION TEST CHART
NATIONAL BUREAU OF STANDARDS-1963-A

ARL-TR-79-44

Copy No. 63

AN EXAMINATION OF COUPLED MODE THEORY AS APPLIED TO UNDERWATER SOUND PROPAGATION

Steven R. Rutherford

APPLIED RESEARCH LABORATORIES
THE UNIVERSITY OF TEXAS AT AUSTIN
POST OFFICE BOX 8029, AUSTIN, TEXAS 78712

28 July 1979

Technical Report

APPROVED FOR PUBLIC RELEASE;
DISTRIBUTION UNLIMITED.

Prepared for:

NAVAL OCEAN RESEARCH AND DEVELOPMENT ACTIVITY
NSTL STATION, MS 39562

79 09 25 015

AN EXAMINATION OF COUPLED MODE THEORY AS APPLIED

TO UNDERWATER SOUND PROPAGATION

by

STEVEN ROSS RUTHERFORD, B.S., M.S.

DISSERTATION

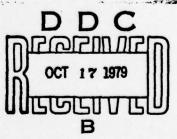Presented to the Faculty of the Graduate School of

The University of Texas at Austin

in Partial Fulfillment

of the Requirements

for the Degree of

DOCTOR OF PHILOSOPHY

THE UNIVERSITY OF TEXAS AT AUSTIN

26 JULY 1979

SECURITY CLASSIFICATION OF THIS PAGE *(When Data Entered)*

REPORT DOCUMENTATION PAGE		READ INSTRUCTIONS BEFORE COMPLETING FORM
1. REPORT NUMBER	2. GOVT ACCESSION NO.	3. RECIPIENT'S CATALOG NUMBER
4. TITLE *(and Subtitle)* AN EXAMINATION OF COUPLED MODE THEORY AS APPLIED TO UNDERWATER SOUND PROPAGATION		5. TYPE OF REPORT & PERIOD COVERED technical report
		6. PERFORMING ORG. REPORT NUMBER ARL-TR-79-44
7. AUTHOR(s) Steven R. Rutherford		8. CONTRACT OR GRANT NUMBER(s) N00014-78-C-0113
9. PERFORMING ORGANIZATION NAME AND ADDRESS Applied Research Laboratories The University of Texas at Austin Austin, TX 78712		10. PROGRAM ELEMENT, PROJECT, TASK AREA & WORK UNIT NUMBERS 224
11. CONTROLLING OFFICE NAME AND ADDRESS Naval Ocean Research and Development Activity NSTL Station, MS 39529		12. REPORT DATE 26 July 1979
		13. NUMBER OF PAGES 216
14. MONITORING AGENCY NAME & ADDRESS *(If different from Controlling Office)*		15. SECURITY CLASS. *(of this report)* UNCLASSIFIED
		15a. DECLASSIFICATION/DOWNGRADING SCHEDULE N/A

16. DISTRIBUTION STATEMENT *(of this Report)*

Approved for public release; distribution unlimited.

17. DISTRIBUTION STATEMENT *(of the abstract entered in Block 20, if different from Report)*

18. SUPPLEMENTARY NOTES

19. KEY WORDS *(Continue on reverse side if necessary and identify by block number)*

coupled mode theory
normal mode theory
adiabotic approximation

20. ABSTRACT *(Continue on reverse side if necessary and identify by block number)*

(U) The work presented in this dissertation is a theoretical investigation of the mathematical formalism of coupled mode theory as applied to underwater sound propagation in a range dependent, ocean environment. The range dependence of an acoustic medium may be characterized by two types, range variability of the geoacoustic parameters such as sound speed and range variability of the boundary conditions. This dissertation focuses on both types of range variation and examines coupled mode theory and its various approximations with respect to the

DD FORM 1473 EDITION OF 1 NOV 65 IS OBSOLETE UNCLASSIFIED

SECURITY CLASSIFICATION OF THIS PAGE *(When Data Entered)*

20. (Cont'd)

range variability of the ocean bottom. There are two approximations that
arise in applications of coupled mode theory. The adiabatic approximation,
which becomes valid in the limit of slight range variability of the medium,
involves the neglect of the mode-mode energy coupling process. Another
approximation which is inherent in the theory involves a boundary condition
approximation which must be made in applications involving range variable
boundaries. The adiabatic approximation is examined with respect to its
validity as a function of sediment type and bottom range variability
(bottom slope and radial sound speed gradient). The raypath properties of
the adiabatic approximation are also examined with respect to the multipath
conversion process caused by a sloping bottom and are shown to agree with a
ray theory view of the process. The boundary condition approximation which
arises in applications of the theory to problems with nonhorizontal boundaries
is also investigated. It is shown that the effect of this approximation is
an acoustic field that does not have the proper energy flow characteristics.
A modification of the theory that is first order in the bottom slope is
derived which alleviates this problem. Numerical calculations for the field
in a wedge shaped waveguide are presented to illustrate the effects of the
boundary condition approximation and to show how the modifications to the
theory produce the desired results. Throughout the dissertation the mathemati-
cal formalism is presented in a form amenable to numerical calculations. Also,
numerical methods for implementing the theory are described and discussed.

ACCESSION for

NTIS	White Section	✓
DDC	Buff Section	☐
UNANNOUNCED		☐
JUSTIFICATION		

BY _____
DISTRIBUTION/AVAILABILITY CODES

Dist.	AVAIL. and/or SPECIAL
A	

TABLE OF CONTENTS

iv

LIST OF NOTATION

$\overset{\bullet}{A}$ Partial or total range derivative of A as appropriate

A' Partial or total z derivative of A as appropriate

A_{mn} Coupling coefficient defined in Chapter II

B_{mn} Coupling coefficient defined in Chapter II

$c(r,z)$ Sound speed as a function of depth and range

f Frequency

f_r Radial flux

F_m Reduced radial function defined by $F_m = \sqrt{r}\, R_m$

G_m Reduced radial function with corrections for nonhorizontal
boundaries, $G_m = \sqrt{r}\, X_m$

H_i Depth of ith boundary interface, can be a function of
range

I_{mn} $\displaystyle\int_0^\infty \rho\phi_m \delta\phi_n dz$

J_r Total power flow in radial direction

$J_r^{(m)}$ Power transported in radial direction by mth mode

$k(z,r)$ Wave number, $k = \omega/c(z,r)$

k_m Horizontal wave number associated with mode m,

$$k_m = \sqrt{k^2 - \kappa_m^2}$$

p Acoustic pressure

R_m Radial function

X_m Radial function with corrections for nonhorizontal boundaries; $X_m = R_m + \delta R_m$

α Bottom slope angle

$\alpha(z,r)$ Attenuation as a function of depth and range

$\delta_{n,m}$ Kronecker delta

$\delta(r)$ Dirac delta function

$\delta\phi_m$ Correction to depth function for mode m

δR_m Correction to radial function for mode m

Θ_m Equivalent ray angle of mode m

κ_m Vertical wave number associated with mode m,

$$\kappa_m = \sqrt{k^2 - k_m^2}$$

ρ Material density

ϕ_m Normal mode depth function for mode m, also called mode function

Φ_m $\Phi_m = \phi_m + \delta\phi_m$

$\psi(r,z)$ Acoustic velocity potential field as a function of depth and range

ω Circular frequency, $\omega = 2\pi f$

$\nabla_{\perp}$ Normal derivative operator

RHS   Right-hand side

LHS   Left-hand side

CHAPTER I

INTRODUCTION

The analytical description of sound propagation in a range changing, ocean environment is a topic of fundamental interest to acousticians because the horizontal stratification of acoustic media is a condition that is rarely realized in the physical world. In underwater sound propagation there is a genuine need for the calculational ability to realistically model a range variable ocean environment. A wealth of acoustical data already exists which cannot be analyzed properly without taking into account the range variability of the acoustic medium.

The types of methods for modeling sound propagation in a range dependent medium are the same as for a horizontally invariant medium and may be generally classified as ray theoretical or wave theoretical. Ray theory is an analytic method that associates the propagation of energy between source and receiver positions with particular raypath trajectories. Wave theory methods, on the other hand, are based on the solution of the wave equation satisfied by the acoustic field.

The main advantage of a ray theory approach to the description of sound propagation is in its physically intuitive notion of propagation along raypaths. In many situations a ray theory viewpoint is useful for developing an understanding of the physical processes and phenomenology of underwater sound

1

propagation. There are several disadvantages associated with ray theory, however. The raypath description of sound propagation in ray theory is based on a WKB[1.1-1.3] asymptotic solution of the acoustic wave equation, and as such, is valid only in the limit of high frequencies and slowly varying media. Also associated with the theory are infinities connected with caustics[1.4] and shadow zones. In addition, in most implementations of ray theory methods in range dependent propagation media (see Refs. 1.5 and 1.6) one is restricted in the level of detail with which the ocean bottom may be described.

There have in the past been many applications of ray theory methods to sound propagation in a range variable environment. Weston[1.7,1.8] has used ray theory methods to investigate horizontal refraction and guided propagation in weakly range dependent media. Smith[1.9] has employed ray theory methods to examine the averaged transmission loss for range dependent sound channels, and Harrison[1.10] has used raypath invariants discovered by Weston to describe horizontal ray curvature effects in ocean basins and troughs, and near seamounts. Modifications to asymptotic, ray theory solutions of the wave equation for a range dependent medium have also been proposed (see Refs. 1.11-1.14). These modifications, for the most part, have involved slightly different asymptotic expansions of the solution to the acoustic wave equation in an effort to lower the frequency range of applicability and to impart more wave-like properties to the resulting solution.

When one considers a wave theory approach to the numerical modeling of sound propagation in a range dependent medium there are three ways to proceed. One way is a full three-dimensional numerical solution of the wave equation. Another is through the use of the parabolic equation method. The final method is the subject matter of this dissertation, the coupled mode theory approach. A wave theory description of sound propagation is desirable because it is an exact treatment of the problem in formulation, valid for all frequencies. Most applications of wave theory, however, are to low frequency sound propagation because the numerical sampling of the medium, which is wavelength dependent, becomes so fine at higher frequencies that a numerical solution is not practical.

Of the previously mentioned wave theoretical methods, only two have been applied to acoustic wave propagation, the parabolic equation method and coupled mode theory. In the parabolic equation[1.15-1.22] method, which has seen wide use in the underwater acoustics modeling community, the Helmholtz equation for the acoustic field is approximated by a differential equation which is parabolic in form. The nature of the parabolic approximation, however, is such that the field so obtained is not valid at ranges near the source position and involves the neglect of backscattered energy. The parabolic equation method is capable of describing range changes in the water column but suffers from some serious disadvantages concerning the description of the bottom. The

numerical methods employed in the solution of the parabolic differential equation are such that the bottom is characterized by a critical grazing angle below which the bottom is perfectly reflecting and above which it is perfectly absorbing. Needless to say, this restriction is serious if one is interested in the influence a realistic ocean bottom has on sound propagation in the water layer.

The subject matter of this dissertation is the application of coupled mode theory to the description of sound propagation in a range changing, ocean environment. Coupled mode theory was proposed for use in underwater acoustic propagation applications by Pierce[1.23] in 1965 and again by Milder[1.24] in 1969. Coupled mode theory is a formalism built around conventional normal mode theory. As with other wave theory methods coupled mode theory is computationally feasible only at low frequencies. One advantage to a normal mode description of sound propagation is that the ocean bottom is included as part of the propagation from the beginning with its acoustic properties capable of being described in detail. The detailed description of the bottom afforded by coupled mode theory is an important advantage when considering low frequency sound propagation in an ocean waveguide since bottom attenuation effects are reduced at low frequencies; with the reduced attenuation, acoustic energy refracting through the bottom can greatly influence the acoustic field in the water column in a manner that is sensitive to the geoacoustic properties of the subbottom. Hence,

the coupled mode theory formalism is expected to be most useful in acoustic propagation problems involving significant bottom interaction.

The coupled mode theory formalism is not restricted to acoustics applications. Very similar types of theories have been applied to electromagnetic wave propagation. Wait and Spies[1.25] used coupled mode theory to examine mode conversion in atmospheric VLF radio wave propagation. Wexler[1.26] has also used the coupled mode formalism in describing microwave propagation in waveguides having discontinuities along the path of propagation. In a book by Unger[1.27] the coupled mode theory has been used to describe guided propagation in fiber waveguides.

In underwater acoustics applications, coupled mode theory has been applied to a variety of range dependent propagation media. S. T. McDaniel[1.28-1.30] has applied coupled mode theory to the description of mode-mode coupling induced by a randomly rough, water-sediment interface. Tappert and Dozier[1.31,1.32] have also used the theory to investigate the fluctuation statistics of the acoustic field in an ocean waveguide having a water sound speed profile that varies randomly as a function of depth and range.

Applications of coupled mode theory to underwater acoustics problems of a more deterministic nature have been relatively few. Most applications of the theory have involved the adiabatic approximation which is discussed in Chapter III. Within the adiabatic approximation, which is expected to be valid for weakly range

dependent media, the mode-mode coupling effects are ignored. Graves et al.[1.33] applied the adiabatic approximation of coupled mode theory to an isovelocity, wedge-shaped model of an oceanic waveguide. Nagl et al.[1.34] and Graves et al.[1.35] considered the adiabatic approximation applied to realistic ocean waveguides having range variable sound speed profiles. Chwieroth et al.[1.36] applied the full formalism of coupled mode theory to the problem of an acoustic waveguide having a range variable, parabolic sound speed profile. Variations of coupled mode theory where the acoustic medium is partitioned into range segments in which the acoustic properties are range independent have been used by Waits[1.37] and MacPherson[1.38] to describe sound propagation in a waveguide of range dependent dimensions.

Until now, the applications of coupled mode theory to deterministic problems have either focused on range variations of the properties of the water layer or have employed the adiabatic approximation. No applications of the full coupled mode theory have been made in problems involving lateral variations in the bottom or range variable boundaries. The material in this dissertation focuses on these types of problems and is concerned with the application of the theory to low frequency, acoustic propagation over bottom structures whose depth and acoustic properties vary with range. Coupled mode theory is especially well suited to the description of acoustic propagation over range variable ocean

bottoms because of the detailed manner in which the bottom may be described.

The purpose of this dissertation is threefold. First, it presents a general mathematical description of coupled mode theory in a form that is convenient for numerical calculation. Second, it examines the adiabatic approximation with regard to its validity when applied to propagation over range dependent ocean bottoms. Third, it exposes an inconsistency in the theory when applied to propagation in waveguides having nonhorizontal boundaries. The inconsistency is related to approximations on the physically proper boundary conditions to be satisfied by the acoustic field and it is shown that the inconsistency can be remedied by modification of the theory.

The originality of the work presented in this dissertation lies in its focus on the ocean bottom. All previous applications of the theory have considered range variations in the water layer and have not considered sloping boundaries at all. Since many important propagation situations involve propagation over sloping bottoms and bottoms of range variable composition, it is clearly important that the theory and its various approximations be placed on a firm theoretical foundation for use in problems such as these.

The work presented in this dissertation is divided into six chapters of which this is the first. In Chapter II the mathematical formalism of coupled mode theory as originally proposed by Pierce[1.23] and Milder[1.24] is presented in detail. In Chapter II all

quantities occurring in the theory are expressed in a form convenient for numerical computation. Also included in Chapter II is a discussion of how coupled mode theory is implemented in acoustic propagation problems of practical interest along with a review of mode theory for range invariant waveguides.

In Chapter III the adiabatic approximation to coupled mode theory is considered. The approximation and its implications are discussed and the energy flow characteristics of the field so obtained are examined. Next the sensitivity of the adiabatic approximation to the range dependence of the bottom is considered. Lateral changes in the sediment sound speed profile and water-sediment interface slope are examined using an adiabacity criterion developed by Milder.[1.24] Finally the adiabatic approximation is examined with respect to the process of multipath conversion. It is concluded that the geometric (raypath) properties of acoustic propagation are described quite well in the adiabatic approximation.

In Chapter IV application of coupled mode theory to propagation over range variable ocean bottoms is considered. During the course of research it was discovered that boundary condition approximations which are made in problems involving range variable interfaces cause the field so obtained to have physically improper energy flow characteristics. These improper energy characteristics are a consequence of the inconsistency of the boundary condition approximations. This problem has not risen until now

because all previous applications of the theory have been to waveguides with horizontal boundaries. This problem is exposed and discussed in detail in Chapter IV. Also considered in Chapter IV is a correction to coupled mode theory which remedies the inconsistent boundary condition approximation and energy flow characteristics of the field.

Chapter V presents numerical calculations to verify the assertions and proposed corrections to coupled mode theory given in Chapter IV. The waveguide model used in the numerical calculations is an isovelocity wedge having a pressure release surface and a rigid sloping bottom. The calculations presented in Chapter V are the first reported results of an application of coupled mode theory to a waveguide with nonhorizontal boundaries, excluding the adiabatic approximation. Calculations of the rate of energy transport and various other quantities associated with the theory are presented. The numerical methods employed in the calculations are also described.

Chapter VI, the final chapter of the dissertation, is devoted to a summary of the results and conclusions of Chapters II-V. Also included in Chapter VI is a discussion of potentially useful and interesting applications of coupled mode theory along with suggestions for future work.

CHAPTER II

FUNDAMENTALS OF COUPLED MODE THEORY

The purpose of this chapter is to describe the mathematical formalism of coupled mode theory and to derive mathematical expressions which will be used throughout this report. In the first part of this chapter, normal mode theory for a horizontally stratified propagation medium will be reviewed. Next, range dependence of the medium will be introduced and the mathematical formalism of coupled mode theory derived. The chapter will conclude with a brief discussion of how coupled mode theory is implemented.

In the derivations performed in this chapter, a cylindrical coordinate system will be employed. The symmetry axis (z-axis) is perpendicular to the ocean surface and extends downward in the positive z direction toward the ocean bottom. Azimuthal symmetry about the z-axis is also assumed.

A.   Review of Normal Mode Theory for a Range Invariant
        Medium

In a horizontally stratified medium, the variations in the properties of the waveguide are restricted to the z-direction. The types of variations of the medium encountered in the ocean are depth changing sound speed and density. These changes can be of a continuous or discontinuous nature. Of course range dependence in the ocean is always present, though it is in general much weaker

10

than the depth dependence. Therefore the assumption of horizontal stratification of the ocean medium is always an approximation to the actual physical situation, and depending on the degree of range variability, this approximation can be quite good or quite poor.

The time independent wave equation to be solved is

$$\nabla^2 \psi(r,z) + k^2(z)\psi(r,z) = 0 \qquad . \qquad (2.1)$$

In Eq. (2.1), ψ is the time harmonic acoustic velocity potential for a fluid medium. The quantity $k(z)$ is equal to $\omega/c(z)$ where ω is 2π times the frequency and $c(z)$ is the sound speed in the fluid medium as a function of depth. Equation (2.1) is not valid when continuous depth variations of density within a layer are present. Rutherford and Hawker[2.1] have shown that continuous density variations of a magnitude likely to be found in the oceanic waveguide are of negligible importance. Therefore, throughout this dissertation, continuous density variations within layers will be ignored. Discontinuous density variations across an interface separating two media of differing acoustic properties do not affect the form of (2.1) and are allowed.

A solution of Eq. (2.1) in terms of acoustic normal modes may be obtained in a number of ways (see Refs. 2.2-2.6). The method employed here is one used by Mitchell.[2.2] Equation (2.1) can be expressed in terms of products of radial and depth functions each depending only on r and z, respectively.

$$\psi(r,z) = R(r)\phi(z) \tag{2.2}$$

The differential equation governing $R(r)$ and $\phi(z)$ may be obtained by substituting Eq. (2.2) into (2.1) to get

$$\left[\frac{\partial^2}{\partial r^2} + \frac{1}{r}\frac{\partial}{\partial r} + \frac{\partial^2}{\partial z^2} + k^2(z)\right] R(r)\phi(z) = 0 \quad . \tag{2.3}$$

Equation (2.3) can be rewritten as

$$\frac{1}{R(r)}\left(\frac{d^2}{dr^2}R(r) + \frac{1}{r}\frac{dR(r)}{dr}\right) = \frac{-1}{\phi(z)}\left[\frac{d^2}{dz^2} + k^2(z)\right]\phi(z) \quad . \tag{2.4}$$

Since the left-hand side (LHS) of (2.4) is a function of r alone and the right-hand side (RHS) of (2.4) a function of z alone, the LHS and RHS must both be equal to a separation constant $-\kappa^2$. Therefore the equations for $R(r)$ and $\phi(z)$ are given by

$$\frac{d^2}{dr^2}R(r) + \frac{1}{r}\frac{d}{dr}R(r) + \kappa^2 R(r) = 0 \quad , \tag{2.5}$$

and

$$\frac{d^2}{dz^2}\phi(z) + \left[k^2(z) - \kappa^2\right]\phi(z) = 0 \quad . \tag{2.6}$$

Equation (2.5) is recognized to be Bessel's Equation. If a solution involving outgoing waves is desired, the appropriate solution to (2.5) for $e^{-i\omega t}$ time dependence is

$$R(r) = H_0^{(1)}(\kappa r) \tag{2.7}$$

where $H_0^{(1)}$ is the zero order Hankel function of the first kind.

Equation (2.6) has simple analytic solutions only for specific types of depth dependence of $k(z)$. For example, if $k(z)$ is constant in depth, $\phi(z)$ is a combination of sine and cosine functions. If $k^2(z)$ is linear with depth $\phi(z)$ is given by combinations of Airy functions.[2.2,2.4] The boundary conditions to be satisfied by (2.6) are obtained from the boundary conditions to be satisfied by the total field ψ of Eqs. (2.1) and (2.2). The boundary conditions on ψ and its derivatives appropriate for an oceanic waveguide are that: (1) ψ vanish at $z=0$ (pressure release surface), (2) ψ vanish at $z=\infty$, (3) the acoustic pressure be continuous across any surfaces of discontinuity, and (4) the normal component of particle velocity be continuous across any surfaces of discontinuity. Boundary condition (2) is a consequence of the fact that the sound speed structure in the ocean bottom is generally increasing with depth in the bottom and attains values much larger than those occurring in the water column. Should condition (2) not be satisfied guided propagation is not possible.

The acoustic pressure p is given by

$$p = - \rho \frac{\partial \psi}{\partial t} = i \omega \rho \psi \quad . \quad (2.8)$$

Boundary condition (3) requires that the product of density ρ and depth function $\phi(z)$ be continuous across a surface of discontinuity. Boundary condition (4) requires that the normal component of particle velocity given by $\frac{\partial \psi}{\partial z}$ be continuous across any surfaces of discontinuity. This in turn requires that

$$\frac{\partial \phi(z)}{\partial z} \quad (2.9)$$

be continuous across layer boundaries.

Figure II.1 shows the depth structure of a typical oceanic waveguide. The first layer is the water layer which overlies sediment layers which are treated as fluids supporting only compressional waves. The water and sediment layers overlie an infinite, isovelocity half-space which may be considered to have solid properties without unduly complicating the problem (see Ref. 2.7). The material densities are assumed constant within each layer while the compressional wave sound speeds are allowed to vary continuously in the water and sediment layers.

r

z

$\rho_0,\ c_0(z),\ \phi_{0n}$ WATER LAYER

$z = H_0$

$\rho_1,\ c_1(z),\ \phi_{1n}$ SEDIMENT

$z = H_1$

$\rho_2,\ c_2(z),\ \phi_{2n}$

$\rho_i,\ c_i(z),\ \phi_{in}$ SEDIMENT

$z = H_i$

$\rho_{i+1},\ c_{i+1}(z),\ \phi_{i+1,n}$ SEDIMENT

$z = H_{i+1}$

$\rho_{i+2},\ c_{i+2},\ \phi_{i+2,n}$ SUBSTRATE HALF-SPACE
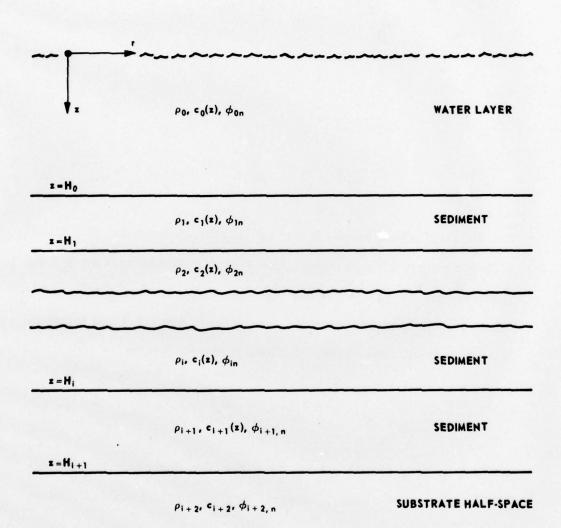
FIGURE II.1
LAYER STRUCTURE FOR A HORIZONTALLY
STRATIFIED OCEANIC WAVEGUIDE

In terms of the notation of Fig. II.1, boundary conditions (1)-(4) become:

$$(1) \qquad \phi(0) = 0$$

$$(2) \qquad \phi(\infty) = 0 \qquad\qquad (2.10)$$

$$(3) \quad \rho_i \phi^{(i)}(H_i) = \rho_{i+1} \phi^{(i+1)}(H_i)$$

$$(4) \quad \frac{\partial}{\partial z} \phi^{(i)}(H_i) = \frac{\partial}{\partial z} \phi^{(i+1)}(H_i) \qquad . \qquad (2.11)$$

The boundary conditions (2.10) and (2.11) along with Eq. (2.6) define an eigenvalue problem. The spectrum of eigenvalues k_n, in general, has a finite number of discrete elements and a continuously distributed component (see Refs. 2.8 and 2.9 and Appendix A). The normal mode depth equations therefore become

$$\frac{d^2}{dz^2} \phi_n(z) + \left(k^2(z) - k_n^2 \right) \phi_n(z) = 0 \qquad (2.12)$$

subject to Eqs. (2.10) and (2.11). The mode functions thus determined form an orthogonal, complete set of functions normalized so that

$$\int_0^\infty \rho \phi_n(z) \, \phi_m(z) \, dz = \delta_{n,m} \qquad . \qquad (2.13)$$

In (2.13) ρ is the material density of the medium taken to be constant within a layer. Any type of compressional wave, acoustic

disturbance in the oceanic waveguide can be described in terms of the radial and depth functions as follows

$$\psi(r,z) = \sum_n {}' a_n H_o^{(1)}(k_n r) \, \phi_n(z) \qquad . \tag{2.14}$$

The Σ' symbol denotes summation over discrete and integration over continuum eigenvalues. In most applications the contribution to Eq. (2.14) from the continuous modes is negligible (see Ref. 2.2, pp. 24-25); therefore, as is customary in underwater acoustics, the continuum contribution to the field will be neglected in the following analysis. See Appendix A for a more detailed description of the properties of the mode depth functions.

One particularly useful solution of the wave equation is the one for a point source of volume velocity located at $\vec{r}=\vec{r}_o$. The equation describing the field in this situation is

$$\nabla^2 \psi(r,z) + k^2(z)\psi(r,z) = -4\pi\delta(\vec{r}-\vec{r}_o) \qquad . \tag{2.15}$$

After Eq. (2.15) is integrated over the azimuthal angle, it becomes

$$\left(\frac{\partial^2}{\partial r^2} + \frac{1}{r}\frac{\partial}{\partial r} + \frac{\partial^2}{\partial z^2}\right)\psi(r,z) + k^2(z)\psi(r,z) = -\frac{2\delta(r-r_o)}{r}\delta(z-z_o) \tag{2.16}$$

Upon substituting (2.14) into (2.16) one obtains

$$\sum_n a_n \phi_n(z) \left(\frac{d^2}{dr^2} + \frac{1}{r} \frac{d}{dr} + k_n^2 \right) H_o^{(1)}(k_n r) = \frac{-2}{r} \delta(r-r_o) \delta(z-z_o) \quad (2.17)$$

where Eq. (2.12) has been employed. If the orthonormality proper-

ties of ϕ_n are exploited (see Eq. (2.13)) (2.17) becomes

$$a_m \left(\frac{d^2}{dr^2} + \frac{1}{r} \frac{d}{dr} + k_m^2 \right) H_o^{(1)}(k_m r) = \frac{-2}{r} \delta(r-r_o) \rho(z_o) \phi_m(z_o) \quad . \quad (2.18)$$

The constants a_m can be determined by recognizing that $H_o^{(1)}(k_m r)$ is

the two-dimensional freefield Green's function (see Ref. 2.10,

Chapter VII) satisfying

$$\left[\frac{d^2}{dr^2} + \frac{1}{r} \frac{d}{dr} + k_m^2 \right] H_o^{(1)}(k_m r) = \frac{2i}{\pi} \frac{\delta(r-r_o)}{r} \quad . \quad (2.19)$$

Equations (2.18) and (2.19) combine to yield

$$\frac{2i}{\pi} \frac{\delta(r-r_o)}{r} a_m = \frac{-2}{r} \delta(r-r_o) \rho(z_o) \phi_m(z_o)$$

$$(2.20)$$

$$a_m = i\pi \rho(z_o) \phi_m(z_o) \quad .$$

Therefore the velocity potential due to a point source at $\vec{r} = \vec{r}_o$ is

given by

$$\psi(r,z) = i\pi\rho(z_o) \sum_n H_o^{(1)}(k_n r) \phi_n(z) \phi_n(z_o) \quad (2.21)$$

where the contribution from the continuum has been neglected (see Appendix A). With the derivation of Eq. (2.21) the review of range stratified normal mode theory is concluded. The next section of this chapter will extend the ideas of normal mode theory to a range dependent medium.

B.   Basics of Coupled Mode Theory

The theory of acoustic propagation via coupled normal modes was proposed independently in papers written by Pierce[2.11] in 1965 and Milder[2.12] in 1969. The mathematical formalism of coupled mode theory was described in these two papers though both authors were more concerned with situations in which the mode coupling process could be ignored (the adiabatic approximation).

The wave equation for the velocity potential in a medium with depth and range dependence is

$$\nabla^2 \psi(r,z) + k^2(r,z)\, \psi(r,z) = 0 \quad . \tag{2.22}$$

In Eq. (2.22) the range dependence of the medium enters in two ways. One is through the range dependence of the wave number. Additional sources of range dependence enter through the boundary conditions. The boundary conditions on ψ are applied at surfaces of discontinuity whose depth might vary with range (i.e., sloping layers). The boundary conditions on ψ also involve the density which could be range dependent. The range dependence of the boundary conditions therefore contributes to the radial dependence of the field. As in

the horizontally stratified case, Eq. (2.22) is expressed in cylindrical coordinates and azimuthal symmetry is assumed. The extention to three-dimensional coupled mode theory formulated in cartesian coordinates is given later in this chapter.

Because of the radial dependence of k, a complete separation of variables is possible only for $k^2(r,z)$ of the form

$$k^2(r,z) = k^2(r) + k^2(z) \quad .$$

Since this form for the wave number is unduly restrictive and not physically realistic, it will not be considered further.

Coupled mode theory is implemented by attempting a partial separation of variables. In analogy with conventional mode theory, Pierce postulated a solution of Eq. (2.22) of the form

$$\psi(r,z) = \sum_n R_n(r) \, \phi_n(z;r) \tag{2.23}$$

where $\phi_n(z;r)$ satisfies

$$\left[\frac{\partial^2}{\partial z^2} + k^2(r,z) - k_n^2(r) \right] \phi_n(z;r) = 0 \quad . \tag{2.24}$$

The boundary conditions which ϕ_n is to satisfy are that $\rho\phi_n$ and $\partial\phi_n/\partial z$ be continuous at surfaces of discontinuity. These conditions arise from requiring continuity of pressure and z-component of particle velocity across interfaces. The depth

functions ϕ_n satisfy (2.24) locally which gives rise to a parametric dependence of the mode functions and eigenvalues on range.

The partial separation of variables indicated by (2.23) and (2.24) plus boundary conditions is exact only for range variable media having horizontal interfaces and boundaries. In this case the z-component of particle velocity, $\partial\phi/\partial z$, and pressure must be continuous across boundaries. Hence the boundary conditions on ψ may be transferred directly to $\phi_n(z;r)$. When nonhorizontal boundaries are present, it is the normal component of particle velocity, $\nabla_{\perp}\phi$, and pressure that are required to be continuous. For a nonhorizontal boundary defined by $z=H(r)$, $\nabla_{\perp}$ is given by

$$\nabla_{\perp} = \frac{1}{\sqrt{1+\dot{H}^2}} \left(\frac{\partial}{\partial z} - \dot{H} \frac{\partial}{\partial r} \right)$$

(2.25)

$$\dot{H} = \frac{dH(r)}{dr} \quad .$$

When nonhorizontal boundaries are present, the boundary conditions on ψ do not transfer to $\phi_n(z;r)$ alone and nothing is gained by expressing the field as in Eq. (2.23). In other words, not even a partial separation of variables is possible, greatly complicating the solution of Eq. (2.22).

The intent of Pierce was that the formalism of coupled mode theory be applied to problems having nonhorizontal boundaries even though the theory is not strictly valid in these cases. The reasoning behind this assumption was that for small slope angles,

i.e., small $\dot{H}$, the normal derivative is approximately the z-derivative; hence, the true boundary conditions could be replaced with continuity of z derivative boundary conditions while incurring negligible errors of order $\dot{H}$. It turns out that this practice is not justified and can introduce serious problems. Chapter IV is concerned with correcting coupled mode theory for use in problems with nonhorizontal boundaries. The rest of this chapter will derive the mathematical formalism of coupled mode theory as proposed by Pierce and will not be concerned with the improper boundary conditions that must be imposed in problems with sloping boundaries.

1. Derivation of Radial Equations

To derive the differential equation for the radial functions $R_n(r)$ Eq. (2.23) is first substituted into Eq. (2.22) to yield

$$\sum_n \ddot{R}_n\phi_n + 2\dot{R}_n\dot{\phi}_n + \frac{R_n\dot{\phi}_n}{r} + \frac{\dot{R}_n}{r}\phi_n + R_n\ddot{\phi}_n \tag{2.26}$$
$$+ R_n\left(\frac{\partial^2\phi_n}{\partial z^2} + k^2(r,z)\phi_n\right) = 0 \quad.$$

In Eq. (2.26) and in the rest of the dissertation, the dot symbol stands for derivative with respect to r. The depth functions $\phi_n(z,r)$, at each range point r, form an orthonormal complete set of functions such that

$$\int_0^\infty \rho \phi_n(z;r) \; \phi_m(z;r) \; dz = \delta_{n,m} \qquad . \qquad (2.27)$$

If Eq. (2.26) is multiplied by $\rho \phi_m(z;r)$ and integrated over depth, the following differential equation for $R_n(r)$ results

$$\ddot{R}_m(r) + \frac{1}{r} \dot{R}_m(r) + k_m^2(r) \; R_m = -\sum_n A_{mn} R_n + B_{mn} \left(\frac{R_n}{r} + 2\dot{R}_n \right) (2.28)$$

The A_{mn} and B_{mn} are functions of range defined by

$$A_{mn}(r) = \int_0^\infty \rho(z) \; \phi_m(z;r) \; \ddot{\phi}_n(z;r) \; dz \qquad , \qquad (2.29)$$

$$B_{mn}(r) = \int_0^\infty \rho(z) \; \phi_m(z;r) \; \dot{\phi}_n(z;r) \; dz \qquad , \qquad (2.30)$$

and are referred to as the coupling coefficients. For reasons related to numerical solutions of differential equations, a more convenient differential equation is sometimes the reduced wave equation which is obtained from (2.28) by substituting $F_n(r)/\sqrt{r}$ in place of $R_n(r)$. The reduced wave function $F_n(r)$ satisfies

$$\ddot{F}_m(r) + \left(k_m^2(r) + \frac{1}{4r^2} \right) F_m(r) = -\sum_n (A_{mn} F_n + 2B_{mn} \dot{F}_n) \qquad . (2.31)$$

The radial wave functions of Eqs. (2.28) and (2.31) satisfy a set of coupled differential equations. The exchange of energy between normal modes or the mode coupling process is

described by the coupled differential equations which the radial functions satisfy. The RHS of Eqs. (2.28) and (2.31) can be thought of as a spatial distribution of sources feeding or absorbing amplitude to or from mode m. The coupling coefficients, A_{mn} and B_{mn}, are therefore proportional to radial rates of interchange of amplitude between modes m and n.

An intuitive picture of sound propagation via coupled normal modes is as follows. In the range stratified case, the proportion of energy alloted to each normal mode of oscillation remains constant in range. In other words, the partitioning of energy among the modes does not vary. When a range dependence of the medium is introduced, an exchange of energy between modes occurs and the partitioning of energy between the modes changes with range from the source. The increase or decrease of amplitude of the modes as a function of range is described by the behavior of the amplitude of the radial function.

At this point it is interesting to note that the mathematical formalism of coupled mode theory reduces to range invariant mode theory as the range dependence of the medium goes to zero. As the medium approaches horizontally stratified, the $\phi_n(z;r)$ and $k_n(r)$ become range independent. When this occurs, the coupling coefficients defined by Eqs. (2.29) and (2.30) vanish and Eqs. (2.28) and (2.24) reduce to the same ones encountered in conventional mode theory.

2. Derivation of Expressions for the Coupling Coefficients

The coupling coefficients defined in Eqs. (2.29) and (2.30) are important functions in the coupled mode theory formalism. The radial functions cannot be determined until the coupling coefficients as a function of range are known. The definition of the coupling coefficients given in Eqs. (2.29) and (2.30) are not convenient for numerical computation because they entail calculation of range derivatives of the $\phi_n(z;r)$ over the entire range of z occurring in the problem. In the following analysis expressions for A_{mn} and B_{mn} more amenable to numerical calculation are derived.

To derive an alternate expression for B_{mn}, one starts with Eq. (2.24). After differentiating with respect to range, (2.24) becomes

$$\frac{\partial^2}{\partial z^2}\dot{\phi}_n + 2(k\dot{k} - k_n\dot{k}_n)\,\phi_n + (k^2 - k_n^2)\,\dot{\phi}_n = 0 \qquad . \qquad (2.32)$$

If (2.32) is multiplied by $\rho\phi_m(z;r)$ and integrated over depth, the result is

$$\int_o^\infty \rho\phi_m \frac{\partial^2}{\partial z^2}\dot{\phi}_n\,dz + \int_o^\infty (k^2 - k_n^2)\rho\phi_m\dot{\phi}_n\,dz = 2k_n\dot{k}_n\delta_{n,m}$$

$$(2.33)$$

$$-\int_o^\infty 2\rho k\dot{k}\phi_m\dot{\phi}_n\,dz \qquad ,$$

where the orthonormality property (Eq. 2.27) of the ϕ_n has been exploited. To illustrate the computational technique, a two-layered waveguide geometry, as pictured in Fig. II.2, will be assumed. The extension to waveguides having more layers is straightforward. Due to the discontinuous nature of the depth functions at layer interfaces, the integrals from 0 to ∞ in (2.33) are shorthand notation for

$$\int_0^\infty = > \int_0^{H(r)} + \int_{H(r)}^\infty \quad . \tag{2.34}$$

With Eq. (2.34) in mind, the first integral in Eq. (2.33) may be integrated twice by parts with respect to z to yield

$$\int_0^\infty \rho \phi_m \frac{\partial^2}{\partial z^2} \dot{\phi}_n \, dz = \int_0^\infty \rho \dot{\phi}_n \frac{\partial^2 \phi_m}{\partial z^2} \, dz + \rho_1 \phi_{1m} \frac{\partial}{\partial z} \dot{\phi}_{1n} \Big|_0^{H(r)}$$

$$+ \rho_2 \phi_{2m} \frac{\partial}{\partial z} \dot{\phi}_{2n} \Big|_{H(r)}^\infty - \rho_1 \dot{\phi}_{1n} \frac{\partial}{\partial z} \phi_{1m} \Big|_0^{H(r)} \tag{2.35}$$

$$- \rho_2 \dot{\phi}_{2n} \frac{\partial}{\partial z} \phi_{2m} \Big|_{H(r)}^\infty \quad .$$

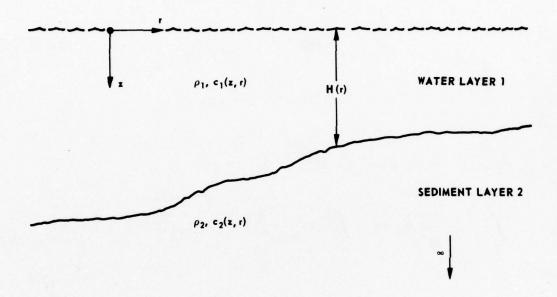In (2.35), the subscript preceding the mode index on the ϕ_n denotes

FIGURE II.2
WAVEGUIDE GEOMETRY FOR DERIVATION OF ALTERNATE
EXPRESSIONS FOR COUPLING COEFFICIENTS

the depth function in the ith layer. The boundary conditions satisfied by ϕ_n are:

$$\phi_{1m}(z=0) = \dot{\phi}_{1m}(z=0) = 0$$

$$\phi_{2m}(z=\infty) = \dot{\phi}_{2m}(z=\infty) = 0$$

$$\rho_1\phi_{1m} = \rho_2\phi_{2m}\Big|_{z=H(r)} \qquad (2.36)$$

$$\frac{\partial}{\partial z}\phi_{1m} = \frac{\partial}{\partial z}\phi_{2m}\Big|_{z=H(r)} \qquad .$$

Equation (2.36) combines with (2.35) to give

$$\int_o^\infty \rho\phi_m \frac{\partial^2}{\partial z^2}\dot{\phi}_n\,dz = \int_o^\infty \rho\dot{\phi}_n \frac{\partial^2\phi_m}{\partial z^2}\,dz + \rho_1\phi_{1m}\left[\frac{\partial}{\partial z}\dot{\phi}_{1n} - \frac{\partial}{\partial z}\dot{\phi}_{2n}\right]\Bigg|_{z=H(r)}$$

$$(2.37)$$

$$- \frac{\partial}{\partial z}\phi_{1m}\left[\rho_1\dot{\phi}_{1n} - \rho_2\dot{\phi}_{2n}\right]\Bigg|_{z=H(r)} \qquad .$$

Equation (2.37) can be used in (2.33) to get

$$\left[k_m^2(r) - k_n^2(r)\right]\int_o^\infty \rho\phi_m\dot{\phi}_n\,dz = 2k_n\dot{k}_n\delta_{n,m} - 2\int_o^\infty \rho k\dot{k}\phi_m\dot{\phi}_n\,dz$$

$$- \rho_1\phi_{1m}\left[\frac{\partial}{\partial z}\dot{\phi}_{1n} - \frac{\partial}{\partial z}\dot{\phi}_{2n}\right]_{z=H(r)}$$

$$(2.38)$$

$$+ \frac{\partial}{\partial z}\phi_{1m}\left[\rho_1\dot{\phi}_{1n} - \rho_2\dot{\phi}_{2n}\right]_{H(r)} \qquad .$$

In obtaining (2.38), $\frac{\partial^2}{\partial z^2}\phi_m$ was replaced with $\left[k_m^2(r) - k^2(z,r)\right]\phi_m$.

Note that the integral on the LHS of (2.38) is simply the definition of B_{mn}; hence (2.38) becomes

$$
B_{mn}(r) = \left[k_n^2(r) - k_m^2(r)\right]^{-1}\left\{2\int \rho k\dot{k}\phi_m\phi_n\,dz\right.
$$

$$
+ \rho_1\phi_{1m}\left[\frac{\partial}{\partial z}\dot{\phi}_{1n} - \frac{\partial}{\partial z}\dot{\phi}_{2n}\right]_{H(r)} \quad (2.39)
$$

$$
\left. - \frac{\partial}{\partial z}\phi_{1m}\left[\rho_1\dot{\phi}_{1n} - \rho_2\dot{\phi}_{2n}\right]_{H(r)}\right\} m \neq n \quad .
$$

The discontinuity terms in (2.39) may be eliminated by use of the boundary conditions on ϕ_n which are

$$
\rho_1\phi_{1n}\left[r,\ z = H(r)\right] = \rho_2\phi_{2n}\left[r,\ z = H(r)\right] \quad , \quad (2.40)
$$

$$
\frac{\partial}{\partial z}\phi_{1n}\left[r,\ z = H(r)\right] = \frac{\partial}{\partial z}\phi_{2n}\left[r,\ z = H(r)\right] \quad . \quad (2.41)
$$

By taking the total range derivative of Eqs. (2.40) and (2.41) it is possible to derive the following expressions.

$$
\left[\rho_1\dot{\phi}_{1n} - \rho_2\dot{\phi}_{2n}\right]_{z=H(r)} = \dot{H}(\rho_2-\rho_1)\left.\frac{\partial\phi_{1n}}{\partial z}\right|_{H(r)} \quad . \quad (2.42)
$$

$$\left[\frac{\partial}{\partial z} \dot{\phi}_{1n} - \frac{\partial}{\partial z} \dot{\phi}_{2n} \right]_{H(r)} = \dot{H} \left[\left(k_n^2(r) - k_2^2 \right) \frac{\rho_1}{\rho_2} \right.$$

$$\left. - \left(k_n^2 - k_1^2 \right) \right] \phi_{1n} \Bigg|_{H(r)} \quad . \tag{2.43}$$

Equations (2.42) and (2.43) combined with (2.39) give

$$B_{mn}(r) = \left[k_n^2(r) - k_m^2(r) \right]^{-1} \left\{ 2 \int_0^\infty \rho k \dot{k} \phi_m \phi_n \, dz + H(r) \sigma_{1mn} \right\} \tag{2.44}$$

where σ_{1mn} is given by

$$\sigma_{1mn}(r) = \left\{ \rho_1 \phi_{1m} \phi_{1n} \left[\frac{\rho_1}{\rho_2} \left(k_n^2 - k_2^2 \right) + \left(k_1^2 - k_n^2 \right) \right] \right.$$

$$\left. - \frac{\partial \phi_{1m}}{\partial z} \frac{\partial \phi_{1n}}{\partial z} (\rho_2 - \rho_1) \right\}_{z=H(r)} \quad . \tag{2.45}$$

Equation (2.44) is much more convenient than (2.30) for numerical calculation because it contains no terms involving radial derivatives of normal mode functions. All of the quantities necessary to evaluate (2.44) are known once the depth functions for a given range have been computed.

Equation (2.44) is not valid for $m = n$. To derive an expression for B_{nn}, one takes the range derivative of the mode orthogonality relationship as follows.

$$\frac{d}{dr}\left[\int_0^{H(r)} \rho_1 \phi_{1m} \phi_{1n} dz + \int_{H(r)}^\infty \rho_2 \phi_{2m} \phi_{2n} \, dz\right] = 0$$

$$(2.46)$$

$$\int_0^{H(r)}\left(\rho_1 \dot{\phi}_{1m} \phi_{1n} + \rho_1 \phi_{1m} \dot{\phi}_{1n}\right) dz + \int_{H(r)}^\infty \left(\rho_2 \dot{\phi}_{2m} \phi_{2n} \, dz + \rho_2 \phi_{2m} \dot{\phi}_{2n}\right) dz$$

$$= -\dot{H}\rho_1 \phi_{1m} \phi_{1n} \Big|_{H(r)} + \dot{H}\rho_2 \phi_{2m} \phi_{2n} \Big|_{H(r)} \quad .$$

The integrals in Eq. (2.46) may be expressed in terms of the B_{mn} through the use of (2.30).

$$B_{mn}(r) + B_{nm}(r) = 2B_{mn}^S(r) = -\dot{H}\rho_1 \phi_{1m} \phi_{1n} \, (1-\rho_1/\rho_2)\Big|_{z=H(r)} \quad . (2.47)$$

In (2.47) the superscript S means the symmetric part of B_{mn}. The diagonal elements of B_{mn} are easily obtained from (2.47) and are given by

$$B_{nn}(r) = - \frac{\dot{H}\rho_1 [\phi_{1n}]^2}{2} \, (1-\rho_1/\rho_2)\Big|_{z=H(r)} \quad . \qquad (2.48)$$

Equation (2.47) can also be derived from the closure relationship for the mode functions. Closure is a property of complete, ortho-normal sets of functions and is expressed as

$$\sum_n \rho \phi_n(z;r) \, \phi_n(z';r) = \delta(z-z') \quad .$$

$$(2.49)$$

An expression for A_{mn} can be obtained by differentiating the integral defining B_{mn} with respect to range.

$$\frac{d}{dr} B_{mn}(r) = \frac{d}{dr} \left\{ \int_o^{H(r)} \rho_1 \phi_{1m} \dot{\phi}_{1n} \, dz + \int_{H(r)}^{\infty} \rho_2 \phi_{2m} \dot{\phi}_{2n} \, dz \right\}$$

$$(2.50)$$

$$\dot{B}_{mn}(r) = \int \rho \phi_m \ddot{\phi}_n \, dz + \int \rho \dot{\phi}_m \dot{\phi}_n \, dz + \dot{H} \left[\rho_1 \phi_{1m} \dot{\phi}_{1n} - \rho_2 \phi_{2m} \dot{\phi}_{2n} \right]_{H(r)} \cdot$$

With Eq. (2.29), (2.50) becomes

$$A_{mn}(r) = \dot{B}_{mn}(r) - \int \rho \dot{\phi}_m \dot{\phi}_n \, dz - \dot{H} \rho_1 \phi_{1m} \left[\dot{\phi}_{1n} - \dot{\phi}_{2n} \right]_{H(r)} \cdot (2.51)$$

It is possible to derive an expression for $\dot{\phi}_n$ from the closure relation of Eq. (2.49). If (2.49) is differentiated with respect to range multiplied by $\phi_m(z;r)$ and then integrated over z, $\dot{\phi}_n$ can be shown to be given by

$$\dot{\phi}_n(z;r) = -\sum_{\ell} E_{n\ell} \, \phi_{\ell}(z;r) \quad , \tag{2.52}$$

with

$$E_{n\ell}(r) = B_{n\ell}(r) + \dot{H} \rho_1 \phi_{1\ell} \phi_{1n} (1 - \rho_1/\rho_2) \Big|_{H(r)} \quad . \tag{2.53}$$

In deriving Eq. (2.52) use was made of the fact that the density has a step function discontinuity at $z=H(r)$, i.e.,

$$\rho(z,r) = \rho_1 \textcircled{H} [H(r) - z] - \rho_2 \textcircled{H} [z - H(r)] \qquad (2.54)$$

$$\dot{\rho}(z,r) = \dot{H}[\rho_1 \delta(H(r)-z) - \rho_2 \delta(z-H(r)] \qquad \cdot \qquad (2.55)$$

In (2.54) $\textcircled{H}(x)$ is the Heavyside unit step function defined by

$$\textcircled{H}(x) \approx \begin{cases} 1 & x>0 \\ \\ 0 & x<0 \end{cases} \qquad .$$

Using Eq. (2.52) in (2.51), one may obtain

$$A_{mn}(r) = \dot{B}_{mn}(r) - \sum_{\ell} E_{n\ell} E_{m\ell} - \dot{H}\rho_1 \phi_{1m} (\dot{\phi}_{1n} - \dot{\phi}_{2n}) \Big|_{H(r)} \cdot \qquad (2.56)$$

In the preceding derivations, any range dependence of the density other than of the form in Eq. (2.54) was not considered. As with the case of continuous variation of density with depth, the continuous radial variation of density within a layer is expected to be of negligible importance. Should one desire to include radial density variations within a layer, the wave equation for the acoustic field is changed (see Ref. 2.13) and the preceding developments and derivations must be altered.

C.   Implementation of Coupled Mode Theory

The application of coupled mode theory to underwater sound propagation is accomplished in four stages. The first stage entails computation of sets of normal mode functions on a mesh of range values covering the radial distance of interest. In the second stage, the normal mode functions are used to compute the coupling coefficients as a function of range through the use of Eqs. (2.44) and (2.56). In the third step, the radial functions defined by Eqs. (2.28) or (2.31) are computed. The last stage combines the normal mode and radial functions according to Eq. (2.23) to produce the field. In each of stages 1 through 4 there are questions concerning choice of the range mesh appropriate for a given problem. These questions are essentially numerical analysis concerns and are not considered in this dissertation. Suffice it to say, the range sampling must be fine enough to allow sufficiently accurate numerical solutions of the differential equations for the radial functions.

1.   Solution of Depth Equations

The numerical solution of the depth equation (2.24) subject to the appropriate boundary conditions is a numerical problem familiar to many areas of engineering and physics. In quantum mechanics,[2.14,2.15] for example, the one-dimensional Schroedinger equation has the same form as Eq. (2.24) where

and
$$k^2(r,z) = -\frac{2m}{\hbar^2} V(z)$$

$$k_n^2(r) = \frac{2m}{\hbar^2} E_n \quad .$$

In the above two expressions $V(z)$ is the potential energy felt by a particle of mass m, E_n is the energy eigenvalue, and $\hbar$ is Plank's constant divided by 2π. Returning now to underwater acoustics, the numerical solution of Eq. (2.24) subject to the previously described boundary conditions is a familiar and well documented procedure and will not be discussed in any detail. References 2.2, 2.7, and 2.16 describe three different methods of solution of Eq. (2.24).

2. Solution of Radial Equations

The solution of the radial equations (2.28) or (2.31) is not a routine matter and will be discussed in more detail here. Assuming that the coupling coefficient matrices as a function of range are known, one can proceed toward a solution of the radial equations in a number of ways. A method used in making the numerical calculations reported later in this dissertation is an iterative technique. In this approach, the set of coupled differential equations is replaced by the following inhomogeneous equations which are solved iteratively.

$$\ddot{F}_m^{(o)} + \left(k_m^2(r) + \frac{1}{4r^2} \right) F_m^{(o)} = 0 \quad . \tag{2.57}$$

$$\ddot{F}_m^{(i+1)} + \left(k_m^2(r) + \frac{1}{4r^2}\right) F_m^{(i+1)} = -\sum_n \left(A_{mn} F_n^{(i)} + 2B_{mn} \dot{F}_m^{(i)}\right) \cdot \quad (2.58)$$

The iteration process on Eq. (2.58) is continued until the procedure converges, i.e., until $F_m^{(i+1)} = F_m^{(i)}$ to the desired accuracy. For typical range variations found in the ocean, the coupling coefficients are expected to be relatively small and slowly varying. For this reason, it is expected that the iterative procedure just described will converge fairly rapidly. However, as with all iterative computational schemes one must be prepared to encounter unstable systems of equations which will not converge under the iterative procedure.

The iterative solution of the radial equations is very similar to the "self-consistent fields" method employed in atomic physics to compute the Hartree-Fock atomic wave functions (see Refs. 2.17 and 2.18). The Hartree-Fock wave functions satisfy a set of coupled, integro-differential equations; however, the iterative process employed in their solution is identical to the one just described.

A second type of iterative procedure that is very similar to the one described in Eqs. (2.57) and (2.58) is a Green's function method. Using this approach, one replaces Eq. (2.31) with the following equation which is solved iteratively

$$F_m^{(i+1)}(r) = F_m^{(o)}(r) - \sum_n \int_0^\infty \left(A_{mn} F_n^{(i)} + 2B_{mn} F_m^{(i)}\right) g_m^{(o)}(r,r')dr' \cdot$$
$$(2.59)$$

The Green's function $g_m^{(o)}$ is obtained from the homogeneous equation for F_m (Eq. 2.57) and is given by (see Ref. 2.10, Ch. 5)

$$g_m^{(o)}(r,r') = \begin{cases} \dfrac{F_{1m}(r)\ F_{2m}(r')}{\Delta(r')} & r \geq r' \\ \\ \dfrac{F_{1m}(r')\ F_{2m}(r)}{\Delta(r')} & r \leq r' \end{cases} \qquad . \quad (2.60)$$

In (2.60), F_{1m} and F_{2m} are two linearly independent solutions to Eq. (2.57). This technique has been used by Williams[2.19] to calculate radial wave functions for the isovelocity, wedge shaped waveguide.

Another method that has been used to solve coupled differential equations is a matrix method. In this technique, a range dependent similarity transformation is obtained such that Eqs. (2.28) or (2.31) are diagonalized. The ensuing system of differential equations are not coupled and may be solved by conventional methods. After solution of the noncoupled system of equations, the desired solutions, i.e., the R_m or F_m, are obtained by applying the inverse similarity transformation to the noncoupled solutions. More details concerning this method may be obtained from Refs. 2.20, 2.21, and 2.22.

3.   Initial Conditions

Before any type of numerical solution for the radial functions can be implemented, the proper initial conditions of the functions must be known.   The type of problem in underwater acoustics most likely to be attacked with coupled mode theory involves computation of the field due to a monochromatic point source in a range dependent medium.   In this situation it can be assumed that in the neighborhood of the point source, the field is essentially the same as the field predicted by range invariant mode theory.   This assumption is expected to be quite good unless severe range variations of the medium occur very near the source. Excluding these pathological cases of near-source, severe range variations, one obtains the initial conditions for the radial functions by requiring that they match the field for a range invariant medium at some point $r=r_s$ which is close to the source region.

Figure II.3 shows a portion of what might be considered a typical range dependent waveguide.   In the notation of Fig. II.3, the initial conditions for the radial functions and their derivatives are taken to be (see Eqs. 2.21 and 2.23)

$$R_m(r_s) = i\pi \, H_o^{(1)}(k_m r_s) \, \phi_m(z_o) \, \rho(z_o)$$

$$\dot{R}_m(r_s) = \rho(z_o) i\pi \, k_m \, \dot{H}_o^{(1)}(k_m r_s) \, \phi_m(z_o)$$

$$= -i\pi \, k_m \, H_1^{(1)}(k_m r_s) \, \phi_m(z_o) \, \rho(z_o) \quad .$$
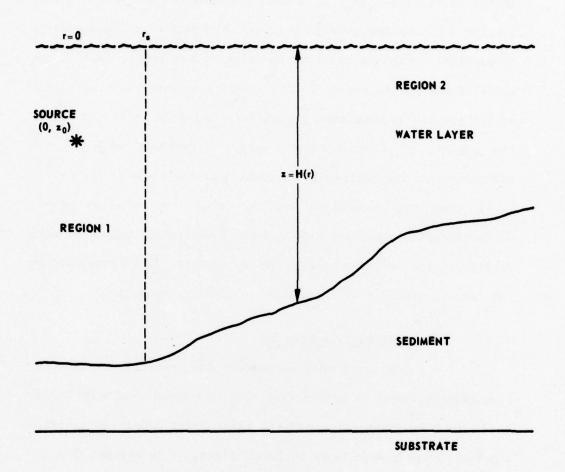
(2.61)

FIGURE II.3
WAVEGUIDE STRUCTURE USED TO DISCUSS INITIAL CONDITIONS OF RADIAL EQUATIONS

In Eq. (2.61) the $\phi_m(z_o)$ is a mode function for the source region (region 1) computed using the local bathymetry and geoacoustic parameters. With the initial conditions given by Eq. (2.61), the radial functions in region 2 can be computed numerically using one of the previously mentioned techniques. Implicit in Eq. (2.61) is the neglect of backscattered energy. Previous work[2.19] has indicated that the backscattered portion of the field is negligibly small. For this reason and the fact that the inclusion of the backscattered field makes a formidable numerical problem even more difficult, the incoming portion of the acoustic field generated by the range dependence of the medium is usually neglected.

4. Attenuation Effects

Up until now, no mention has been made of attenuation effects. What is customarily done in conventional mode theory is to include attenuation effects using first order perturbation theory. The procedure is as follows. First, it is assumed that the attenuation effects of the medium may be treated by introducing a small imaginary component of the wave number, i.e., $k(z)$ becomes

$$k(z) + i\alpha(z)$$

$$\alpha \ll k$$

(2.62)

where $\alpha(z)$ is the attenuation as a function of depth in units of nepers per unit length. Equation (2.62) is next used in (2.12) to get

$$\frac{d^2}{dz^2} \phi_n(z) + \left[k^2(z) - k_n^2 + 2i\alpha(z)k(z)\right]\phi_n(z) \qquad , \qquad (2.63)$$

where α^2 has been neglected as a second order quantity. Conventional first order perturbation theory[2.10,2.15] can be applied to Eq. (2.63) to determine the change in k_n^2 due to the perturbing term $2i\alpha(z)k(z)$. The change in k_n^2 is imaginary and is given by

$$i\delta_n = 2i \int_0^\infty \alpha(z)k(z) \, \rho(z) \, \phi_n^2(z) \, dz \qquad . \qquad (2.64)$$

Hence, the new eigenvalue of the problem becomes

$$k_n^2 + i\delta_n = k_n^2 \left(1 + \frac{i\delta_n}{k_n^2}\right) \qquad . \qquad (2.65)$$

From (2.65) the correction to k_n can be found and is seen to be

$$\sqrt{k_n^2 \left(1 + \frac{i\delta_n}{k_n^2}\right)} \simeq k_n \left(1 + \frac{i\delta_n}{2k_n^2}\right) = k_n + \frac{i\delta_n}{2k_n} \qquad . \qquad (2.66)$$

Attenuation effects are built into the field by retaining the unperturbed mode functions while using Eq. (2.66) in the radial equations. The field in a range invariant medium including attenuation effects becomes from Eq. (2.21)

$$\psi = i\pi\rho(z_o) \sum_n H_o^{(1)}\left(k_n r + \frac{i\delta_n r}{2k_n}\right)\phi_n(z)\,\phi_n(z_o) \qquad . \tag{2.67}$$

If one uses the asymptotic form of the Hankel function valid for $k_n r \geq 1$, (2.67) becomes

$$\psi(r,z) = i\sqrt{\frac{2\pi}{r}} \sum_n \frac{e^{ik_n r}}{\sqrt{k_n}}\,\phi_n(z)\,\phi_n(z_o)\,e^{-\delta_n r/2k_n} \qquad . \tag{2.68}$$

The extension of this perturbation approach to coupled mode theory is straightforward. Since in coupled mode theory the eigenvalues k_n^2 are range dependent, so too are the perturbation corrections to $k_n(r)$. Therefore $k_n(r)$ is replaced with

$$k_n(r) + \frac{i\delta_n(r)}{2k_n(r)} \qquad , \tag{2.69}$$

in analogy with Eq. (2.66). The $\delta_n(r)$ is given by

$$\delta_n(r) = 2\int_o^\infty \alpha(z,r)\,k(z,r)\,\rho(z)\,\phi_n^2(z;r)\,dz \qquad . \tag{2.70}$$

Equation (2.70) is simply (2.64) with range dependence of the modes, wave number, and attenuation allowed for. When the depth functions and eigenvalues for a given range have been computed, the attenuation coefficients $\delta_n(r)$ can easily be calculated via (2.70). When all of the normal mode quantities and the attenuation

coefficients have been determined on the desired range grid, the attenuation effects can be fed into the radial equations (2.28) or (2.31) by replacing $k_m(r)$ with Eq. (2.69).

In the preceding developments the source of the attenuation is not mentioned. Whether it is caused by thermo-viscous effects, relaxation mechanisms, or any other number of mechanisms is not important. One must simply know the attenuation as a function of depth and range for the waveguide irregardless of what caused it. In low frequency underwater sound propagation, the attenuation process is dominated by volume absorption effects in the sediment layers. Published experimental work[2.23,2.24] is readily available documenting the results of measurement of α for oceanic sediments.

5.   Three-Dimensional Coupled Mode Theory

When cylindrical coordinates and azimuthal symmetry are not appropriate for the problem at hand, a more general, three-dimensional coupled mode theory of the following form can be employed. In three-dimensional cartesian coordinates, Eq. (2.22) becomes

$$\nabla^2 \psi(x,y,z) + k^2(x,y,z) \, \psi(x,y,z) = 0 \quad . \quad (2.71)$$

Employing the same methods as used in section B of this chapter, ψ is assumed to be given by

$$\psi(x,y,z) = \sum_n R_n(x,y)\ \phi_n(z;x,y) \qquad , \qquad (2.72)$$

with R_n and ϕ_n satisfying

$$\frac{\partial^2}{\partial x^2} R_m + \frac{\partial^2 R_m}{\partial y^2} + k_m^{\ 2}(x,y)\ R_m = -\sum_n \left(A'_{mn}\ R_n + \vec{B}'_{mn} \cdot \nabla_t\ R_n \right) \quad (2.73)$$

$$\left[\frac{\partial^2}{\partial z^2} + k^2(x,y,z) - k_n^{\ 2}(x,y) \right] \phi_n(z;x,y) = 0 . \qquad (2.74)$$

In Eq. (2.73) ∇_t is the transverse gradient operator defined by

$$\nabla_t = \hat{x}\frac{\partial}{\partial x} + \hat{y}\frac{\partial}{\partial y} \qquad , \qquad (2.75)$$

and A'_{mn} and $\vec{B}'_{mn}$ are given by

$$A'_{mn}(x,y) = \int_o^\infty \rho \phi_m \nabla_t^{\ 2} \phi_n\ dz \qquad . \qquad (2.76)$$

$$\vec{B}'_{mn}(x,y) = \int_o^\infty \rho\ \phi_m \nabla_t \phi_n\ dz \qquad . \qquad (2.77)$$
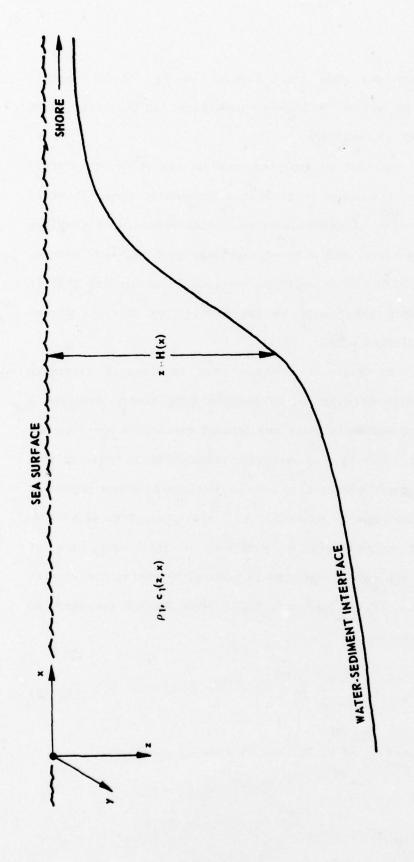
As in the previous case the $\phi_n(z;x,y)$ of Eq. (2.74) satisfy continuity of $\rho\phi_n$ and $\partial\phi_n/\partial z$ boundary conditions and form a complete, orthonormal set of functions.

The task of applying coupled mode theory to a truly three-dimensional problem is at best a formidable one. It would entail computation of depth functions, eigenvalues, and coupling coefficient matrices over a two-dimensional grid of (x,y) points. The amount of effort that would be required to accomplish this is probably greater than would be expended in an outright three-dimensional solution of Eq. (2.71).

One type of problem that requires a cartesian coordinate system formulation of coupled mode theory involves a range dependent medium in which the lateral variations occur in one dimension only. This type of waveguide scenario might reasonably be applied to acoustic propagation over a continental slope region in which the bottom slope is a function of x alone (see Fig. II.4). To apply coupled mode theory to problems of this sort, the y-dependence of the radial equation is removed by taking the Fourier transform of Eq. (2.73) (see Ref. 2.25). The Fourier transform of $R_m(x,y)$ is given by

$$R_m(x,\gamma) = \frac{1}{\sqrt{2\pi}} \int_{-\infty}^{+\infty} dy \, e^{i\gamma y} \, R_m(x,y) \qquad . \qquad (2.78)$$

Taking the transform of (2.73) one obtains

FIGURE II.4

WAVEGUIDE GEOMETRY FOR MEDIUM IN WHICH RANGE DEPENDENCE OCCURS IN x-DIRECTION

THIS DEPICTION IS INVARIANT WITH RESPECT TO TRANSLATION IN THE y-DIRECTION

$$(2.79)$$

$$\frac{d^2}{dx^2} R_m(x,\gamma) + \left[k_m^2(x) - \gamma^2 \right] R_m(x,\gamma) = - \sum (A'_{mn} + \vec{B}'_{mn} \cdot \nabla_t) R_n \quad \cdot$$

Equation (2.79) is to be solved over a sufficient range of γ such that the inverse transform of $R_m(x,y)$ can be computed using

$$R_m(x,y) = \frac{1}{\sqrt{2\pi}} \int_\infty^\infty d\gamma e^{-i\gamma y} R_m(x,\gamma) \quad . \qquad (2.80)$$

Having determined $R_m(x,y)$ according to Eqs. (2.79) and (2.80), the field is constructed from Eq. (2.72) where ϕ_n now depends only on z and x.

At this point it is worth pointing out the differences between the two-dimensional coupled mode theory described in section B of this chapter and the formalism of the theory for range variations occurring in one dimension that was just described. If the formalism of section B were to be applied to a waveguide as pictured in Fig. II.4, one would actually be considering a bowl shaped structure obtained by rotating Fig. II.4 about an axis perpendicular to the ocean surface and passing through the source position. In many applications, this would be a poor approximation to the physical system being modeled. However, in many types of problems in which the source is some distance removed from the areas of significant range variation, the differences between the two different formalisms of coupled mode theory might reasonably be expected to become small. The reason

that the differences are expected to become small is related to the
fact that at large distances from the source, the rotation of a
waveguide such as shown in Fig. II.4 about the source position is a
good approximation to a translation in the y direction, even for
angles of rotation that are fairly large. In other words, the bowl
becomes so large and the curvature so small that the sound field
loses knowledge of the basin-like structure it is propagating in
and becomes a good approximation to the field in the waveguide being
modeled.

The advantage of applying an azimuthally symmetric
cylindrical coordinate system whenever possible is that it elimi-
nates the need to perform the inverse Fourier transform procedure
of Eq. (2.80). Since the inverse transform procedure involves
solution of (2.79) for many values of γ, the savings in computational
effort can be quite significant. A distant deep water source
radiating energy toward a continental slope is an example of a
propagation problem which can reasonably be handled using an
azimuthally symmetric, cylindrical coordinate system formulation.

CHAPTER III

COUPLED MODE THEORY IN THE ADIABATIC APPROXIMATION

In this chapter the adiabatic approximation to coupled mode theory is examined. The adiabatic approximation is an approximation on the set of coupled radial equations in which all mode-mode coupling effects are ignored. In the adiabatic approximation the amount of energy initially associated with a mode remains with that mode since energy exchange between modes has been neglected.

The adiabatic approximation to coupled mode theory has been a basic part of the formalism of the theory from the very beginning. In the two benchmark papers by Pierce[3.1] and Milder[3.2] in which the full framework of coupled mode theory was described, it was the adiabatic approximation to coupled mode theory that was actually the focal point. Pierce applied ray theory methods to the solution of the adiabatic range equations while Milder derived ray theory and wave theory criteria for the validity of the approximation. A large portion of all applications of coupled mode theory in underwater acoustics has been within the adiabatic approximation (see Refs. 3.3-3.7).

The material contained in this chapter will be presented according to the following format. First, the basics of the adiabatic approximation will be examined. This will include a discussion of energy conservation and a validity criterion for the

49

approximation. Second, the sensitivity of the adiabatic approximation to the range dependence of the ocean bottom will be examined. This examination will take place within the context of a realistic model of a deep water oceanic waveguide. Finally, the field in the adiabatic approximation is examined with regard to the multipath conversion processes present in waveguides having nonhorizontal boundaries and interfaces. This will involve drawing an analogy between wave theory and ray theory.

A.   Background

The term "adiabatic approximation" or "adiabatic variation" arises in many branches of physics. These terms were originally coined in the Hamilton-Jacobi[3.8-3.11] theory of action-angle variables in classical mechanics. In quantum mechanics, an adiabatic approximation (see Ref. 3.12, Chapter 8) is used in the solution of the Schrödinger equation for a weakly time-dependent Hamiltonian. Another quantum mechanical approximation that is mathematically identical to the adiabatic approximation of coupled mode theory is the Born-Oppenheimer[3.13-3.15] approximation used to separate the electron and nuclear motions in the solution of Schrödinger's equation in atomic physics applications.

In the application to coupled mode theory, "adiabatic variation" refers to the range dependence of the properties of the acoustic medium in question. An adiabatic variation of some

property of a waveguide, e.g., the sound speed, is a finite change
in that parameter occurring such that locally

$$\frac{\partial c}{\partial r} \to 0$$

while r goes to infinity in a manner that

$$\int_0^r \frac{\partial c}{\partial r} \, dr = \Delta c \quad ,$$

with Δc being a finite change in the parameter. An adiabatic
variation of a parameter can involve quite large changes, just so
long as the local rate of change is small. The "adiabatic
approximation" considered in this chapter is based upon the
assumption of adiabatic range variability of the acoustic medium
and is expected to be valid in the limit of very slow local radial
rates of change of the geoacoustic parameters of the waveguide.

1. Fundamentals of the Adiabatic Approximation

The adiabatic approximation is an approximation
applied to the set of coupled radial equations arising from the
coupled mode theory. The approximation is based on the assumption
that for sufficiently slow range variation of the medium, the
effects of mode-mode coupling become small and may be neglected.
Based on this assumption the radial equations in the adiabatic
approximation become from (2.28) and (2.31)

$$\ddot{R}_m(r) + \frac{\dot{R}_m(r)}{r} + k_m^2(r) R_m(r) = 0 \qquad . \qquad (3.1)$$

$$\ddot{F}_m(r) + \left(k_m^2(r) + 1/4r^2 \right) F_m(r) = 0 \qquad . \qquad (3.2)$$

In Eqs. (3.1) and (3.2) the coupling coefficients which describe the mode-mode interactions have been neglected. From Eqs. (2.44) and (2.56) it is apparent that the B_{mn} and A_{mn} are proportional to first and second range derivatives of the properties of the propagation medium ($k(z,r)$ and $H(r)$). Hence, the neglect of the coupling coefficients is based on the assumption that, locally, the properties of the medium are slowly varying and this is consistent with the definition of adiabatic variation.

The acoustic field computed in the adiabatic approximation differs from the field computed using the full coupled mode formalism only in the radial equations ((3.1) and (3.2) versus (2.28) and (2.31)) that are employed. Of course the main advantage of the adiabatic approximation is that a set of uncoupled radial equations is to be solved rather than a coupled set. Since solving uncoupled equations is a much simpler task than solving coupled equations, it is clearly important to be able to take advantage of the adiabatic approximation whenever possible. A comparison of Eqs. (2.5) and (3.1) shows that the adiabatic range

equations differ from the horizontally stratified equations only through the range dependence of the eigenvalue $k_m(r)$. Therefore, it is expected that for waveguides having slow range dependence, Eq. (3.1) will exhibit behavior similar to a Hankel function.

In the developments of Chapter II it was revealed that coupled mode theory when applied to waveguides having range variable boundaries involves an approximation to the physically proper boundary conditions satisfied by the field. In Chapter IV it will be shown that this approximation is not consistent with the theory obtained. In the adiabatic approximation to coupled mode theory no such consistency problem arises because the assumption of adiabatic variation of the medium is of the same order, or is consistent with the approximation to the physically proper boundary conditions.

The partial separation of radial and depth variables effected in coupled mode theory requires that the normal derivative of the field at a nonhorizontal boundary be approximated with the z-derivative. This amounts to a zero order approximation of Eq. (2.25).

$$\nabla \simeq \frac{\partial}{\partial z} + O(\dot{H}) \quad . \tag{3.3}$$

Since the coupling coefficients which are of order $\dot{H}$ and $\dot{H}^2$ are neglected in the adiabatic approximation, the boundary condition approximation of Eq. (3.3) is consistent with the assumption of

adiabatic variation of the medium. The significance of the consistency will become more apparent in Chapter IV.

In the first part of this chapter it was stated that the energy initially associated with a mode remains with that mode in the adiabatic approximation. To illustrate this point consider the radial energy flux f_r given by (see Refs. 3.16 and 3.17)

$$f_r = \frac{1}{2} \text{Re} \ (pv_r^*) \qquad . \qquad (3.4)$$

In (3.4) p is the acoustic pressure and v_r is the radial component of particle velocity given by

$$p = -\rho \frac{\partial \psi}{\partial t} = i\omega\rho\psi \qquad . \qquad (3.5)$$

$$v_r = \frac{\partial \psi}{\partial r} \qquad . \qquad (3.6)$$

In (3.5) the time dependence of the field was taken to be $e^{-i\omega t}$ and "Re" in (3.4) means real part of. For the field expressed in the form

$$\psi(r,z) = \sum_n R_n(r) \ \phi_n(z;r) \qquad , \qquad (3.7)$$

Eq. (3.4) becomes

$$f_r = \frac{i\omega\rho}{4} \left\{ \sum_{n,m} \left(R_n \dot{R}^*_n - R^*_n \dot{R}_n \right) \phi_n \phi_m + \left(R_n R^*_m - R^*_n R_m \right) \phi_n \dot{\phi}_m \right\} \quad , \quad (3.8)$$

where the dot symbol denotes differentiation with respect to range. The time rate of change of energy in the radial direction, J_r, is obtained by integrating (3.8) over the surface of a cylinder centered about the depth axis at range $r=0$. (See Fig. III.1.) This yields

$$J_r = \int_0^\infty 2\pi r \, f_r \, dz$$

$$J_r = \frac{i\pi\omega r}{2} \left\{ \sum_n \left(R_n \dot{R}^*_n - R^*_n \dot{R}_n \right) + \sum_{n,m} \left(R_n R^*_m - R^*_n R_m \right) B_{nm} \right\} \quad (3.9)$$

where the definition for B_{nm} in Eq. (2.30) along with (2.27) were employed.

In the adiabatic approximation all quantities involving coupling coefficients are neglected; hence, (3.9) becomes in the adiabatic approximation

$$J_r = \frac{i\pi\omega r}{2} \sum_n \left(R_n \dot{R}^*_n - R^*_n \dot{R}_n \right) \quad . \quad (3.10)$$

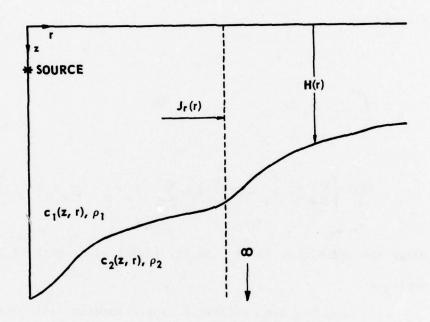If Eq. (3.1) is multiplied by R^*_m and subtracted from its complex conjugate, it is easy to show that

FIGURE III.1
WAVEGUIDE GEOMETRY FOR DERIVATION OF RADIAL ENERGY FLUX

$$R_n \ddot{R}_n^* - R_n^* \ddot{R}_n + \frac{R_n \dot{R}_n^* - R_n^* \dot{R}_n}{r} = 0 \quad ,$$

$$\frac{d}{dr}\left(R_n \dot{R}_n^* - R_n^* \dot{R}_n\right) + \frac{\left(R_n \dot{R}_n^* - R_n^* \dot{R}_n\right)}{r} = 0 \quad , \tag{3.11}$$

$$\frac{d}{dr}\left[r\left(R_n \dot{R}_n^* - R_n^* \dot{R}_n\right)\right] = 0 \quad .$$

Equation (3.11) shows that in *the adiabatic approximation*, the quantity

$$r\left(R_n \dot{R}_n^* - R_n^* \dot{R}_n\right) = \beta_n \tag{3.12}$$

is constant in range and that the radial flux of energy through a cylindrical surface transported by the nth mode, $J_r^{(n)}$, is range independent

$$J_r^{(n)} = \frac{i\pi\omega}{2}\beta_n \quad . \tag{3.13}$$

This verifies that, in the absence of attenuation, the amount of energy initially associated with a particular mode remains with that mode in the adiabatic approximation to coupled mode theory. Moreover, the total radial energy flux through a cylindrical surface given by

$$J_r = \sum_n J_r^{(n)} \tag{3.14}$$

is also seen to be range independent, indicating that energy is conserved within the *context of adiabatic mode theory*.

An estimate of the adiabatic power amplitude associated with a given normal mode may be made based on the WKB approximate solution of Eq. (3.1) (see Refs. 3.1, 3.12, 3.17, 3.18) given by

$$R_n(r) \simeq i\sqrt{2\pi}\; \rho(z_o)\; \phi_n(z_o;0)\; \frac{e^{\;i\int^r k_n(r')dr'\; -\; i\pi/4}}{\sqrt{k_n(r)r}} \qquad . \quad (3.15)$$

In Eq. (3.15) the multiplicative constants were chosen such that the field reduces to the field for a range invariant medium near the source located at $(z_o,0)$ (see Chapter II, section C-3). Equations (3.12)-(3.15) give

$$J_r^{(n)} \simeq 2\pi^2 \omega\rho(z_o)^2 \phi_n^2(z_o;0) \qquad . \qquad (3.16)$$

$$J_r \simeq 2\pi^2 \omega\rho(z_o)^2 \sum_n \phi_n^2(z_o;0) \qquad . \qquad (3.17)$$

Equations (3.16) and (3.17) are the adiabatic power amplitudes evaluated within the WKB approximation and depend on the amplitude of the mode functions at the source location.

2. Derivation of Adiabacity Criterion

In this subsection of Chapter III a validity criterion for the adiabatic approximation that will be used in later sections of this chapter is derived. This criterion is based on coupled mode wave theory and was originally derived by Milder.[3.2] The derivation presented here is a reproduction of Milder's derivation. Other validity criteria for adiabacity have been derived (see Refs. 3.4 and 3.6); however, Milder's criterion is of a form most suitable for the investigations presented later in this chapter.

The derivation starts with Eq. (2.31) approximated as

$$\left[\frac{d^2}{dr^2} + k_m^2(r)\right] F_m(r) = -2 \sum_n B_{mn}(r) \dot{F}_n(r) \quad . \quad (3.18)$$

In writing (2.31) as (3.18) it has been assumed that the range variations of interest are far enough from the source that the $1/4r^2$ term may be neglected and that A_{mn} which is second order in the range dependence of the medium is negligible compared to B_{mn}. The solution to Eq. (3.18) can be expressed in terms of a homogeneous solution, $F_m^{(0)}$, and a particular solution, $F_m^{(1)}$.

$$F_m(r) = F_m^{(0)} + F_m^{(1)} \qquad (3.19)$$

The solution $F_m^{(0)}$ is of course the adiabatic solution. The particular solution $F_m^{(1)}$ can be written in terms of a Green's function as

$$F_m^{(1)}(r) = -2 \sum_n \int_0^r B_{mn}(r') \, \dot{F}_n(r') g_m(r,r') dr' \qquad . \quad (3.20)$$

In (3.20) g_m is the Green's function appropriate to the homogeneous form of (3.18). In evaluating (3.20), WKB approximations for the quantities in the integral are employed. These are

$$g_m(r,r') \simeq \frac{1}{2ik_m} \exp\left[i\int_{r'}^r k_m(x)dx\right] \qquad (3.21)$$

$$F_n(r') \simeq \exp\left\{i\int^{r'} k_n(x)dx\right\} \qquad (3.22)$$

$$\dot{F}_n(r') \simeq ik_n(r') \, F_n(r') \qquad . \qquad (3.23)$$

Equations (3.21) - (3.23) in (3.20) give

$$F_m^{(1)}(r) \simeq -2 \sum_n \int_0^r \frac{B_{mn}(r')ik_n(r')}{2ik_m(r')} \exp\left\{i\int^{r'}\left[k_n(x) - k_m(x)\right]dx\right\}$$

$$\times \exp\left\{i\int^r k_m(x)dx\right\} dr' \qquad . \qquad (3.24)$$

In order to derive a criterion that does not depend on the particular details of a given propagation medium, the following assumptions are made. First, it is assumed that the range variations of the medium occur only over a region of space between 0 and r_o. Second, it is assumed that the eigenvalues and B_{mn} are slowly varying functions of range. In problems involving realistic deep water, oceanic waveguides this assumption is quite good. Under the above two assumptions Eq. (3.24) becomes

$$F_m^{(1)}(r) \simeq - \sum_n B_{mn}(r) \, e^{ik_m r} \int_o^{r_o} e^{i(k_n - k_m)r'} \, dr' \quad . \qquad (3.25)$$

$$F_m^{(1)}(r) \simeq - \sum_n B_{mn}(r) \, e^{ik_m r} \, \frac{e^{i(k_m - k_n)r_o} - 1}{i(k_m - k_n)} \quad . \qquad (3.26)$$

In obtaining (3.26) the ratio k_n/k_m in (3.24), which is a term of order unity, was replaced by 1.

Milder's criterion is obtained from (3.26) by requiring that the magnitude of $F_m^{(1)}$ be much less than the magnitude of the WKB form of adiabatic solution in Eq. (3.22). Hence, for the effects of mode coupling to be small,

$$\left| F_m^{(1)}(r) \right| \ll 1 \quad . \qquad (3.27)$$

Equation (3.27) will be satisfied if, term by term from (3.26),

$$\left| \frac{2B_{mn}(r)}{k_m(r) - k_n(r)} \right| \ll 1 \qquad . \tag{3.28}$$

Equation (3.28) states that if the coupling coefficient B_{mn} describing the mode interaction between modes m and n is small compared to the difference in eigenvalues, then adiabatic mode invariance is assured. Equation (3.28) is to be satisfied for all combinations of m and n, especially for those where m and n differ by 1 and $k_m - k_n$ is the least. A somewhat relaxed version of (3.28) is obtained by requiring the coupling between nearest neighbor modes to be small.

$$\left| \frac{2B_{m,m+1}}{k_m - k_{m+1}} \right| \ll 1 \tag{3.29}$$

Equation (3.29) is the adiabacity criterion that will be used in the next section of this chapter. In terms of the mode cycle distance, x_m, defined by

$$x_m = \frac{2\pi}{k_m - k_{m+1}} \qquad , \tag{3.30}$$

Eq. (3.29) becomes

$$\left| \frac{B_{m,m+1} \, x_m}{\pi} \right| = \varepsilon \ll 1 \tag{3.31}$$

where ε is a smallness parameter.

3. Types of Problems Suitable for the Adiabatic

Approximation

The requirement of adiabatic range dependence of the medium narrows the scope of problems that may be attacked using adiabatic mode theory. Since interchange of energy is not allowed in adiabatic mode theory, it is probably not suited for use in waveguides in which the number of propagating modes varies drastically in range. Such a situation would occur if adiabatic mode theory were applied to a continental slope propagation problem.

For a 20 Hz source located in deep water (5000 m) there would typically be about 110 propagating modes. For a receiver located on the continental shelf in shallow water (700 m) there would exist about 20 propagating modes. In this situation one could not expect the adiabatic approximation to work very well over extended ranges since the energy associated with a particular mode disappears from the problem when that mode reaches cutoff. Clearly the process of mode conversion in which energy is transferred among the modes would be important in this case.

The types of problems that are likely candidates for the use of adiabatic mode theory are those in which the principle of conservation of mode index applies. The principle of conservation of mode index was used by Pierce[3.1] to describe propagation situations in which the number of propagating modes remained

constant in range. In this case, the range dependence of the medium is assumed to be accommodated by small adjustments of the mode functions in range without the need of energy transfer. Conservation of mode index can reasonably be expected to apply to waveguides having relatively horizontal boundaries and geoacoustic parameters that are weakly dependent on range. Since the number of propagating modes is particularly sensitive to water depth, wave-guides having large depth variations cannot be treated as adiabatic. On the other hand, if one wanted to describe the propagation of sound over a relatively flat ocean basin where the sediment composition varied slowly with range, then the adiabatic approximation is likely to be quite good.

B.   Sensitivity of Adiabatic Approximation to Ocean Bottom Properties

In the study of underwater sound propagation in the ocean it is customary to consider the waveguide in terms of two component parts, the water layer and the bottom. The bottom is considered to begin at the water-sediment interface and continue into the substrate to infinity. Depending on the frequency of interest, the bottom can influence the field in the water column to a great extent. At low frequencies where normal mode techniques are most applicable, the bottom is an important part of the propagation medium.

In this section of Chapter III the sensitivity of the adiabatic approximation to the range dependence of the ocean bottom is examined. Previous work along these lines (see Refs. 3.2 - 3.5) has focused on range variability in the water column alone. In most realistic, deep water oceanic waveguides the water layer is sufficiently slowly varying with range that the adiabatic approximation is valid. Milder showed that for typical horizontal sound speed gradients in the ocean, adiabatic propagation in the water layer was assured for frequencies less than 600 Hz.

The ocean bottom is not nearly as stable as the water column and much larger range variability is present. The work presented here will focus on two range dependent bottom parameters, sediment sound speed and water-sediment interface slope, and will explore how the adiabatic approximation depends on these parameters.

The method used to examine the sensitivity of the adiabatic approximation to the bottom parameters is through the use of Milder's criterion given in Eq. (3.31). The procedure is to select a value for ϵ in (3.31) and compute, for each mode number m, the magnitude of $B_{m,m+1}$ at which the equality in (3.31) is satisfied. The magnitude of $B_{m,m+1}$ depends on the properties of the bottom in question. This allows one to determine the values of sediment radial sound speed gradient and water-sediment interface slope that may be tolerated within the adiabatic approximation.
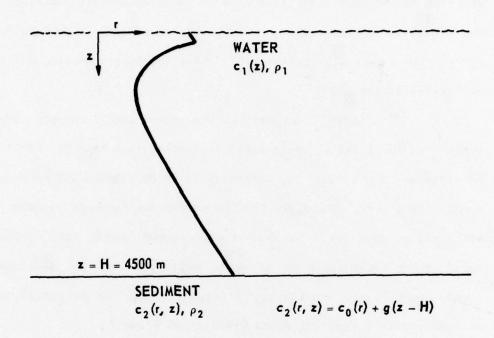
In the choice of ε in (3.31) one is allowed a certain amount of latitude. Only when the adiabatic solution can be directly compared with the full coupled mode solution will it be possible to determine the proper value of the smallness parameter ε to ensure adiabacity. Since a coupled mode theory calculation for a general oceanic waveguide is not yet able to be done, it is possible only to select what is considered to be a safe value for ε and proceed with the investigation. Hence, it is not now possible to determine absolutely the magnitude of bottom slope and radial sound speed gradient that may be treated adiabatically though the relative sensitivity of the adiabatic approximation among different bottom types can be studied and understood. The value of ε used in the studies presented here is $\varepsilon = 0.1$.

1. Dependence on Radial Sound Speed Gradient

The first range dependent parameter to be investigated is the sediment sound speed. Figure III.2 depicts the waveguide geometry used in the numerical calculations that were performed. The first layer is water 4500 m deep having an arbitrary sound speed profile. (For the calculations presented here, a mid-Pacific type profile was used.) The sediment layer is 300 m deep and is assumed to depend on range and depth as

$$c_2(r,z) = c_o(r) + g(z-H) \quad .$$

In other words, the sound speed varies with range and depth in such a way that the depth variation is linear and the radial gradient of

FIGURE III.2
WAVEGUIDE LAYER AND SOUND SPEED STRUCTURE
FOR EXAMINATION OF THE EFFECTS OF RADIAL AND
SOUND SPEED DERIVATIVES IN THE SEDIMENT LAYER

sound speed is depth independent. The sediment layer will be treated as clay, silt, and sand. These sediment types span the spectrum of sediment porosities usually found in oceanic sediments. The substrate is treated as an infinite isovelocity liquid half-space. The geoacoustic parameters[3.19] for the layers in Fig. III.2 are listed in Table I.

Figure III.3 depicts the relationship between mode number and local radial sound speed derivative such that Eq. (3.31) is satisfied for $\varepsilon = 0.1$. The frequency is 20 Hz and the sediment is treated as a clay. There are 106 discreet modes for this frequency and layering geometry. Two curves are present in Fig. III.3. The solid curve corresponds to no depth dependence of the sediment sound speed, i.e., isovelocity in depth, while the dotted curve corresponds to a constant depth gradient of 1 $\sec^{-1}$.

The curves in Fig. III.3 were generated from Eq. (2.44) using $\dot{H} = 0$.

$$B_{mn}(r) = \frac{1}{\left[k_n^2 - k_m^2\right]} \int_0^\infty 2\rho k \dot{k} \phi_n \phi_m dz \qquad (3.32)$$

Since the range variations are restricted to the sediment layer and are given by

$$c_2(r,z) = c_o(r) + g(z-H) \qquad , \qquad (3.33)$$

Eq. (3.32) becomes

TABLE I

SEDIMENT AND SUBSTRATE GEOACOUSTIC PARAMETERS[3.19]

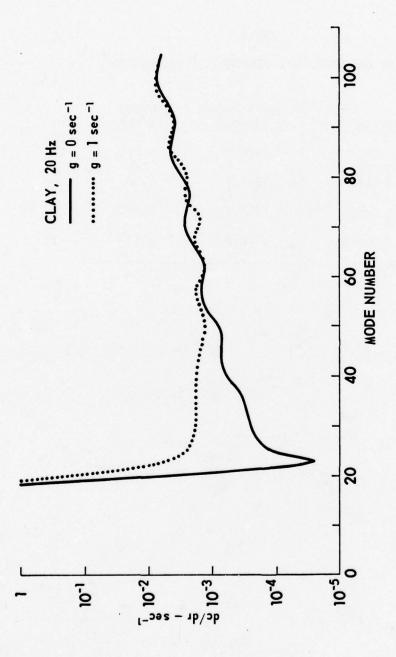| Bottom Type	Sound Speed (m/sec)	Density (g/cc)
Clay	1526.6	1.27
Silt	1563.0	1.60
Sand	1723.8	2.08
Substrate	2700.0	2.60

FIGURE III.3

CURVE REPRESENTING THE RELATIONSHIP BETWEEN MODE NUMBER
AND MAXIMUM RADIAL SEDIMENT SOUND SPEED DERIVATIVE THAT
MAY BE TOLERATED WITHIN THE ADIABATIC APPROXIMATION

$$B_{mn}(r) = \frac{-2\omega^2 \dot{c}_o(r)\rho_2}{\left[k_n^2 - k_m^2\right]} \int_{sed} \frac{\phi_n(z;r)\ \phi_m(z;r)}{c_2^3(r,z)}\, dz \quad . \qquad (3.34)$$

From Eq. (3.34) it is straightforward to determine the values of $\dot{c}_o(r)$ that cause Eq. (3.31) to be satisfied for a particular choice of ε. In this manner Fig. III.3 and all similar curves were generated. The mode functions, ϕ_n, used in the computation of (3.34) were obtained by numerical integration[3.20,3.21] of the depth equation (2.24).

There are several interesting features in Fig. III.3. First, note the large dip in the curve for g=0 at about mode number 24. This dip marks the dividing line between modes with turning points in the water and those with turning points in the sediment. The term "turning point" refers to points at which the vertical wavenumber $\kappa_n^2(z;r)=k^2(r,z)-k_n^2(r)$ in (3.35) becomes zero.

$$\left[\frac{\partial^2}{\partial z^2} + \kappa_n^2(z;r)\right]\phi_n(z;r) = 0 \qquad (3.35)$$

Hence, a turning point separates regions in which the mode functions ϕ_n are oscillatory and exponential in behavior. For a typical deep water sound speed profile as shown in Fig. III.2, the modes of low index number have turning points wholly within the water column and are exponential in the bottom region. These modes are said to be trapped in the water column. As mode index increases, the lower turning points begin to occur within the bottom and oscillatory behavior of the mode function occurs over a

portion of the bottom. Such modes are said to be bottom interacting modes.

In Fig. III.3, the modes of index less than 24 are trapped in the water columns and are exponential in the bottom region where the range changes are occurring. Hence, these modes are insensitive to what is happening in the bottom and may be treated adiabatically for quite large radial sound speed gradients.

Another feature of Fig. III.3 is that the presence of a depth gradient washes out the large dip beginning at mode number 24 and approaches the curve for g=0 at the higher mode numbers. The general features of both curves in Fig. III.3 may be understood with reference to Fig. III.4. When a mode has a turning point in the sediment, it may be viewed as a ray of equivalent bottom angle, θ_m, given by

$$\theta_m = \cos^{-1} \frac{c_1(H)}{V_m}$$

$$V_m = \omega/k_m \qquad .$$

where V_m is the phase velocity of the nth mode. The equivalent bottom grazing angle is an increasing function of mode number.

The large dip in the solid curve of Fig. III.3 at mode number 24 corresponds to the first mode with a turning point in the sediment layer. This mode corresponds to an equivalent ray of very shallow grazing angle. When no depth gradients are present in
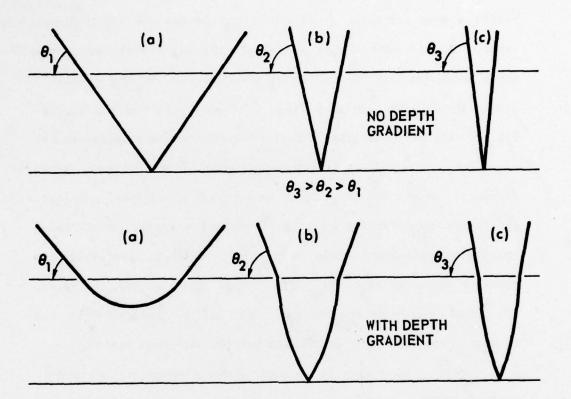
FIGURE III.4
SEDIMENT RAY PATHS FOR DIFFERENT BOTTOM GRAZING ANGLES
WITH AND WITHOUT SEDIMENT SOUND SPEED DEPTH GRADIENT

the bottom, this ray covers the largest radial distance through the sediment on its path to the substrate and back to the water column. This equivalent ray, therefore, is exposed to the largest relative radial change in sound speed as it cycles through the sediment layer. As the mode number increases, the equivalent ray bottom angle increases and the radial distance covered by the ray as it cycles through the sediment layer decreases (see top row in Fig. III.4). The adiabatic approximation depends on the relative amount of radial change in sediment sound speed over the mode cycle distance. Hence, for the case of no vertical sound speed gradient, the higher modes should be able to withstand larger radial sound speed gradients and remain adiabatic. This is precisely the behavior of the solid curve in Fig. III.3. One sees that the amount of radial sound speed gradient that may be tolerated in the adiabatic approximation increases steadily with mode number.

When a vertical sound speed gradient is present in the bottom, the previous situation is altered somewhat (see bottom row in Fig. III.4). When g=0, the mode with the shallowest equivalent bottom angle no longer corresponds to the largest cycle distance through the sediment due to the refraction caused by the vertical sound speed gradient. As the mode number and hence the equivalent bottom angle is increased, the cycle distance through the sediment begins to increase until the mode turning points reach the substrate. At this time, the cycle distances begin to decrease and approach the cycle distances for g=0 as the equivalent bottom

angles become so steep that the refractive effects of the vertical gradient become negligible. This is the behavior exhibited by the dotted curve in Fig. III.3. The large dip around mode 24 vanishes due to the decreased cycle distances of these modes when a vertical gradient is present and the dotted curve approaches the solid curve as mode number increases and the cycle distances for the two cases become similar.

Figures III.5 and III.6 are the same type curves as Fig. III.3 except that the sediment is treated as silt and sand. Figures III.5 and III.6 exhibit the same type of behavior as Fig. III.3 except that the large dip in the solid curves corresponding to the first mode with a turning point in the bottom occurs at higher mode numbers because of higher surficial sound speed values in silt and clay.

Figure III.7 is a superposition of Figs. III.3, III.5, and III.6 for g=1. Based on Fig. III.7 and a choice of ϵ=0.1, it can be said that a radial sediment sound speed gradient of about 10^{-3} sec^{-1} could be tolerated within the adiabatic approximation for all the sediment types and all mode numbers.

In the lower mode number portions (less than m 60) of Fig. III.7, the curves lie in the order sand, silt, and clay. In this low mode region the sand can withstand the highest radial gradients followed by silt, and then clay. This behavior is related to the fact that the characteristic acoustic impedance of sand is

FIGURE III.5
CURVE REPRESENTING THE RELATIONSHIP BETWEEN MODE NUMBER AND MAXIMUM RADIAL SEDIMENT SOUND SPEED DERIVATIVE THAT MAY BE TOLERATED WITHIN THE ADIABATIC APPROXIMATION
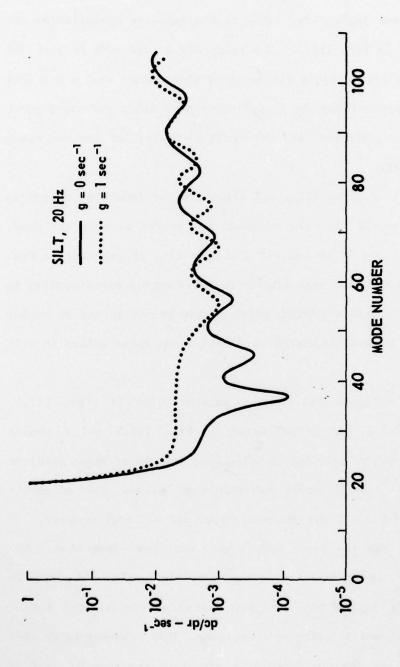
FIGURE III.6

CURVE REPRESENTING THE RELATIONSHIP BETWEEN MODE NUMBER
AND MAXIMUM RADIAL SEDIMENT SOUND SPEED DERIVATIVE THAT
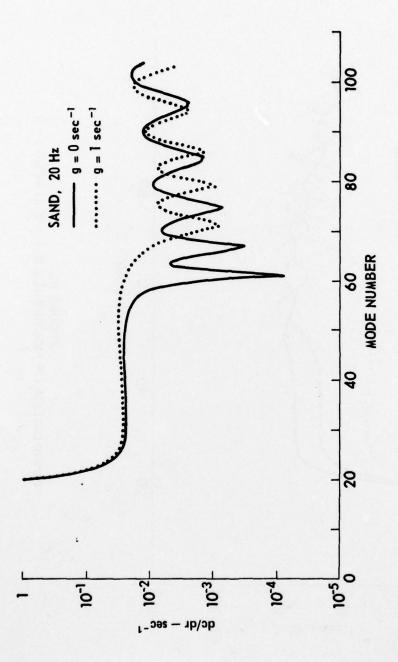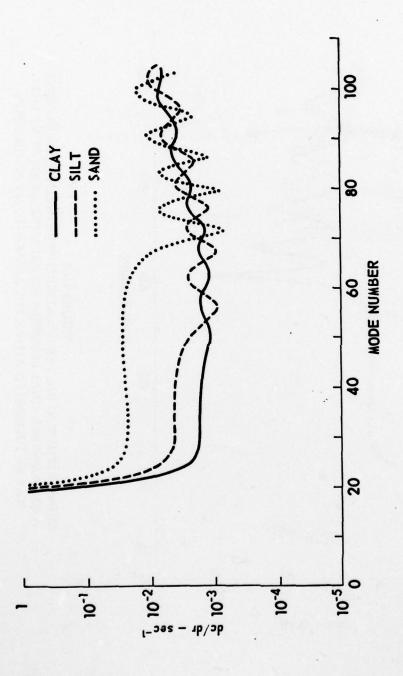MAY BE TOLERATED WITHIN THE ADIABATIC APPROXIMATION

FIGURE III.7

SUPERPOSITION OF FIGURES III.3, III.5, and III.6 FOR g = 1

higher than that of silt, which is higher than that of clay. Hence, for the low mode numbers in question, the sand bottom has the lowest portion of acoustic energy present in the bottom and is least affected by the presence of a radial sediment sound speed gradient. Silt is affected to a greater degree since its characteristic impedance is less than that of sand. Clay has the smallest impedance and is affected to the greatest degree.

In long range propagation problems it is likely that only the lower modes are of importance at long ranges from the source because of attenuation of the bottom interacting modes. In a situation such as this, the magnitude of radial sound speed gradient that may be handled within the adiabatic approximation can be seen to vary over an order of magnitude as the bottom type varies from clay to sand.

2.   Dependence on Local Bottom Slope

The next parameter isolated and examined is the local bottom slope. The waveguide geometry that was used for the calculation of the normal modes, coupling coefficients, and mode cycle distances is shown in Fig. III.8. In this figure there is a water layer of variable depth given by $H(r)$ overlying isovelocity sediment and substrate layers. The calculations to be presented were performed at a range where the water depth was 4500 m and the sediment depth 300 m. Again, the water sound speed profile is a typical mid-Pacific type profile.
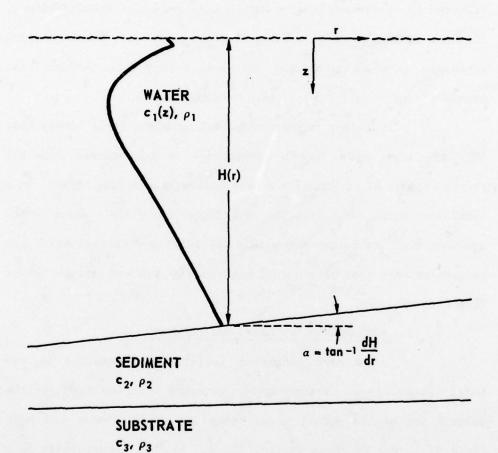
FIGURE III.8
WAVEGUIDE LAYER AND SOUND SPEED STRUCTURE
FOR EXAMINATION OF THE EFFECTS OF A SLOPING
WATER-SEDIMENT INTERFACE

Figure III.9 shows the relationship between mode number and local bottom slope, dH/dr, such that Eq. (3.31) is satisfied for $\varepsilon=0.1$, with the sediment being treated as a clay. For a given mode number m, values of dH/dr lying beneath the curve correspond to slopes that may be treated adiabatically while those lying above the curve correspond to slopes that may not be treated adiabatically. Based on the choice of $\varepsilon=0.1$, Fig. III.9 reveals that most of the modes propagate adiabatically for slopes up to about $0.5°$.

As was done in the previous case, the curve in Fig. III.9 was generated from Eq. (2.44), this time with k=0.

$$B_{mn} = \frac{1}{k_n^2 - k_m^2} \dot{H}(r)\sigma_{1mn} \tag{3.36}$$

From (3.36) and the expression for σ_{mn} given in (2.45), the values of H that satisfy the equality in (3.31) can be found once the mode functions and eigenvalues are known.

The curves in Figs. III.10 and III.11 are the same type as the one shown in Fig. III.9 except that the sediment layer is treated as silt and sand, respectively. Figures III.9, III.10, and III.11 are similar in that they are oscillatory over a large portion of the mode numbers present. The oscillatory behavior begins at the mode number corresponding to the first mode with a turning point in the sediment. The oscillatory regions of the

FIGURE III.9
CURVE REPRESENTING THE RELATIONSHIP BETWEEN MODE NUMBER AND MAXIMUM LOCAL BOTTOM SLOPE THAT MAY BE TOLERATED WITHIN THE ADIABATIC APPROXIMATION

FIGURE III.10

CURVE REPRESENTING THE RELATIONSHIP BETWEEN MODE NUMBER
AND MAXIMUM LOCAL BOTTOM SLOPE THAT MAY BE TOLERATED
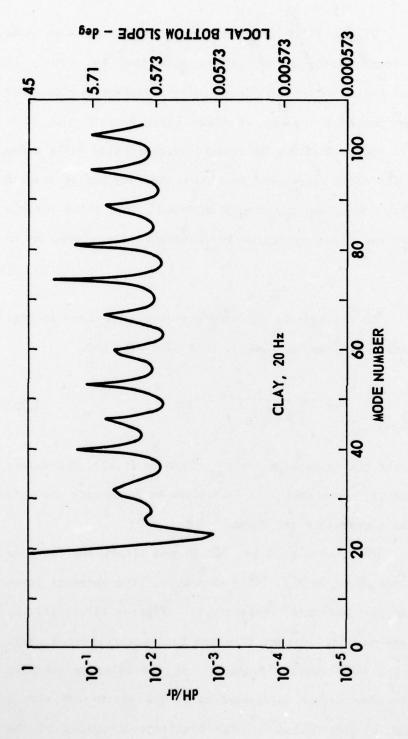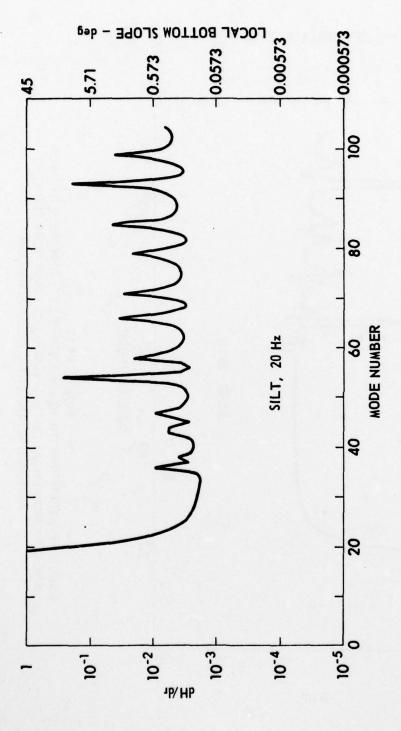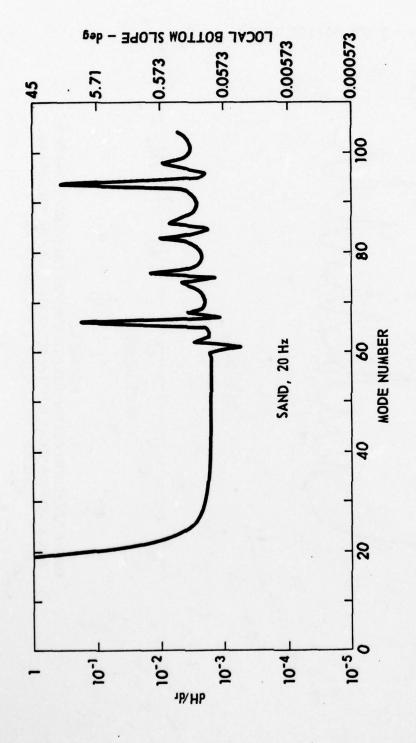WITHIN THE ADIABATIC APPROXIMATION

FIGURE III.11
CURVE REPRESENTING THE RELATIONSHIP BETWEEN MODE NUMBER
AND MAXIMUM LOCAL BOTTOM SLOPE THAT MAY BE TOLERATED
WITHIN THE ADIABATIC APPROXIMATION

84

curves for silt and sand are delayed in mode number relative to the clay case because of critical angle effects present in silt and sand that increase the mode number at which bottom penetration first occurs.

Figure III.12 is a superposition of Figs. III.9, III.10, and III.11. Note that the curves tend to lie in the order clay, silt, and sand, with clay being able to tolerate more slope angle than sand. This ordering follows the ordering of the characteristic acoustic impedances of the sediment, with clay having the smallest and sand the largest. This behavior is not inconsistent with the notion that an acoustically hard sloping bottom would give rise to more mode conversion than an acoustically softer, more penetrable bottom. The curves in Fig. III.12, for the choice $\varepsilon=0.1$, indicate that mode conversion effects begin to arise in sand for local bottom slopes between 0.057° and 0.57° whereas for clay, mode conversion effects begin at slope angles on the order of 0.5° to 1.0°. Hence, the mode conversion process due to a sloping bottom seems to be fairly sensitive to bottom type.

3. Summary

The dependence of the adiabatic approximation on the geoacoustic parameters of the bottom has been examined using a criterion developed by Milder which requires that the amount of mode coupling occurring over a mode cycle distance be small. It has been shown that the magnitude of local sound speed gradient that may
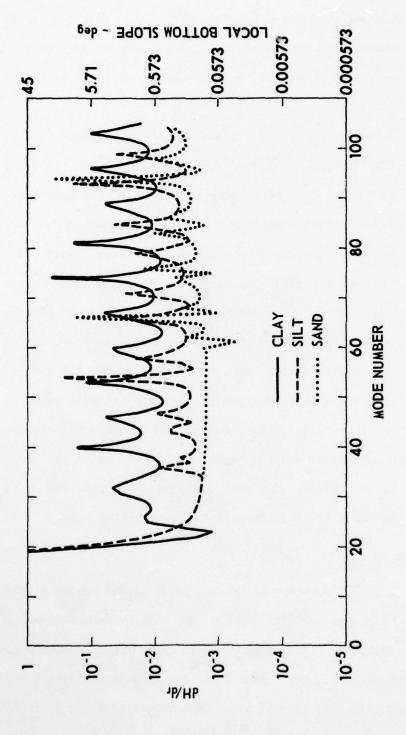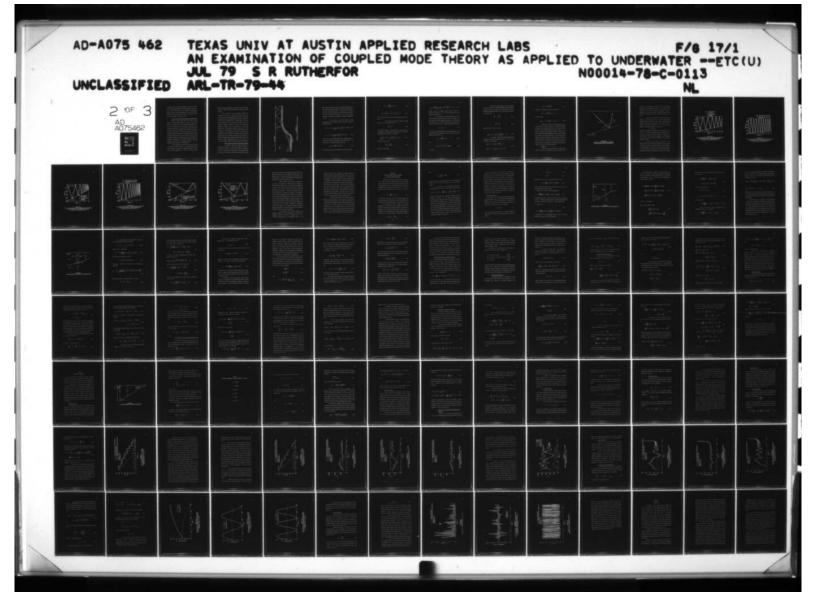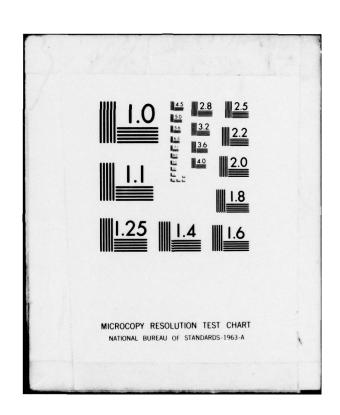
FIGURE III.12
SUPERPOSITION OF FIGURES III.9, III.10, AND III.11

MICROCOPY RESOLUTION TEST CHART

NATIONAL BUREAU OF STANDARDS-1963-A

be handled within the adiabatic approximation can vary over more than an order of magnitude as the sediment type varies from clay to sand. It has also been shown that the magnitude of local bottom slope can vary over an order of magnitude as the sediment changes from clay to sand; the acoustically softer clay bottom causes less mode conversion than the harder sand bottom.

C.   Multipath Information Within the Adiabatic Approximation

Recently, Tindle and Guthrie[3.22] published a paper exploring the relationship between ray theory and normal mode theory in horizontally stratified acoustic propagation geometries. Their basic conclusion was that raypaths correspond to the constructive interference of a group of normal modes centered about the mode of index that corresponds to the equivalent ray angle of the ray path in question. This conclusion allowed them to draw a connection between ray theory, with its physically intuitive notion of raypaths, and mode theory, which is exact but often not useful for gaining insight into the physical processes which influence the propagation of underwater sound. The idea of raypaths arising from constructive interference of neighboring modes has also been discussed by Tolstoy and Clay[3.17] and Weston.[3.23]
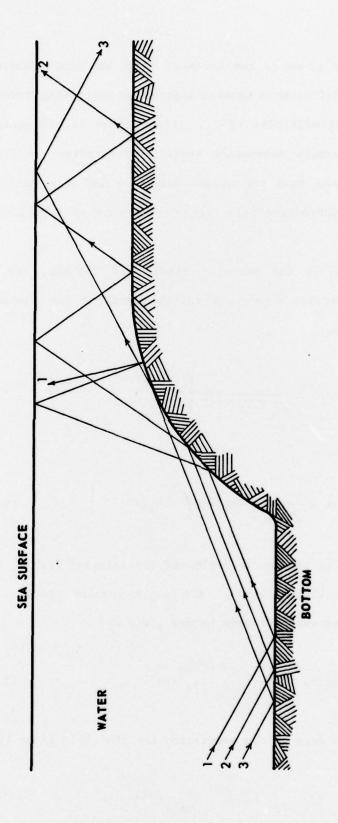
The work reported in this section concerns an extension of the work of Tindle and Guthrie to a range dependent medium. Their techniques are extended to an adiabatic wave theory description of sound propagation in an effort to determine whether

multipath conversion phenomena are contained within the adiabatic solution or whether they are attributable to mode-mode coupling processes.

What is meant by the term "multipath conversion" is illustrated in Fig. III.13. Figure III.13 shows how three rays initially having the same grazing angles with respect to horizontal are converted into three completely different types of raypaths by virtue of their interactions with a sloping bottom. With each bottom interaction a ray is converted into another ray that is steeper or shallower in angle by twice the local bottom slope depending on whether the ray is traveling up or down slope, respectively. The multipath conversion process has a great influence on sound propagation over range variable bottoms and it is important to know whether the process is contained within adiabatic mode theory or whether it was discarded with the coupling coefficients and the assumption of adiabacity of the medium. If multipath conversion is not contained within adiabatic mode theory, then the adiabatic approximation would be of little use in realistic propagation problems involving range variable boundaries.

1. Raypaths Within the Context of Adiabatic Mode Theory

In analogy to the work of Tindle and Guthrie in range invariant media, it is assumed that raypaths linking source and receiver correspond to groups of normal modes in the summation of Eq. (3.7) that interfere constructively. This assumption, which was shown to be correct in the horizontally stratified case, means

FIGURE III.13

SCHEMATIC ILLUSTRATION OF MULTIPATH CONVERSION

that a raypath is given by the locus of range and depth points at which the phase differences between a group of successive terms in (3.7) are integer multiples of 2 . Since there is, in general, more than one raypath connecting source and receiver locations, there will be more than one unique set of r and z points that correspond to constructive interference of groups of normal modes in (3.7).

As in the work of Tindle and Guthrie, the WKB approximations for the depth and radial functions are employed. These are given by

$$\phi_n(z;r) = \text{const} \times \frac{1}{\sqrt{\kappa_n(z;r)}} \exp\left\{\pm i \int_{z_o}^{z} \kappa_n(z';r)dz'\right\} \quad . \quad (3.37)$$

$$R_n(r) = \text{const} \times \frac{1}{\sqrt{k_n(r)r}} \exp\left\{i \int_{o}^{r} k_n(r')dr'\right\} \quad . \quad (3.38)$$

In Eq. (3.37) z_o is the source depth and the integral from z_o to z may proceed directly or through the upper turning point. The function κ_n is the vertical wave number given by

$$\kappa_n(z;r) = \sqrt{k^2(z,r) - k_n^2(r)} \quad . \quad (3.39)$$

The phase of each term in the expression for the field given by

$$\psi(r,z) = \sum_n R_n(r) \, \phi_n(z;r) \qquad (3.40)$$

is

$$\Gamma_n(z,r) = \pm \int_{z_0}^{z} \kappa_n(z';r)dz' + \int_0^r k_n(r')dr' \qquad . \qquad (3.41)$$

The ± sign in (3.41) accounts for up and downgoing paths from the source.

As stated earlier, a raypath is assumed to be given by the set of r and z points such that

$$\frac{\Delta \Gamma_n}{\Delta n} = 2\ell\pi \qquad , \qquad (3.42)$$

with ℓ being an integer. The quantity $\Delta \Gamma_n/\Delta n$ means change in Γ_n corresponding to a change of mode index of one unit. If $\Delta/\Delta n$ is approximated by $\partial/\partial n$, (3.41) in (3.42) gives

$$\pm \int_{z_0}^{z} \frac{\partial \kappa_n}{\partial n}(z';r)dz' + \int_0^r \frac{\partial k_n}{\partial n}(r')dr' = 2\ell\pi \qquad . \qquad (3.43)$$

From (3.39) it follows that

$$\frac{\partial \kappa_n}{\partial n} = - \frac{k_n}{\kappa_n} \frac{\partial k_n}{\partial n} \qquad ; \qquad (3.44)$$

hence, Eq. (3.43) becomes

$$\mp k_n(r) \frac{\partial k_n(r)}{\partial n} \int_{z_o}^{z} \frac{dz'}{\kappa_n(z';r)} + \int_o^r \frac{\partial k_n(r')}{\partial n} dr' = 2\ell\pi \qquad . \quad (3.45)$$

Equation (3.45) is an integral equation which is assumed to prescribe combinations of r and z points corresponding to rays emanating from the source.

To see whether the raypaths described by (3.45) exhibit multipath conversion effects, a test case is designed. The test case will consider propagation upslope in an isovelocity, wedge shaped ocean. The source is taken to be at the surface z=0 and the bottom is taken to have a linearly decreasing depth given by

$$H(r) = H_o(1 - \beta r) \qquad . \qquad (3.46)$$

In (3.46) β is a positive constant for upslope propagation. For a rigid sloping bottom and pressure release surface the normalized depth functions are given by

$$\phi_n(z;r) = \sqrt{\frac{2}{H(r)}} \sin \kappa_n z \qquad , \qquad (3.47)$$

with

$$\kappa_n(r) = \sqrt{k^2 - k_n^2(r)} = \frac{(n + 1/2)\pi}{H(r)} \qquad (3.48)$$

and $k = \omega/c$.

The test case chosen here has an obvious advantage in that the vertical and horizontal wavenumbers κ_n and k_n are known analytically and that conventional ray theory paths are easily generated for comparison with Eq. (3.45). From (3.47) and (3.48) it is easily seen that

$$\frac{\partial k_n}{\partial n} = -\frac{\kappa_n}{k_n}\frac{\partial \kappa_n}{\partial n} \quad . \tag{3.49}$$

$$\frac{\partial \kappa_n}{\partial n} = \frac{\pi}{H(r)} \quad . \tag{3.50}$$

Equations (3.48)-(3.50) in (3.45) give

$$\pm \frac{\pi}{H(r)} (z - z_0) - \int_0^r \frac{(n + 1/2)\pi^2}{k_n(r')H^2(r')} dr' = 2\ell\pi \quad . \tag{3.51}$$

The integral in (3.51) may be done analytically by changing the variable of integration from r' to H. With this procedure, Eq. (3.51) becomes

$$\pm \frac{\pi}{H(r)} (z - z_0) + \frac{\pi}{H_o\beta} \cos^{-1}\left(\frac{\kappa_n}{k}\right)\Bigg|_0^r = 2\ell\pi$$

$$\tag{3.52}$$

$$\pm \frac{\pi}{H(r)} (z - z_0) + \frac{\pi}{\beta H_o} [\sigma_n(r) - \sigma_n(0)] = 2\ell\pi \quad .$$

$$\sigma_n(r) = \cos^{-1}\left[\frac{\kappa_n(r)}{k}\right] \quad . \tag{3.53}$$

In terms of the equivalent ray angle $\theta_n(r)$ defined by

$$\theta_n(r) = \cos^{-1}\left[\frac{k_n(r)}{k}\right] = \sigma_n(r) - \pi/2 \quad ,$$

Eq. (3.52) becomes

$$\pm \frac{\pi}{H(r)}(z - z_o) + \frac{\pi}{H_o\beta}[\theta_n(r) - \theta_n(0)] = 2\ell\pi \quad . \tag{3.54}$$

Equation (3.54) gives the relationship between r and z that describes the paths of constructive interference emanating from the source at a grazing angle of $\theta_n(0)$. The integer ℓ denotes the number of bottom bounces incurred along the raypath. To see whether the adiabatic solution exhibits multipath conversion, the paths of constructive interference given by (3.54) will be compared to conventional ray theory paths for the same sloping bottom geometry. When a ray encounters a sloping bottom it is converted to a grazing angle that is steeper by twice the bottom slope α as shown in Fig. III.14. If Eq. (3.54) gives this same sort of behavior it will be possible to conclude that the adiabatic solution contains within it the effects of multipath conversion.

2. Results

In this section, the results of ray tracing via Eq. (3.54) will be shown. For simplicity the source is taken to be at
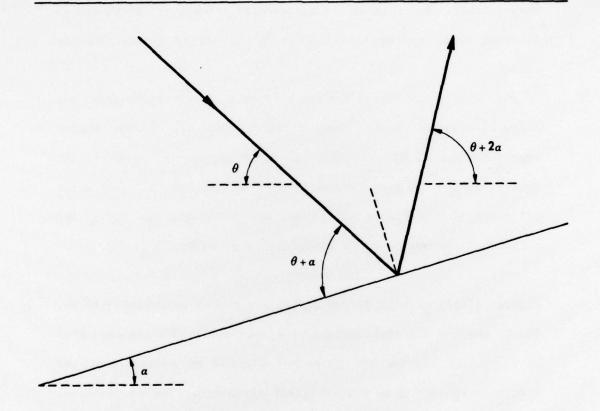
FIGURE III.14
SCHEMATIC VIEW OF RAY ANGLE STEEPENING
DUE TO REFLECTION FROM A SLOPING BOTTOM

the surface. In the examples to be presented, the isovelocity wedge was taken to be 0.5 km deep at the source, i.e., $H_o=0.5$ km. The frequency and sound speed were taken to be 20 Hz and 1.5 km/sec, respectively. For this set of geoacoustic parameters, there are 13 discreet modes having mode numbers 0 through 12 present at the source.

Ray traces for two different launch angles and three different bottom slopes are given. The two launch angles considered are $10.81°$ and $39.61°$. These angles correspond to the equivalent ray angles of modes 2 and 8 at the source. The three different bottom slopes considered are $0.5°$, $2°$, and $10°$. The tangent of the bottom slope angle (α) is given by

$$\tan \alpha = H_o \qquad .$$

Figures III.15 through III.20 depict ray traces performed with Eq. (3.54) for the six combinations of slopes and launch angles. Also shown on the figures are raypaths obtained by conventional ray tracing methods. Note the excellent agreement. The conventional ray traces were obtained from a two-dimensional ray trace program developed at ARL:UT.

In Figs. III.15 through III.20 there is good agreement between the conventional ray paths and those calculated using Eq. (3.54), even for a bottom slope of $10°$. This finding is a bit puzzling especially in light of the work presented in section B of this chapter where it was found that the adiabatic approximation can begin to be suspect for bottom slopes as small as $0.5°$. Figures
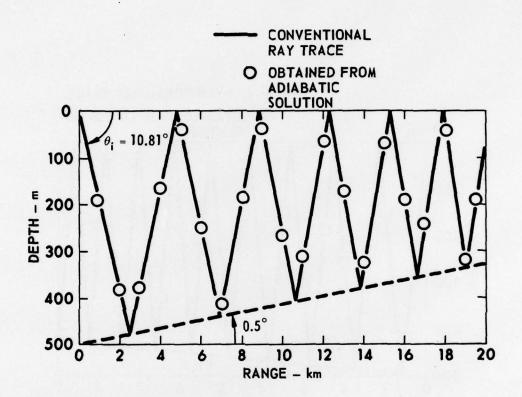
FIGURE III.15
RAY TRACE PERFORMED BOTH BY CONVENTIONAL METHODS AND
WITHIN THE CONTEXT OF ADIABATIC MODE THEORY
RAY ANGLE = 10.81°, SLOPE ANGLE = 0.5°

FIGURE III.16
RAY TRACE PERFORMED BOTH BY CONVENTIONAL METHODS AND
WITHIN THE CONTEXT OF ADIABATIC MODE THEORY
RAY ANGLE = 39.61°, SLOPE ANGLE = 0.5°
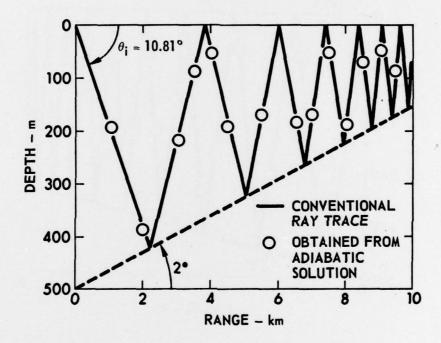
FIGURE III.17
RAY TRACE PERFORMED BOTH BY CONVENTIONAL METHODS AND
WITHIN THE CONTEXT OF ADIABATIC MODE THEORY
RAY ANGLE = 10.81°, SLOPE ANGLE = 2.0°
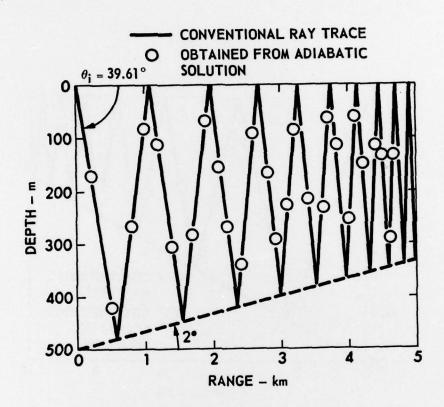
FIGURE III.18
RAY TRACE PERFORMED BOTH BY CONVENTIONAL METHODS AND
WITHIN THE CONTEXT OF ADIABATIC MODE THEORY
RAY ANGLE = 39.61°, SLOPE ANGLE = 2.0°
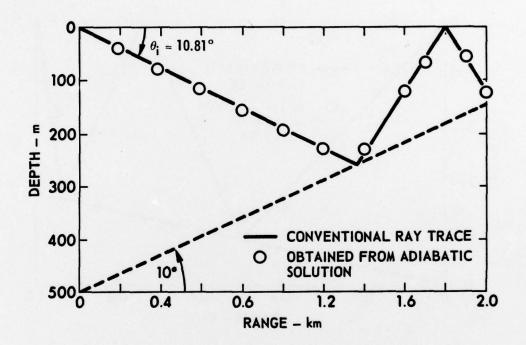
FIGURE III.19
RAY TRACE PERFORMED BY BOTH CONVENTIONAL METHODS AND
WITHIN THE CONTEXT OF ADIABATIC MODE THEORY
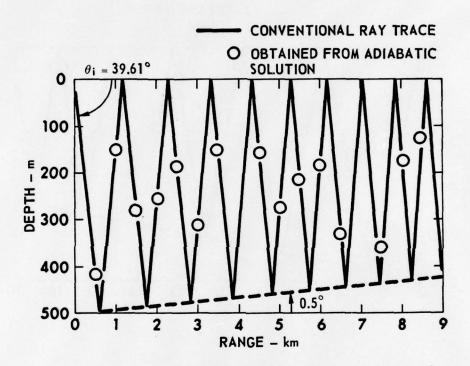RAY ANGLE = 10.81°, SLOPE ANGLE = 10°
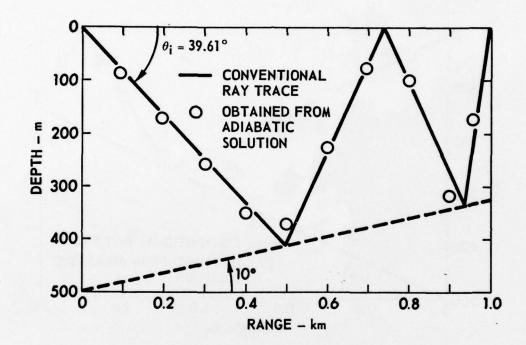
FIGURE III.20
RAY TRACE PERFORMED BOTH BY CONVENTIONAL METHODS AND
WITHIN THE CONTEXT OF ADIABATIC MODE THEORY
RAY ANGLE = 39.61°, SLOPE ANGLE = 10°

III.15-III.20 indicate that the adiabatic solution describes the geometric characteristics of the propagation quite well for slope angles up to 10°. This apparent paradox is due to the fact that the work presented in section B considers amplitude interchange between modes while the work just described does not.

Milder's criterion used in section B involves the B_{mn} which are proportional to radial rates of interchange of amplitude between modes m and n. This amplitude interchange does not occur in the adiabatic solution and hence the criteria for adiabacity given in section B are based on amplitude interchange between modes being small. The work just presented does not consider amplitudes. It examines the geometric or ray properties of the adiabatic approximation and has shown that the adiabatic solution gives the proper geometrical properties of the field even for quite large bottom slope angles. These findings lead one to conclude that the adiabatic solution describes the phase of the acoustic field quite well and that the coupling coefficients, which are neglected in the adiabatic approximation, predominately influence the magnitudes of the radial distribution of amplitude among the normal modes. This conclusion will be tested by numerical calculation and shown to be valid in Chapter V.

The conclusions just reached concerning the geometrical properties of sound propagation contained within the adiabatic solution were arrived at through the use of an isovelocity, wedge model for the propagation medium. It is

asserted now that these conclusions are general because the isovelocity wedge with a rigid bottom is about the most severe case one could apply the adiabatic approximation to. In section B of this chapter it was seen that the harder the bottom became in terms of characteristic acoustic impedance, the less the local bottom slope that could be tolerated in the adiabatic approximation. A rigid bottom is infinitely hard in terms of acoustic impedance; hence, the mode conversion effects in the test case considered are expected to be maximal with the adiabatic approximation being the most sensitive to bottom slope. The finding that the adiabatic approximation gives the geometric properties of the field in this case, even for quite large bottom slopes, leads one to conclude that it does so in less severe, more realistic waveguides also.

Another characteristic of the isovelocity wedge that makes it a severe test case is the fact that all of the mode depth functions have turning points at the surface and on the bottom. In a realistic oceanic waveguide the water sound speed profile often traps modes in the water column away from sloping bottom interfaces; hence, only a certain portion of the discrete modes present interact with the bottom and experience mode conversion effects. In the isovelocity wedge each and every mode present interacts with the bottom and experiences mode conversion effects.

CHAPTER IV

COUPLED MODE THEORY APPLIED TO PROBLEMS

WITH RANGE DEPENDENT BOUNDARIES

In Chapter II it was pointed out that the partial separation
of the radial and depth variables was not strictly possible
whenever range variable boundaries and/or interfaces were present
in the propagation medium. This nonseparability arises from the
requirement that the particle velocity normal to a surface of
discontinuity be continuous across that surface. For a field given
by

$$\psi(r,z) = \sum_n R_n(r) \, \phi_n(z;r) \quad , \tag{4.1}$$

the requirement that normal velocity be continuous entangles the
radial and depth functions with the net result being that there is
no advantage to be had by expressing the field in the form of (4.1).

As was pointed out earlier in Chapter II, a natural
approximation to be made when range dependent boundaries are
present is to approximate the normal derivative of the field at a
boundary with the z-derivative and require this quantity to be
continuous. For a waveguide having a range variable boundary as
shown in Fig. II.2, this approximation is mathematically stated by

$$\nabla_{\!\perp} \psi \Big|_{z=H(r)} \simeq \frac{\partial \psi}{\partial z} \Big|_{z=H(r)} \quad , \tag{4.2}$$

105

with

$$\nabla_{\perp} = \frac{1}{\sqrt{1+\dot{H}^2}} \left[\frac{\partial}{\partial z} - H \frac{\partial}{\partial r} \right] \quad . \tag{4.3}$$

Equation (4.2) involves an approximation to the normal derivative operator of Eq. (4.3) that is of zero order in the local bottom slope $\dot{H}$.

In the derivation of the mathematical formalism of coupled mode theory, the radial functions R_m were shown to satisfy

$$\ddot{R}_m + \frac{1}{r} \dot{R}_m + k_m^2(r) R_m = - \sum_n \left\{ A_{mn} R_n + B_{mn} \left(\frac{R_n}{r} + 2\dot{R}_n \right) \right\} \tag{4.4}$$

From Eqs. (2.44) and (2.51) it is apparent that B_{mn} is of order $\dot{H}$ and A_{mn} is of order $\dot{H}^2$. This fact makes the approximation of Eq. (4.2) suspect in that terms of order $\dot{H}$ and higher are dropped in (4.2) while they are retained in (4.4). In other words the approximation in Eq. (4.2), though necessary to obtain a workable theory, is not a consistent approximation. To make the theory consistent with (4.2) would require neglecting the right-hand side of (4.4). This leads to the adiabatic approximation discussed in Chapter III. Hence as things now stand, the only consistent application of coupled mode theory to problems involving range variable boundaries is within the adiabatic approximation.

Later in this chapter it is shown that if one ignores the inconsistency of Eq. (4.2) and uses the full framework of coupled mode theory, the result is a field which does not conserve energy. The nonconservation of energy is caused by the imposition of physically improper boundary conditions on the field. Therefore, to apply the notion of sound propagation via coupled normal modes to problems having range variable boundaries, a new theory must be constructed. The purpose of this chapter is to show that the application of conventional coupled mode theory to problems with range dependent boundaries results in nonconservation of energy and to develop a corrected coupled mode theory which can be applied when nonstratified boundaries are present.

A. Energy Considerations

In this section it will be shown that applying coupled mode theory with the approximation of Eq. (4.1) to waveguides having range dependent boundaries leads to a theory in which energy is not conserved. To illustrate this point, one first considers the time averaged radial energy flux, f_r, given by (see Ref. 4.1, Chapter V)

$$f_r = \frac{1}{2} \, \mathrm{Re}(pv_r^*) \quad , \tag{4.5}$$

where p is the acoustic pressure and v_r is the radial component of particle velocity. In terms of the velocity potential, ψ, p and v_r are given by

$$p = - \rho \frac{\partial \psi}{\partial t} = i\omega\rho\psi \quad . \tag{4.6}$$

$$v_r = \frac{\partial \psi}{\partial r} \quad . \tag{4.7}$$

Equations (4.1), (4.6), and (4.7) combine with (4.5) to give

$$f_r = \frac{1}{2} \text{Re} \left\{ i\omega\rho \sum_{n,m} R_n \phi_n \left[\dot{R}_m^\star \phi_m + R_m^\star \dot{\phi}_m \right] \right\} \quad . \tag{4.8}$$

In Eq. (4.8) the mode functions ϕ_n are real and the dot symbol denotes differentation with respect to range.

Equation (4.8) can be put in the following form.

$$f_r = \frac{i\omega\rho}{4} \left\{ \sum_{n,m} \left(R_n \dot{R}_n^\star - R_n^\star \dot{R}_m \right) \phi_n \phi_m + \left(R_n R_m^\star - R_n^\star R_m \right) \phi_n \dot{\phi}_m \right\} \quad . \tag{4.9}$$

To compute the time rate of change of energy in the radial direction J_r, Eq. (4.9) is integrated over the surface of a cylinder centered about the depth axis at range r=0. (See Fig. IV.1.) This procedure gives

$$J_r = \int_o^\infty 2\pi r \, f_r \, dz$$

$$\tag{4.10}$$

$$J_r = \frac{i\pi\omega r}{2} \left\{ \sum_n \left(R_n \dot{R}_n^\star - R_n^\star \dot{R}_n \right) + \sum_{n,m} \left(R_n R_m^\star - R_n^\star R_m \right) B_{nm} \right\} \quad .$$

In obtaining (4.10), the orthonormality property of Eq. (2.27) and the definition for B_{nm} in Eq. (2.30) were employed.
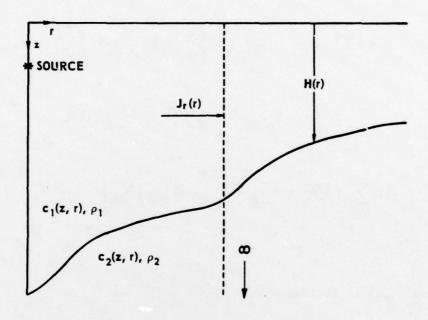
FIGURE IV.1
WAVEGUIDE GEOMETRY FOR DERIVATION OF RADIAL ENERGY FLUX

The time averaged rate of change of energy (power flow) given by (4.10) is a quantity that should be independent of range in the absence of attenuation. The range independence of J_r is equivalent to conservation of energy. If Eq. (4.10) is differentiated with respect to range, the result is

$$\dot{J}_r = \frac{i\pi\omega}{2} \left\{ \sum_n \left(R_n \dot{R}_n^* - R_n^* \dot{R}_n \right) + \sum_{n,m} \left(R_n R_m^* - R_n^* R_m \right) B_{nm} \right.$$

$$+ r \sum_n \left(R_n \ddot{R}_n^* - R_n^* \ddot{R}_n \right) + r \sum_{n,m} \left(R_n R_m^* - R_n^* R_m \right) \dot{B}_{nm} \qquad (4.11)$$

$$\left. + r \sum_{n,m} \left(\dot{R}_n R_m^* + R_n \dot{R}_m^* - \dot{R}_n^* R_m - R_n^* \dot{R}_m \right) B_{nm} \right\} \quad .$$

From (4.4) it follows that

$$\left(R_n \ddot{R}_n^* - R_n^* \ddot{R}_n \right) + \frac{1}{r} \left(R_n \dot{R}_n^* - R_n^* \dot{R}_n \right)$$

$$= - \sum_m \left\{ A_{nm} \left(R_n R_m^* - R_n^* R_m \right) \right. \qquad (4.12)$$

$$\left. + B_{nm} \left[\frac{\left(R_n R_m^* - R_n^* R_m \right)}{r} + 2 \left(R_n \dot{R}_m^* - R_n^* \dot{R}_m \right) \right] \right\} \quad .$$

Equation (4.12) can be used to replace the first and third terms of (4.11) yielding

$$\dot{J}_r = \frac{i\pi\omega}{2} \sum_{n,m} \left\{ r\left(\dot{B}_{nm} - A_{nm}\right)\left(R_n R_m^* - R_n^* R_m\right) \right.$$

$$\left. + r\, B_{nm}\left(\dot{R}_n R_m^* - \dot{R}_n^* R_m - R_n \dot{R}_m^* + R_n^* \dot{R}_m\right)\right\} \quad . \tag{4.13}$$

With the following definitions

$$Q_{nm} = R_n R_m^* - R_n^* R_m = -Q_{mn} \tag{4.14}$$

$$P_{nm} = \dot{R}_n R_m^* - \dot{R}_n^* R_m - R_n \dot{R}_m^* + R_n^* \dot{R}_m = P_{mn} \quad , \tag{4.15}$$

Eq. (4.13) becomes

$$\dot{J}_r = \frac{i\pi\omega}{2} \sum_{n,m} \left\{ r\left(\dot{B}_{nm} - A_{nm}\right) Q_{nm} + r\, B_{nm}\, P_{nm} \right\} \quad . \tag{4.16}$$

By Eqs. (4.14) and (4.15), Q_{nm} is antisymmetric and P_{nm} is symmetric; therefore, (4.16) becomes

$$\dot{J}_r = \frac{i\pi\omega}{2} \sum_{n,m} \left\{ r\left(\dot{B}_{nm} - A_{nm}\right)^A Q_{nm} + r\, B_{nm}^S\, P_{nm} \right\} \quad . \tag{4.17}$$

In (4.17) the superscript A and S mean "antisymmetric and symmetric parts of," respectively. For a waveguide having one range variable interface as in Fig. II.2, $(\dot{B}_{nm} - A_{nm})^A$ is obtained from Eq. (2.56) and B_{nm}^S is given by (2.47).

$$\left(\dot{B}_{nm} - A_{nm}\right)^A = \dot{H}\rho_1\left[\phi_{1n}\left(\dot{\phi}_{1m} - \dot{\phi}_{2m}\right) - \phi_{1m}\left(\dot{\phi}_{1n} - \dot{\phi}_{2n}\right)\right]_{z=H(r)} \quad (4.18)$$

$$B_{nm}^S = -\frac{\dot{H}\rho_1}{2}\phi_{1m}\phi_{1n}\left(1 - \rho 1/\rho 2\right)\bigg|_{z=H(r)} \quad (4.19)$$

Equations (4.17)-(4.19) indicate that only when $\dot{H}$ is identically zero, i.e., horizontal boundaries, is energy conserved. This discovery is a rather disconcerting one since a theory that fails to conserve energy is highly suspect.

At this juncture it is reasonable to ask what happens to the energy that is removed from the flow in the radial direction? The answer to this question is that the energy flux removed from the radial direction contributes to a nonzero net flux of energy normal to the range variable boundary or boundaries. To illustrate this point, consider Fig. IV.2. It will now be shown that the difference in radial energy flow through the surfaces of cylinders of radii r and r+dr is equal to the net flow of energy normal to the interface z=H(r) between r and r+dr.
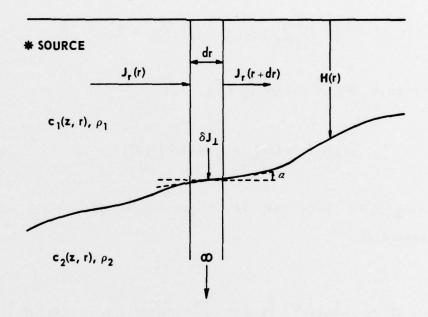
FIGURE IV.2
WAVEGUIDE GEOMETRY FOR ENERGY FLUX CONSIDERATIONS

For an infinitesimal dr, the difference in the rate of energy change between r and r+dr is given by

$$\delta J_r = J_r(r) - J_r(r + dr) = -\dot{J}_r(r) \, dr \qquad . \qquad (4.20)$$

With (4.17), Eq. (4.20) becomes

$$\delta J_r = - \frac{i\pi\omega r}{2} \, dr \left[\sum_{n,m} \left(\dot{B}_{nm} - A_{nm} \right)^A Q_{nm} + B_{nm}^S \, P_{nm} \right] \qquad . \qquad (4.21)$$

The normal flux of energy $f_\perp$ is given by

$$f_\perp = \frac{1}{2} \, \text{Re}[Pv_\perp^*] = \frac{1}{2} \, \text{Re}[i\omega\rho\psi\nabla_\perp\psi^*] \qquad , \qquad (4.22)$$

with $v_\perp = \nabla_\perp \psi$. With Eqs. (4.1) and (4.3), Eq. (4.22) may be expressed as

$$f_\perp = - \frac{\omega\rho}{2} \, \text{Im} \, \frac{1}{\sqrt{1+\dot{H}^2}} \left\{ \sum_{n,m} \left[R_n^* R_m \phi_m \, \frac{\partial\phi_n}{\partial z} - \dot{H}\left(\dot{R}_n^* R_m \phi_n \phi_m + R_n^* R_m \phi_m \dot{\phi}_n \right) \right] \right\} \qquad .$$

$$(4.23)$$

The net flux normal to the interface defined $\bot$, z=H(r) is

$$\delta f_\perp = f_\perp^{(1)} - f_\perp^{(2)} \Big|_{z=H(r)} \qquad (4.24)$$

where the superscript indicates the layer in which the normal flux is to be evaluated. Using Eq. (4.24) and the boundary conditions on ϕ_n in Eq. (4.24), one may obtain

$$\delta f_\perp = \frac{-i\omega\dot{H}}{4\sqrt{1-\dot{H}^2}} \sum_{n,m} \left\{ \rho_1 \phi_{1n} \phi_{1m} \left(1 - \rho_1/\rho_2\right) \left(\dot{R}^*_n R_m - \dot{R}_n R^*_m\right) \right.$$

$$\left. + \left(R^*_n R_m - R_n R^*_m\right) \rho_1 \phi_{1m} \left(\dot{\phi}_{1n} - \dot{\phi}_{2n}\right) \right\}\Bigg|_{z=H(r)} \qquad . \qquad (4.25)$$

Since $\dot{\phi}_{1n}\dot{\phi}_{1m}$ is symmetric, $\dot{R}^*_n R_m - \dot{R}_n R^*_m$ may be replaced with its symmetric part given by

$$\left(\dot{R}^*_n R_m - \dot{R}_n R^*_m\right)^S = \frac{\dot{R}^*_n R_m - \dot{R}_n R^*_m + \dot{R}^*_m R_n - \dot{R}_m R^*_n}{2} = -\frac{P_{nm}}{2} \qquad . \qquad (4.26)$$

With Eqs. (4.26) and (4.14), Eq. (4.25) becomes

$$\delta f_\perp = \frac{-i\omega\dot{H}}{4\sqrt{1-\dot{H}^2}} \sum_{n,m} \left\{ -\rho_1 \phi_{1n} \phi_{1m} \left(1 - \rho_1/\rho_2\right) \frac{P_{nm}}{2} \right.$$

$$\left. - Q_{nm}\rho_1 \phi_{1m} \left(\dot{\phi}_{1n} - \dot{\phi}_{2n}\right) \right\}\Bigg|_{z=H(r)} \qquad . \qquad (4.27)$$

Since Q_{nm} is antisymmetric, Eqs. (4.18) and (4.19) combine with (4.27) to yield

$$\delta f_\perp = \frac{-i\omega}{4\sqrt{1-\dot{H}^2}} \sum_{n,m} B^S_{nm} P_{nm} + Q_{nm}\left(\dot{B}_{nm} - A_{nm}\right)^A \qquad . \qquad (4.28)$$

The time rate of change of energy normal to $z=H(r)$ between r and $r + dr$ is obtained from (4.28)

$$\delta J_\perp = \delta f_\perp \, \delta S \quad . \tag{4.29}$$

In (4.29) δS is the surface area normal to $z=H(r)$ between r and $r+dr$ and is given by

$$\delta S = \frac{2\pi r \, dr}{\cos \alpha} = 2\pi r \, dr \, \sqrt{1+\dot{H}^2} \quad . \tag{4.30}$$

The angle α in (4.30) is the local slope angle of the surface $z=H(r)$ at range r, i.e., $\dot{H}=\tan\alpha$. From (4.28)-(4.30) $\delta J_\perp$ becomes

$$\delta J_\perp = - \frac{i\omega\pi r \, dr}{2} \sum_{n,m} B_{nm}^S \, P_{nm} + \left(\dot{B}_{nm} - A_{nm}\right)^A \quad . \tag{4.31}$$

A comparison of Eqs. (4.21) and (4.31) shows that they are the same; hence, the change in radial energy flow occurring over an increment dr is due to the net flow of energy normal to the sloping interface in the same increment.

The nonzero net flow of energy normal to range variable boundaries is a consequence of the approximate boundary conditions imposed on the field. The mathematical formalism of coupled mode theory determines a field satisfying precisely the boundary

conditions it was requested to (continuity of pressure and z-component of particle velocity). Should such a medium exist that required continuity of pressure and z-component of particle velocity, conventional coupled mode theory would produce the correct field and radial energy flow would not be range independent. However, when this field is used to approximate a field which is supposed to satisfy the physically proper boundary conditions (continuity of pressure and normal particle velocity) the the nonconservation of energy byproduct is unacceptable.

The ultimate importance of the nonconservation of energy effect in realistic applications of coupled mode theory depends on its importance compared to any attenuation effects expected to be present in the problem. An estimate of the relative importance of energy and attenuation effects can be made as follows. Equations (4.10) and (4.17) may be expressed as

$$J_r = \sum_n J_r^{(n)} \tag{4.32}$$

$$\dot{J}_r = \sum_n \dot{J}_r^{(n)} \tag{4.33}$$

with

$$J_r^{(n)} = \frac{i\pi\omega r}{2} \left[-\frac{P_{nn}}{2} + \sum_m B_{nm} Q_{nm} \right] \quad , \tag{4.34}$$

$$\dot{J}_r^{(n)} = \frac{i\pi\omega r}{2} \sum_m B_{nm}^S P_{nm} + \left(\dot{B}_{nm} - A_{nm}\right)^A Q_{nm} \quad . \tag{4.35}$$

In Eqs. (4.34) and (4.35) P_{nm} and Q_{nm} are given by (4.14) and (4.15). The $J_r^{(n)}$ may be thought of as the time rate of change of energy in the radial direction associated with mode number n.

The ratio of Eq. (4.35) to (4.34) to first order in the bottom slope, $\dot{H}$, is given by

$$\beta_n = \frac{\dot{J}_r^{(n)}}{J_r^{(n)}} = \sum_m - 2 \frac{B_{nm}^S P_{nm}}{P_{nn}} + O(\dot{H}^2) \quad . \tag{4.36}$$

The quantity β_n may be thought of as an effective power attenuation coefficient describing the reduction in radial energy flow due to the nonconservation of energy effects. From Eq. (4.36) it follows that

$$J_r^{(n)}(r) = J_r^{(n)}(r_o) \exp\left\{\int_{r_o}^{r} \beta_n(r')dr'\right\} \tag{4.37}$$

with $J_r^{(n)}(r_o)$ being the time rate of energy flow associated with mode n at some reference range r_o.

The attenuation of the power associated with mode n may be estimated from the results of Chapter II. From Eqs. (2.69) and (2.70), the imaginary part of the eigenvalue resulting from attenuation in the medium is seen to be

$$\text{Im}[k_n(r)] = \frac{i\delta_n(r)}{2k_n(r)} \quad . \tag{4.38}$$

The attenuation to the radial functions R_n caused by the imaginary part of k_n can be approximately included by replacing R_n with

$$R_n \exp\left\{-\int_{r_o}^{r} \frac{\delta_n(r')}{2k_n(r')} dr'\right\} \quad . \tag{4.39}$$

Since the power associated with mode n is quadratically related to the amplitude R_n, the power attenuation due to absorption in the medium is expressed approximately by

$$\exp\left\{-\int_{r_o}^{r} \frac{\delta_n(r')dr'}{k_n(r')}\right\} \quad . \tag{4.40}$$

A comparison of Eqs. (4.40) and (4.37) indicates that one can expect the nonconservation of energy effect to be negligible compared to normally occurring attenuation when

$$\int_{r_o}^{r} \beta_n(r')dr' \ll \int_{r_o}^{r} - \frac{\delta_n(r')dr'}{k_n(r')} \quad . \tag{4.41}$$

Since Eq. (4.36) is good to $O(\dot{H})$ only, one is entitled to use the adiabatic radial solutions in the evaluation of β_n. Therefore a determination as to the importance of nonconservation of energy effects based on Eq. (4.41) may be made using adiabatic mode theory quantitites which are relatively easy to obtain.

The nonconservation of energy phenomenon has not arisen before in the relatively few applications of coupled mode theory to acoustic propagation problems because most of the applications have involved horizontally stratified boundaries and the rest failed to examine or consider energy conservation. In Refs. 4.2-4.4, the coupled mode theory formalism was applied to underwater acoustic propagation problems involving range dependent sound speed with either no boundaries or horizontally stratified boundaries. In Refs. 4.5-4.7, the existence of nonhorizontal boundaries was allowed for, but energy conservation questions were not considered.

B.   First Order Correction to Coupled Mode Theory

In this section a correction to the original coupled mode theory of Pierce and Milder is proposed and derived. It will be shown that, with rather modest change, coupled mode theory may be applied to problems with range variable boundaries with the field so obtained satisfying the proper boundary conditions and conserving energy, both to first order in the boundary slopes $\dot{H}$.

To derive the appropriate corrections to coupled mode theory, Eq. (4.1) is replaced with

$$\psi(r,z) = \sum_n [R_n(r) + \delta R_n(r)][\phi_n(z;r) + \delta\phi_n(z;r)] \quad . \quad (4.42)$$

In (4.42) the δR_n and $\delta\phi_n$ are correction terms of first order in are included so that ψ can be made to satisfy the physically correct boundary conditions to first order. The ϕ_n and R_n of Eq. (4.42)

are the same as those described in Chapter II. The δR_n is taken to be solely a function r with δR_n and all its range derivatives being of order $\dot{H}$. The $\delta\phi_n$ is the corrective term added to ϕ_n. Like $\phi_n(z;r)$, $\delta\phi_n(z;r)$ is predominately a function of z and is weakly dependent on range.

At this point it is convenient to list various quantities that will arise as to their order in powers of $\dot{H}$.

$$\left.\begin{array}{ll} k_m,\ \phi_m,\ \phi_m',\ \phi_m'',\ R_m,\ \dot{R}_m,\ \ddot{R}_m & = 0(0) \\[2mm] B_{mn},\ \dot{k}_m,\ \dot{\phi}_m,\ \delta\phi_m,\ \delta\phi_m',\ \delta\phi_m'',\ \delta R_m,\ \delta\dot{R}_m,\ \delta\ddot{R}_m & = 0(\dot{H}) \\[2mm] A_{mn},\ \ddot{k}_m,\ \ddot{\phi}_m,\ \delta\dot{\phi}_m & = 0(\dot{H}^2) \end{array}\right\} \quad (4.43)$$

In (4.43) the dot and prime symbols stand for differentiation with respect to r and z, respectively. The corrections to coupled mode theory being proposed in this section are of first order. Therefore any terms of order $\dot{H}^2$ and higher and combinations of terms from (4.43) that are order $\dot{H}^2$ and higher are not carried along.

1. Boundary Conditions on $\delta\phi_n$

The boundary conditions to be satisfied by the $\delta\phi_n$ may be obtained by considering the boundary conditions on ψ. The requirement that pressure be continuous everywhere means

that $\rho\psi$ must be continuous at boundaries and interfaces. The ϕ_n are defined in Chapter II such that $\rho\phi_n$ is a continuous function of depth. Therefore, from (4.42), if $\rho\psi$ is to be a continuous function of depth, $\rho\delta\phi_n$ must be required to be continuous. In addition, since the field must vanish at 0 and ∞, $\delta\phi_n$ must vanish at 0 and ∞ also.

The particle velocity normal to an interface or boundary is also required to be continuous. From Eq. (4.3), the particle velocity normal to an interface defined by $z=H(r)$ is to order $\dot{H}$.

$$\nabla_{\perp}\psi = \frac{\partial\psi}{\partial z} - \dot{H}\frac{\partial}{\partial r}\psi + O(H^2) \tag{4.44}$$

Using Eq. (4.42) in (4.44) one obtains to first order

$$\sum_n \left[\left(R_n + \delta R_n \right) \phi_n' + R_n \delta\phi_n' - \ddot{H}\dot{R}_n\phi_n \right] + O(\dot{H}^2) \quad , \tag{4.45}$$

where (4.43) has been employed. Equation (4.45) is to be continuous at surfaces of discontinuity. Since ϕ_n is defined such that ϕ_n' is continuous everywhere,

$$R_n\delta\phi_n' - \ddot{H}\dot{R}_n\phi_n \tag{4.46}$$

must be required to be continuous. For a nonhorizontal boundary defined by $z=H(r)$ separating two fluids of densities ρ_1 and ρ_2 (see

Fig. II.2) the discontinuity in $\delta\phi_n'$ at $z=H(r)$ obtained from (4.46) is

$$\left[\delta\phi_{1n}' - \delta\phi_{2n}'\right]_{z=H(r)} = \frac{\dot{R}_n}{R_n}\,\dot{H}\phi_{1n}\,(1-\rho_1/\rho_2)\Bigg|_{z=H(r)} \qquad . \qquad (4.47)$$

In (4.47) the subscript preceding the mode index denotes the layer in which the corresponding function is to be evaluated.

2. The Differential Equation for δR_n

An equation for the δR_n may be obtained by using Eq. (4.42) in the differential equation satisfied by ψ.

$$\nabla^2\psi + k^2(r,z)\,\psi = 0 \qquad . \qquad (4.48)$$

Equation (4.42) in (4.48) yields to first order

$$\sum_n\left[\delta\ddot{R}_n + \frac{\delta\dot{R}_n}{r} + k_n^2\delta R_n\right]\phi_n$$

$$(4.49)$$

$$= -\sum_n\left\{\left(\ddot{R}_n + \frac{\dot{R}_n}{r}\right)\delta\phi_n + R_n\left[\delta\phi_n'' + k^2\delta\phi_n\right]\right\} \qquad .$$

In deriving Eq. (4.49) the fact that $\sum R_n\phi_n$ satisfies (4.48) and the equation for ϕ_n, (2.24), was used. If (4.49) is multiplied by $\rho\phi_m$

and integrated over depth and if the orthonormality property of Eq. (2.27) is employed, (4.49) becomes

$$\delta\ddot{R}_m + \frac{\delta\dot{R}_m}{r} + k_m^2\delta R_m = -\sum_n \left\{ \left(\ddot{R}_n + \frac{\dot{R}_n}{r}\right) I_{mn} + R_n \int_0^\infty \rho\phi_m\delta\phi_n'' \, dz \right.$$

$$\left. + R_n \int_0^\infty \rho k^2(z,r)\phi_m\delta\phi_n dz \right\} \tag{4.50}$$

with

$$I_{mn} = \int_0^\infty \rho\phi_m\delta\phi_n dz \quad . \tag{4.51}$$

The second term on the right-hand side of (4.50) may be integrated twice by parts with respect to z. If one recognizes that the integral from 0 to ∞ has the meaning given in Eq. (2.34), the following expression is obtained.

$$\int_0^\infty \rho\phi_m\delta\phi_n'' dz = \left[\rho_1\phi_{1m}\delta\phi_{1n}' - \rho_2\phi_{2m}\delta\phi_{2n}'\right]_{H(r)}$$

$$- \left[\rho_1\phi_{1m}'\delta\phi_{1n} - \rho_2\phi_{2m}'\delta\phi_{2n}\right]_{H(r)} \tag{4.52}$$

$$+ \int_0^\infty \rho\left(k_m^2 - k^2\right)\phi_m\delta\phi_n dz$$

In obtaining (4.52) the fact that ϕ_n and $\delta\phi_n$ vanish at zero and infinity was used. The fact that $\rho\phi_n$ and ϕ_n' are continuous may be used in (4.52) to yield

$$\int_0^\infty \rho\phi_m \delta\phi_n'' dz = \rho_1\phi_{1m}\left[\delta\phi_{1n}' - \delta\phi_{2n}'\right]_{z=H(r)} + \int_0^\infty \rho\delta\phi_n\phi_m'' dz \quad . \quad (4.53)$$

Equation (4.47) in (4.53) gives

$$\int_0^\infty \rho\phi_m \delta\phi_n'' dz = \frac{\dot{R}_n}{R_n}\dot{H}\rho_1\phi_{1m}\phi_{1n}\left(1 - \rho_1/\rho_2\right)\Bigg|_{z=H(r)}$$

$$(4.54)$$

$$+ \int_0^\infty \rho\left(k_m^2 - k^2\right)\phi_m\delta\phi_n dz \quad .$$

Equation (4.54) can be combined with (4.50) to yield

$$\delta\ddot{R}_m + \frac{\delta\dot{R}_m}{r} + k_m^2\delta R_m = -\sum_n\left\{\left(\ddot{R}_n + \frac{\dot{R}_n}{r}\right)I_{mn} + k_m^2 I_{mn}R_n\right.$$

$$(4.55)$$

$$\left. + \dot{R}_n\dot{H}\rho_1\phi_{1m}\phi_{1n}\left(1 - \rho_1/\rho_2\right)_{z=H(r)}\right\} \quad .$$

From Eq. (4.4) it follows that

$$\ddot{R}_m + \frac{\dot{R}_m}{r} = -k_m^2 R_m + O(\dot{H}) \quad .$$

Therefore, since I_{mn} is first order in H, Eq. (4.55) becomes

$$\delta\ddot{R}_m + \frac{\delta\dot{R}_m}{r} + k_m{}^2\delta R_m = -\sum_n \left\{ \left(k_m{}^2 - k_n{}^2 \right) R_m I_{mn} - 2B^S_{mn}\dot{R}_n \right\} \tag{4.56}$$

where

$$B^S_{mn} = \frac{-\dot{H}}{2}\rho_1\phi_{1m}\phi_{1n}\left(1 - \rho_1/\rho_2\right) \tag{4.57}$$

from Eq. (2.47) has been used.

Equation (4.56), though derived with a particular waveguide structure in mind (e.g., Fig. II.2), is completely general in form. If one desired to include more than one non-horizontal interface, Eq. (4.53) would have discontinuity terms at each interface as would (4.57), the net result being that (4.56) would remain identical in form. The derivations presented here are based on one sloping interface defined by z=H(r) solely to illustrate the first order correction technique without unduly complicating the already involved analysis. Before further simplification of Eq. (4.56) can be carried out, the differential equation for $\delta\phi_n$ must be obtained so that I_{mn} may be evaluated.

3. The Equation for $\delta\phi_n$

To obtain an equation for $\delta\phi_n$, one assumes that the combination $\Phi_n = \phi_n + \delta\phi_n$ satisfies an equation very similar to the one satisfied by ϕ_n, e.g.,

$$\left[\frac{\partial^2}{\partial z^2} + k^2(r,z) - \sigma_n{}^2(r) \right]\Phi_n = 0 \tag{4.58}$$

In (4.58) σ_n is an altered eigenvalue which will be shown to differ from k_n by terms of order $\dot{H}$. Since ϕ_n' is continuous everywhere, Φ_n' will satisfy the same boundary conditions as $\delta\phi_n$, i.e.,

$$\Phi'_{1n} - \Phi'_{2n} = \frac{\dot{R}_n \dot{H}}{R_n} \phi_{1n}\left(1 - \rho_1/\rho_2\right)\Bigg|_{z=H(r)}$$

$$\rho_1 \Phi_{1n} = \rho_2 \Phi_{2n}\Big|_{z=H(r)} \quad .$$

(4.59)

The assumption of the form of (4.58) is based on the requirement that Φ_n approach ϕ_n as $\dot{H}$ goes to zero. This must be true because the conventional coupled mode theory is valid for $\dot{H}=0$. From Eq. (4.59) it is apparent that the boundary conditions on Φ_n become the same as those on ϕ_n as $\dot{H}$ goes to zero. With Eqs. (4.58) and (4.59) one is assured that the corrected theory reduces to conventional coupled mode theory in the limit of horizontal boundaries.

The equation satisfied by $\delta\phi_n$ is obtained by substituting the equation for ϕ_n, which is

$$\left[\frac{\partial^2}{\partial z^2} + k^2(r,z) - k_n^2(r)\right]\phi_n(z;r) = 0 \quad , \quad (4.60)$$

into (4.58). This procedure yields

$$\left(\frac{\partial^2}{\partial z^2} + k^2 - \sigma_n^2\right)\delta\phi_n = \left(\sigma_n^2 - k_n^2\right)\phi_n \quad . \quad (4.61)$$

It is now possible to derive an expression for I_{mn}. From (4.60) and (4.61) the following expression may be obtained.

$$\phi_m \delta\phi''_n - \delta\phi_n\phi''_m = \left(\sigma_n^2 - k_m^2\right)\phi_m\delta\phi_n + \left(\sigma_n^2 - k_n^2\right)\phi_n\phi_m \qquad (4.62)$$

If (4.62) is multiplied by ρ and integrated, the following is obtained.

$$\left[\rho_1\phi_{1m}\delta\phi'_{1n} - \rho_2\phi_{2m}\delta\phi'_{2n}\right]_{H(r)} - \left[\rho_1\delta\phi_{1n}\phi'_{1m} - \rho_2\delta\phi_{2n}\phi'_{2m}\right]_{H(r)}$$

$$= \left(\sigma_n^2 - k_m^2\right)\left(I_{mn} + \delta_{n,m}\right) \qquad (4.63)$$

If the boundary conditions satisfied by ϕ_n and $\delta\phi_n$ are used, Eq. (4.63) becomes

$$\rho_1\phi_{1m}\left[\delta\phi'_{1n} - \delta\phi'_{2n}\right]_{H(r)} = \left(\sigma_n^2 - k_m^2\right)\left[I_{mn} + \delta_{n,m}\right] \qquad . \qquad (4.64)$$

Equations (4.47) and (4.57) combine with (4.64) to yield

$$\left[I_{mn} + \delta_{n,m}\right]\left(\sigma_n^2 - k_m^2\right) = -\frac{2\dot{R}_n}{R_n}\ B_{mn}^S \qquad . \qquad (4.65)$$

Two important pieces of information may be obtained from Eq. (4.65). For m=n, (4.65) gives

$$\sigma_n^2 - k_n^2 = - \frac{2\dot{R}_n}{R_n} B_{nn} \frac{1}{(1+I_{nn})} \qquad (4.66)$$

$$\sigma_n^2 - k_n^2 = - \frac{2\dot{R}_n}{R_n} B_{nn} + O(\dot{H}^2) \quad .$$

The second of Eqs. (4.66) is obtained because B_{nn} and I_{nn} are order $\dot{H}$. Equations (4.66) state that the difference between the eigenvalue k_n and the corrected eigenvalue σ_n is first order in $\dot{H}$, verifying that σ_n approaches k_n as $\dot{H}$ goes to zero. For $m{\neq}n$ (4.65) gives

$$\left(\sigma_n^2 - k_m^2\right) I_{mn} = - \frac{2\dot{R}_n}{R_n} B_{mn}^S \quad . \qquad (4.67)$$

Since the difference between σ_n^2 and k_n^2 is first order as is I_{mn}, Eq. (4.67) becomes

$$\left(k_n^2 - k_m^2\right) I_{mn} = - \frac{2\dot{R}_n}{R_n} B_{mn}^S + O(\dot{H}^2) \qquad (4.68)$$

for $m{\neq}n$.

4. Final Expressions for the First Order Correct Field

Now that the equations for δR_m, $\delta\phi_m$, and I_{mn} are known, the component parts of the theory may be assembled in a form that is computationally convenient. Equation (4.42) is best expressed in the form

$$\psi(r,z) = \sum_n \chi_n(r) \left[\phi_n(z;r) + \delta\phi_n(z;r)\right] \quad , \qquad (4.69)$$

with

$$X_n(r) = R_n(r) + \delta R_n(r) \quad . \tag{4.70}$$

The equation for X_n is obtained by adding the equations for R_n and δR_n given in (4.56) and (4.4). This gives

$$\ddot{X}_m + \frac{\dot{X}_m}{r} + k_m{}^2 X_m = -\sum_n \left\{ B_{mn}\left(\frac{R_n}{r} + 2\dot{R}_n\right) + \left(k_m{}^2 - k_n{}^2\right) I_{mn} R_n \right.$$

$$\left. - 2B_{mn}^S \dot{R}_n \right\} \quad . \tag{4.71}$$

With Eq. (4.68), (4.71) becomes

$$\ddot{X}_m + \frac{\dot{X}_m}{r} + k_m{}^2 X_m = -\sum_n \left\{ B_{mn}\left(\frac{R_n}{r} + 2\dot{R}_n\right) + 2B_{mn}^S \dot{R}_n (1-\delta_{m,n}) \right.$$

$$\left. - 2B_{mn}^S \dot{R}_n \right\} \quad . \tag{4.72}$$

In Eq. (4.72), if a term, R_n/r, which is negligible compared to $2R_n$ for r greater than a few wavelengths, is added to the second and third terms in (4.72), an equation comparable in form to (4.4) is obtained. Hence, Eq. (4.72) becomes

$$\ddot{X}_m + \frac{\dot{X}_m}{r} + k_m{}^2 X_m = -\sum_{n \neq m} B_{mn}\left(\frac{R_n}{r} + 2\dot{R}_n\right) \quad . \tag{4.73}$$

In deriving (4.73) the second order terms in (4.4) involving A_{mn} were neglected. Since $R_n = X_n - \delta R_n$ differs from X_n by terms of order $\dot{H}$, one is entitled to write (4.73) as

$$\ddot{X}_m + \frac{\dot{X}_m}{r} + k_m^2 X_m = - \sum_{n \neq m} B_{mn} \left(\frac{X_n}{r} + 2\dot{X}_n \right) \quad . \tag{4.74}$$

Equation (4.74) differs from (4.4) in first order by the exclusion of the m=n term from the summation. When $\dot{H}=0$, Eq. (4.57) shows that B_{nn} is identically zero; hence, the equation for X_n in the limit becomes the same as the one for R_n as required.

The equation for $\delta\phi_n$ given by (4.61) along with (4.66) becomes

$$\left[\frac{\partial^2}{\partial z^2} + k^2 - \sigma_n^2 \right] \delta\phi_n = - \frac{2\dot{R}_n}{R_n} B_{nn}\phi_n \quad . \tag{4.75}$$

As stated before, the desired solution to Eq. (4.75) is the one which vanishes as $\dot{H}$ goes to zero. The homogeneous solution to (4.75) is not the proper one because it approaches ϕ_n as $\dot{H}$ goes to zero. The particular solution of (4.75) is the proper solution that vanishes in the limit since the right-hand side of (4.75) vanishes for $\dot{H}=0$. Equation (4.75) is not particularly useful for computing $\delta\phi_n$ since it involves the solution of an inhomogeneous eigenvalue problem. An approximation to (4.75) involves replacing σ_n^2 with k_n^2. One can make this replacement because $\delta\phi_n$ is first order as is the difference between $\sigma_n^2 - k_n^2$. With this substitution (4.75) becomes

$$\left[\frac{\partial^2}{\partial z^2} + k^2 - k_n^2\right]\delta\phi_n = -\frac{2\dot{R}_n}{R_n}B_{nn}\phi_n \qquad . \qquad (4.76)$$

Equation (4.76) is much easier to solve than (4.75) because it does not involve computing eigenvalues, σ_n^2. Once the ϕ_n and k_n are known, a straightforward integration of (4.76) produces the $\delta\phi_n$. The σ_n^2 are not required to compute the corrected field; hence, a savings in computational effort is to be gained by using (4.76) over (4.75).

To show that $\delta\phi_n$ computed from (4.76) still satisfies (4.47), the following equation formed from (4.76) and (4.60) is considered.

$$\frac{\partial}{\partial z}\left[\phi_m\delta\phi_n' - \delta\phi_n\phi_m'\right] = -\frac{2\dot{R}_n}{R_n}B_{nn}\phi_n\phi_m + \left(k_n^2 - k_m^2\right)\phi_m\delta\phi_n \qquad .(4.77)$$

If (4.77) is multiplied by the density and integrated over depth, (4.77) becomes

$$\rho_1\phi_{1m}\left[\delta\phi_{1n}' - \delta\phi_{2n}'\right]_{z=H(r)} = -\frac{2\dot{R}_n}{R_n}B_{nn}\delta_{n,m} + \left(k_n^2 - k_m^2\right)I_{mn} \quad .(4.78)$$

For m=n, (4.78) gives

$$\left[\delta\phi_{1n}' - \delta\phi_{2n}'\right]_{z=H(r)} = -\frac{2\dot{R}_n}{R_n}\frac{B_{nn}}{\rho_1\phi_{1m}}\bigg|_{z=H(r)} \qquad . \qquad (4.79)$$

With Eq. (4.57), (4.79) is seen to be the same as (4.47).

To summarize, a correction to coupled mode theory that is of first order in the slopes of nonhorizontal boundaries present in the waveguide has been derived. The corrected field is given by Eq. (4.69). The X_n, ϕ_n, and $\delta\phi_n$ satisfy Eqs. (4.74), (4.60), and (4.75), respectively. In the limit of H=0, X_n reduces to R_n and $\delta\phi_n$ goes to zero such that the conventional coupled mode theory formalism is regained.

The main difference between the conventional theory and the corrected theory just derived is the additional quantity $\delta\phi_n$ that must be computed. The correction to the radial function δR_n has been incorporated into the equation for X_n and need not be computed independently. Depending on the type of application, the added computational difficulty imposed by the $\delta\phi_n$ may be negligible compared to the other calculations that must be performed, e.g., solving Eq. (4.74). The $\delta\phi_n$ are not needed until the field is to be constructed from the X_n, ϕ_n, and $\delta\phi_n$. This is not true of the ϕ_n which must be known as a function of range so that the coupling coefficients may be determined. Therefore, in applications of the theory in which one is interested in the field as a function of depth at one particular range, only the $\delta\phi_n$ corresponding to that range need be calculated with a minimal increase in computational effort. If the field as a function of depth and range is desired, then the computation of the $\delta\phi_n$ becomes

more costly in terms of effort, depending on the range grid on which the field is to be computed.

5. Conservation of Energy to First Order

In this final subsection of Chapter IV it will be shown that the field computed including the correction terms just derived conserves energy to first order. In other words, it will be shown that the time rate of change of energy in the radial direction computed from (4.69) is a constant to first order in the boundary slope $\dot{H}$. The calculations presented here are similar to those given in section A of this chapter and are abbreviated somewhat.

In the following developments it is useful to remove the $1/\sqrt{r}$ range dependence from the radial functions. The field therefore is taken in the form

$$\psi = \sum_n \frac{G_n(r)}{\sqrt{r}} \; (\phi_n + \delta\phi_n) \quad . \tag{4.80}$$

The function G_n is related to X_n through

$$G_n(r) = \sqrt{r} \; X_n(r) \quad . \tag{4.81}$$

The equation for G_n is taken from Eq. (4.71) ,

$$\ddot{G}_n + \left(k_n^{\,2} + \frac{1}{4r^2}\right) G_n = \sum_m - 2B_{nm}^A \; \dot{F}_m - \left(k_n^{\,2} - k_m^{\,2}\right) I_{nm} \; F_m \quad , \tag{4.82}$$

where $F_m = \sqrt{r} \, R_m$ and

$$B_{nm}^A = \frac{B_{nm} - B_{mn}}{2} = B_{nm} - B_{nm}^S \quad . \qquad (4.83)$$

The time averaged radial energy flux, f_r, may be obtained by substituting the field given by (4.80) into Eqs. (4.5) – (4.7).

$$f_r = -\frac{\omega\rho}{2r} \, Im \left\{ \sum_{m,n} \left(G_n \dot{G}_m^* - \frac{G_m G_n}{2r} \right) \left(\phi_m + \delta\phi_m^* \right) \left(\phi_n + \delta\phi_n \right) \right.$$

$$\left. + G_m^* G_n \left(\phi_n + \delta\phi_n \right) \left(\dot{\phi}_m + \delta\dot{\phi}_m^* \right) \right\} \qquad (4.84)$$

If terms higher than first order are dropped, Eq. (4.84) becomes

$$f_r = -\frac{\omega\rho}{2r} \, Im \left\{ \sum_{m,n} \left(G_n \dot{G}_m^* - \frac{G_m^* G_n}{2r} \right) \left(\phi_m \phi_n + \phi_m \delta\phi_n + \phi_n \delta\phi_m^* \right) \right.$$

$$\left. + G_m^* G_n \phi_n \dot{\phi}_m \right\} \qquad (4.85)$$

As before, the time rate of change of energy in the radial direction J_r is obtained by integrating (4.85) over a cylindrical surface of radius r.

$$J_r = -\omega\pi \operatorname{Im}\left\{\sum_{m,n}\left(G_n\dot{G}_m^* - \frac{G_m^*G_n}{2r}\right)\left(\delta_{n,m} + I_{nm}^* + I_{mn}\right)\right.$$

$$\left. + G_m^*G_n B_{nm}\right\} \qquad . \tag{4.86}$$

In the following developments certain zero order approximations for G_n and R_n are employed. To zero order in $\dot{H}$, the equations for R_n and G_n are given by the left-hand sides of Eqs. (4.4) and (4.82).

$$\ddot{R}_n + \frac{\dot{R}_n}{r} + k_n^2 R_n = 0 + O(\dot{H}) \tag{4.87}$$

$$\ddot{G}_n + \left(k_n^2 + \frac{1}{4r^2}\right)G_n = 0 + O(\dot{H}) \tag{4.88}$$

The solutions of Eqs. (4.87) and (4.88) for certain purposes will be taken to be the WKB solutions (see Refs. 4.8-4.10) given by

$$R_n(r) = \frac{1}{\sqrt{k_n r}}\exp\left\{i\int^r k_n(r')dr'\right\} + O(\dot{H}) \qquad . \tag{4.89}$$

$$G_n(r) = \frac{1}{\sqrt{k_n}} \exp\left\{ i \int^r k_n(r')dr' \right\} + O(\dot{H}) \qquad . \tag{4.90}$$

Equations (4.89) and (4.90) are useful for replacing radial derivatives of R_n and G_n with the following expressions

$$\dot{R}_n = \left(ik_n - \frac{1}{2r} \right) R_n \simeq ik_n R_n \text{ in farfield} \qquad . \tag{4.91}$$

$$\dot{G}_n = ik_n G_n \qquad . \tag{4.92}$$

Equation (4.68) along with (4.91) reveals that $I_{mn} + I_{mn}^*$ is pure imaginary given by

$$I_{mn} + I_{nm}^* = - \frac{2i \ B_{mn}^S}{k_n - k_m} \qquad . \tag{4.93}$$

With the knowledge that $I_{mn} + I_{nm}^*$ is pure imaginary, Eq. (4.86) can be written as

$$J_r = \frac{i\pi\omega}{2} \left\{ \sum_n \left(G_n \dot{G}_n^* - G_n^* \dot{G}_n \right) + \sum_{n,m} \left(G_n \dot{G}_m^* + G_n^* \dot{G}_m \right) \left(I_{mn} + I_{nm}^* \right) \right.$$

$$\left. + \sum_{n,m} \left(G_n G_m^* - G_n^* G_m \right) B_{nm} \right\} \qquad . \tag{4.94}$$

In (4.94) the terms $G_m^* \dot{G}_n / 2r$ were neglected in comparison to $G_n \dot{G}_m^*$. Since the second and third terms of Eq. (4.94) have multiplying

factors of order $\dot{H}$, the zero order approximation for $\dot{G}_n$ of (4.92) may be used.

$$J_r = \frac{i\pi\omega}{2}\left\{\sum_n \left(G_n\dot{G}_n^* - G_n^*\dot{G}_n\right) + \sum_{m,n}\left(G_nG_m^* - G_n^*G_m\right)B_{nm}\right.$$

$$\left. - ik_m\left(I_{nm}^* + I_{mn}\right)\right\} \tag{4.95}$$

To show that Eq. (4.95) is constant in range to first order, Eq. (4.95) is differentiated with respect to range to get

$$J_r = \frac{i\pi\omega}{2}\left\{\sum_n \frac{d}{dr}\left(G_n\dot{G}_n^* - G_n^*\dot{G}_n\right)\right.$$

$$\left. + \sum_{n,m} i\left(k_n - k_m\right)\left(G_nG_m^* + G_n^*G_m\right)\left[B_{nm} - ik_m\left(I_{mn} + I_{nm}^*\right)\right]\right\} . \tag{4.96}$$

In obtaining (4.96), Eq. (4.92) was employed and terms of order $\dot{H}$ were not differentiated since they give rise to second order quantities. If Eq. (4.82) is multiplied by G_n^* and subtracted from its complex conjugate, the first term in (4.96) is seen to be

$$\frac{d}{dr}\left(G_n\dot{G}_n^* - G_n^*\dot{G}_n\right) = -\sum_m 2B_{nm}^A\left(\dot{F}_m^*G_n - \dot{F}_mG_n^*\right)$$

$$- \sum_m \left(k_m^2 - k_n^2\right)\left(F_m^*G_n + F_mG_n^*\right)I_{nm} . \tag{4.97}$$

The zero order equation for F_m is the same as the one for G_m (see Eqs. (2.31) and (4.88)); therefore, since each term in (4.97) has a first order multiplicative factor, F_m may be replaced with G_m.

$$\frac{d}{dr}\left(G_n \dot{G}^*_n - G^*_n \dot{G}_n\right) = -\sum_m 2B^A_{nm}\left(\dot{G}^*_m G_n - \dot{G}_m G^*_n\right)$$

$$\qquad\qquad -\sum_m \left(k_m^{\,2} - k_n^{\,2}\right)\left(G^*_m G_n + G_m G^*_n\right) I_{nm} \quad .$$

$$(4.98)$$

Equation (4.98) in (4.96) employing (4.92) gives

$$\dot{J}_r = \frac{i\pi\omega}{2}\left\{\sum_{n,m}\left(G_n G^*_m + G^*_n G_m\right)\left[i\left(k_n - k_m\right)B_{nm} + 2ik_m B^A_{nm}\right.\right.$$

$$\left.\left. + k_m\left(k_n - k_m\right)\left(I^*_{nm} + I_{mn}\right) - \left(k_m^{\,2} - k_n^{\,2}\right)I_{nm}\right]\right\} \quad .$$

$$(4.99)$$

Since $G_n G^*_m + G^*_n G_m$ is symmetric with respect to interchange of m and n, the first two terms in (4.99) become

$$\sum_{n,m}\left(G_n G^*_m + G^*_n G_m\right) i\left(k_n - k_m\right) B_{nm} + 2ik_m B^A_{nm}$$

$$= \sum_{n,m}\left(G_n G^*_m + G^*_n G_m\right) i\left(k_n + k_m\right) B^A_{nm} = 0 \quad .$$

Hence, (4.99) becomes

$$\dot{J}_r = \frac{i\pi\omega}{2} \left\{ \sum_{n,m} \left(G_n G^*_m + G^*_n G_m \right) \left[k_m \left(k_n - k_m \right) \left(I^*_{nm} + I_{mn} \right) \right. \right.$$

$$\left. \left. - \left(k_m^2 - k_n^2 \right) I_{nm} \right] \right\} \quad . \tag{4.100}$$

With Eqs. (4.68), (4.93), and (4.91), Eq. (4.100) becomes

$$\dot{J}_r = \frac{i\pi\omega}{2} \left\{ \sum_{n,m} \left(G_n G^*_m + G^*_n G_m \right) \left[\frac{k_m (k_n - k_m)}{k_n - k_m} - k_m \right] \left(-2i \, B^S_{mn} \right) \right\} = 0 \tag{4.101}$$

Therefore

$$\dot{J}_r = 0 + O(\dot{H}^2) \quad . \tag{4.102}$$

Equation (4.102) is the desired result showing that the time rate of change of energy in the radial direction has been made constant to first order by inclusion of the corrections to the theory derived in this chapter.   In the next chapter numerical calculations are presented comparing conventional coupled mode theory and the corrected theory.   These calculations will be seen to verify the mathematical analysis presented in this chapter.

CHAPTER V

NUMERICAL CALCULATIONS

In this chapter some coupled mode theory numerical calculations are presented. The purpose for making these calculations is to illustrate how coupled mode theory is implemented and to verify the assertions and corrections proposed in Chapter IV.

The material in this chapter will be presented in the following format. In section A the waveguide model assumed for the calculations is described. In section B the numerical procedures that are employed to calculate the field are discussed. This discussion includes the numerical technique used to solve the second order, coupled radial equations, initial conditions, convergence criteria, and computer run-time statistics. In section C the numerical calculations are presented. Numerical calculations of power, radial functions, depth functions, and the acoustic field are presented.

A.   Model Description

The waveguide geometry assumed for the calculations to be presented in this chapter is shown in Fig. V.1. Figure V.1 is an isovelocity, wedge shaped model of an oceanic waveguide. The sound speed in the water is taken to be isovelocity and the density constant in depth and range. For the calculations to be presented here the sound speed and density were taken to be 1.5 km/sec and 10^3

141
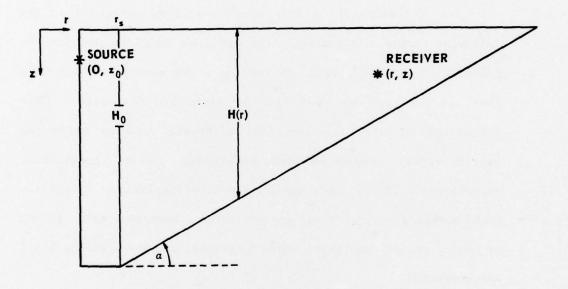
FIGURE V.1
WAVEGUIDE GEOMETRY FOR WEDGE SHAPED OCEAN

kg/m^3, respectively. The source is assumed to be harmonic in time with a frequency of 20 Hz and located at a depth of $z_o=0.2$ km.

The surface of the waveguide is taken to be pressure release and the bottom is assumed to be rigid. The depth of the waveguide is range dependent and is given by

$$H(r) = \begin{cases} H_o & 0 \leq r \leq r_s \\ \\ H_o - \tan\alpha\,(r-r_s) & r > r_s \quad , \end{cases} \tag{5.1}$$

with $r_s=1.0$ km.

The water depth in the source region is taken to be $H_o=0.5$ km. The flat portion of the bottom in the source region is included so that the initial conditions on the field in the range variable region $(r>r_s)$ might be obtained from the analytically known field in the source region $(r \leq r_s)$. In Table II the appropriate geoacoustic parameters are collected in one place.

In the following sections of this chapter the field ψ given by

$$\psi = \sum_n \frac{G_n(r)}{\sqrt{r}} \, [\phi_n(z;r) + \delta\phi_n(z;r)] \tag{5.2}$$

is calculated. For the waveguide of Fig. V.1 the ϕ_n functions are known analytically. The depth functions satisfy

$$\left[\frac{\partial^2}{\partial z^2} + k^2 - k_n^2\right]\phi_n(z;r) = 0 \quad . \tag{5.3}$$

TABLE II

GEOACOUSTIC PARAMETERS OF WAVEGUIDE DEPICTED IN FIGURE V.1

$$\rho = 10^3 \text{ kg/m}^3$$

$$c = 1.5 \text{ km/sec}$$

$$H_o = 0.5 \text{ km}$$

$$z_o = 0.2 \text{ km}$$

$$f = 20 \text{ Hz}$$

$$r_s = 1.0 \text{ km}$$

For a constant $k = \omega/c$, the depth functions are given by

$$\phi_n = a_n \sin \kappa_n z + b_n \cos \kappa_n z \quad , \tag{5.4}$$

$$\kappa_n = \sqrt{k^2 - k_n^2} \quad . \tag{5.5}$$

For a pressure release surface and rigid bottom, b_n in (5.4) must be set to zero. The rigid bottom requires that $\dfrac{\partial \phi_n}{\partial z}$ vanish at the bottom; hence,

$$\phi_n(z;r) = a_n \sin\left[\frac{(n+1/2)\pi z}{H(r)}\right]$$

with

$$\kappa_n(r) = \frac{(n+1/2)\pi}{H(r)} \quad , \tag{5.6}$$

and

$$k_n^2(r) = k^2 - \frac{(n+1/2)^2 \pi^2}{H^2(r)} \quad . \tag{5.7}$$

Since there are no surfaces of discontinuity between the surface and bottom of the waveguide, the depth functions may be normalized such that

$$\int_0^{H(r)} \phi_n \phi_n dz = 1 \quad . \tag{5.8}$$

Hence, the orthonormal ϕ_n are given by

$$\phi_n(z;r) = \sqrt{\frac{2}{H(r)}} \sin\left[\frac{(n+1/2)\pi z}{H(r)}\right] \quad . \tag{5.9}$$

With the field given by (5.2) an assignment of units among the radial and depth functions must be made. It is convenient to take the normalization integral of Eq. (5.8) as unitless. With this convention, the units of the ϕ_n and $\delta\phi_n$ are inverse square root of length or $1/\sqrt{L}$. The units of the velocity potential, ψ, are length square over time or L^2/T; hence, with the unit assigned to ϕ_n and $\delta\phi_n$, $G_n(r)$ must have units of length cubed over time or L^3/T. This unit's convention is followed throughout this chapter.

The calculations described in the next section require a knowledge of the coupling coefficients B_{mn}. Since the ϕ_n are known analytically in the case considered here, the coupling coefficients may also be determined analytically using the techniques of Chapter II. They are seen to be

$$B_{mn}(r) = 2 \frac{(n+1/2)^2 \dot{H}}{H(r)} \left\{\frac{(-1)^{m+n}}{(m+n+1)(m-n)}\right\} \quad . \tag{5.10}$$

The antisymmetric and symmetric parts of B_{mn} are, respectively,

$$B_{mn}^{A} = \frac{B_{mn} - B_{nm}}{2} = (-1)^{m+n} \frac{\dot{H}}{H} \left[\frac{(n+1/2)^2 + (m+1/2)^2}{(m+n+1)(m-n)} \right] \quad , \quad (5.11)$$

and

$$B_{mn}^{S} = \frac{B_{mn} + B_{nm}}{2} = (-1)^{m+n+1} \frac{\dot{H}}{H} \quad . \quad (5.12)$$

In Eqs. (5.10)-(5.12) the density is missing because of the slightly altered orthonormality condition of Eq. (5.8).

B.   Numerical Procedures

In this section the numerical procedures that are used to compute the acoustic field in the waveguide of Fig. V.1 using coupled mode theory are discussed. Since the ϕ_n and B_{mn} are known analytically in this case, two steps in the numerical computations are bypassed. With the field given by (5.2) two quantities remain to be calculated, the G_n and $\delta\phi_n$. It turns out that an analytic solution for $\delta\phi_n$ is possible in the present case; therefore, discussion of the computation of $\delta\phi_n$ is postponed until section C. As indicated in previous chapters, the real challenge in coupled mode theory concerns the solution of the coupled radial equations. This section focuses on that aspect of the computational problem.

The equation for the radial functions G_n is obtained from Eq. (4.74) using $X_m(r) = G_m(r)/\sqrt{r}$. Equation (4.74) is the radial

equation corrected for the presence of nonhorizontal boundaries and is given by

$$\ddot{G}_m + \left(k_m^2(r) + \frac{1}{4r^2} \right) G_m = - \sum_{n=m} 2B_{mn} \dot{G}_n \quad . \qquad (5.13)$$

The numerical procedure applied to the solution of (5.13) is the iterative procedure discussed in Chapter II, section C.2, in which (5.13) is replaced by the following equations to be solved iteratively.

$$\ddot{G}_m^{(0)} + \left[k_m^2(r) + \frac{1}{4r^2} \right] G_m^{(0)} = 0 \quad , \qquad (5.14)$$

$$\ddot{G}_m^{(i)} + \left[k_m^2(r) + \frac{1}{4r^2} \right] G_m^{(i)} = - \sum_{n \neq m} 2B_{mn} \left[\dot{G}_n^{(i-1)}(1-s) + s\dot{G}_n^{(i-2)} \right] \quad .$$

The zeroth iterate, $G_m^{(0)}$, is simply the adiabatic solution. Equations (5.14) differ from (2.57) and (2.58) in the omission of the A_{mn} term which one is not entitled to include in first order calculations, and in the inclusion of a convergence acceleration parameter, s, which is discussed later.

1. Numerical Solution of Second Order Differential Equations

At each step in the iteration described by Eq. (5.14) a set of nonhomogeneous second order differential equations

must be solved. The numerical scheme for solving these differential equations is Numerov's method.[5.1-5.4] Numerov's method is a multistep, 3-point computational scheme applicable to second order differential equations of the form

$$F'' = UF + G \quad . \tag{5.15}$$

Numerov's method is a fast efficient method for solving second order differential equations like Eq. (5.15).

An equation of the form (5.15) is solved numerically in Numerov's method by the following algorithm.

$$F_{i+1} = \left\{ \left[2 + \frac{10h^2}{12} U_i \right] F_i - \left[1 - \frac{h^2}{12} U_{i-1} \right] F_{i-1} \right. \tag{5.16}$$
$$\left. + \frac{h^2}{12} \left[G_{i-1} + 10 \, G_i + G_{i+1} \right] \right\} \bigg/ \left[1 - \frac{h^2}{12} U_{i+1} \right] \quad .$$

In Eq. (5.16) the subscripts refer to the range mesh point at which the appropriate quantity is evaluated, and h is the range mesh increment. To get Numerov's method started, one must supply the initial two values of the function F (F_o and F_1). With F_o and F_1 given, the solution can be marched out using Eq. (5.16). In the

calculations presented later, the initial values of the radial functions were obtained from the analytically known radial functions for the region $r < r_s$ of Fig. V.1.

The global[5.1] or propagation error of Numerov's method is proportional to h^4. The global error is an indication of how much difference one can expect between the true solution of (5.15) and the solution generated by (5.16) at each mesh point. The local error of Numerov's method is proportional to h^6. Reference 5.5 gives a detailed description of what is meant by global and local error.

2. Initial Conditions

As stated in the previous subsection, initial values for the radial equations are required to start the Numerov integration scheme. The initial values of the G_m functions of (5.14) are obtained by requiring the field calculated using coupled mode theory in the region $r \geq r_s$ match the field for the range invariant medium at the point $r = r_s$ (see Fig. V.1).

In the source region, the acoustic field satisfies

$$\nabla^2 \psi + k^2 \psi = -4\pi q_o \, \delta(\vec{r} - \vec{r}_o) \qquad . \qquad (5.17)$$

In Eq. (5.17) the quantity q_o is the source strength in units of volume per unit time. For the calculations to be presented later, the source was taken to have unit source strength with $q_o = 1 \text{ m}^3/\text{sec}$.

The solution to (5.17) in the horizontally stratified source region is given by Eq. (2.21) which is

$$\psi(r,z) = i\pi\rho(z_0) \sum_n H_o^{(1)}(k_n r) \phi_n(z) \phi_n(z_0) \quad . \tag{5.18}$$

In (5.18) the k_n and ϕ_n are the eigenvalues and mode functions for the stratified region $r \leq r_s$ and are independent of range in that region.

The initial values for G_m used to start the Numerov integration scheme are obtained by matching Eq. (5.18) to Eq. (5.2) at r_s. If r_s is the ℓth mesh point in the range grid, then $G_n(r_{\ell-1})$ and $G_n(r_\ell)$ are taken from Eqs. (5.18) and (5.2).

$$G_n(r_j) = i\pi\rho(z_0) \phi_n(z_0) \sqrt{r_j} H_o^{(1)}(k_n r_j)$$

$$\tag{5.19}$$

$$j = \ell - 1, \ell$$

The $\delta\phi_n$ do not enter (5.19) since $\delta\phi_n$ is zero at $r_{\ell-1}$ and r_ℓ because the medium is stratified at these two mesh points. The two initial values given by (5.19) are all that is needed to start the numerical Numerov integration method.

In taking the initial conditions for G_n from (5.18) it is implicit that backscattered energy is being ignored as discussed in Chapter II. A consequence of this assumption is that the field so obtained has only outgoing energy flow. This is the

case because the initial conditions combined with the numerical method allow no mechanism for the generation of a backscattered component of the field.

3. Convergence Criteria

For the iterative process of Eq. (5.14), some method for deciding when the process has converged is required. There are two types of criteria that are appropriate. If G_m is less than one, the iteration is said to have converged if

$$\left| G_m^{(i+1)} - G_m^{(i)} \right| < \epsilon_1 \quad , \tag{5.20}$$

for all ranges. The factor ϵ_1 is the absolute convergence criterion. If G_m is greater than one, the iteration is said to have converged if

$$\left| \frac{G_m^{(i+1)} - G_m^{(i)}}{G_m^{(i)}} \right| < \epsilon_2 \tag{5.21}$$

for all ranges. The ϵ_2 is the relative convergence criterion. Equations (5.20) and (5.21) may be combined into a single criterion given by

$$\left| G_m^{(i+1)} - G_m^{(i)} \right| < \left[\left| G_m^{(i)} \right| \epsilon_2 + \epsilon_1 \right] \quad . \tag{5.22}$$

In the calculations to be presented, Eq. (5.22) was applied to the real and imaginary parts of the radial functions and was required to be satisfied at all range points considered. Both ε_1 and ε_2 were taken to be 10^{-4}. With these values for ε_1 and ε_2 the iteration procedure is required to converge to four significant figures.

For the waveguide parameters given in Table II, there are 13 propagating modes present at the source with mode numbers 0 through 12, and 13 radial functions to be calculated. For a bottom slope of $5°$ a range mesh of 1100 points was used. In this calculation the iterative process converged to four significant figures after 11 iterations. The computer time required for convergence on the Applied Research Laboratories Cyber 171 computer system was about 367 seconds or roughly 6.1 minutes.

In Eq. (5.14) a convergence acceleration parameter, s, was included in the iterative scheme. In the work presented here, no convergence problems were encountered and s was taken to be zero in accordance with Eqs. (2.57) and (2.58). In some circumstances, a nonconverging iterative procedure can be made to converge or a converging procedure accelerated by choosing s not equal to zero (see Refs. 5.3 and 5.4). The principle is similar to the method of successive over-relaxation (SOR) used in the solution of systems of linear equations.

C.   Numerical Results

In this section numerical results obtained by the corrected coupled mode theory presented in Chapter IV are given. The main purpose in presenting these calculations is to illustrate the assertions made in Chapter IV and to compare coupled mode theory with the adiabatic approximation. Concerning the assertions made in Chapter IV, it will be shown here that the original coupled mode theory does not conserve energy when applied to problems having range variable boundaries. It will also be shown that the corrections proposed in Chapter IV alleviate this nonconservation of energy problem to first order in the bottom slope.

1.   Power Calculations

In this subsection some power flow calculations made with the original and the corrected coupled mode theories are compared. The total power flow for the calculations presented here is taken in the following form

$$J_r = \sum_n J_r^{(n)} \quad ,$$

where $J_r^{(n)}$ is the power transported by the nth mode in the radial direction. In the formalism of conventional coupled mode theory, $J_r^{(n)}$ is given by Eq. (4.10), which is reproduced below in slightly altered form.

$$J_r^{(n)} = \frac{i\pi\omega}{2} \left\{ \left(F_n \dot{F}_n^* - F_n^* \dot{F}_n \right) + \sum_m \left(F_n F_m^* - F_n^* F_m \right) B_{nm} \right\} \qquad (5.23)$$

In obtaining (5.23) from (4.10) $F_n = \sqrt{r}\, R_n$ was used. The equation satisfied by F_m is

$$\ddot{F}_m + \left(k_m^2 + \frac{1}{4r^2}\right)F_m = -\sum_n 2\dot{F}_n B_{mn} \quad . \tag{5.24}$$

In the correction to coupled mode theory proposed in Chapter IV the individual mode power amplitudes are obtained from Eqs. (4.93) and (4.94) and are given by

$$J_r^{(n)} = \frac{i\pi\omega}{2}\left\{\left(G_n\dot{G}_n^* - G_n^*\dot{G}_n\right) + \sum_{m\neq n}\left(G_n\dot{G}_m^* + G_n^*\dot{G}_m\right)\left(\frac{-2iB_{mn}^S}{k_n-k_m}\right)\right.$$

$$\left. + \sum_m \left(G_nG_m^* - G_n^*G_m\right)B_{nm}\right\} \quad . \tag{5.25}$$

The function G_m satisfies Eq. (5.13). In the adiabatic approximation $J_r^{(n)}$ is given by Eq. (3.16).

Figure V.2 shows a calculation of total power flow in the radial direction for conventional, corrected, and adiabatic coupled mode theory for a bottom slope of $5°$. The source is of unit strength as defined by (5.17) and the power unit is the watt (1 W = 1 kg m^2/sec^3). The arrows along the range axis denote the cutoff ranges of the normal modes. These cutoff ranges correspond to the ranges at which $k_n^2(r)$ given by Eq. (5.7) becomes negative. Past cutoff the eigenvalues become imaginary and the mode does not propagate but rapidly decays exponentially with range.
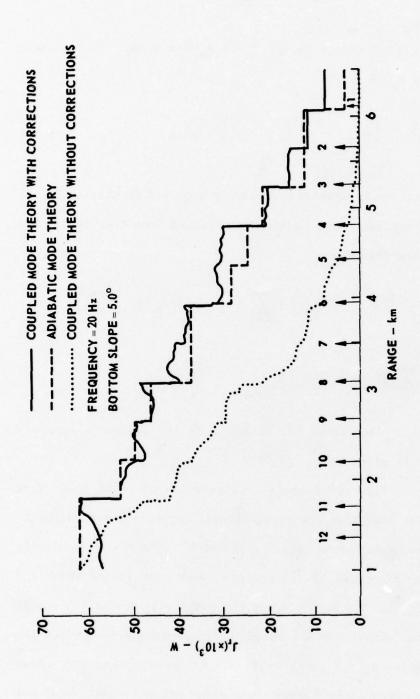
FIGURE Ⅴ.2

TOTAL POWER AMPLITUDE versus RANGE

THE ARROWS DENOTE MODE CUTOFF RANGES

SOURCE DEPTH = 0.2 km, c = 1.5 km/sec

Before discussing Fig. V.2 further, one must know how the total power amplitude should behave in a case in which energy is conserved. It would seem logical to expect the total power flow to be constant for all ranges if energy is conserved. This is not the case depicted in Fig. V.2. The reason for the stair-step type behavior in Fig. V.2 is that only forward going energy is included in the calculation of the power amplitudes. The stair-step behavior of the adiabatic solution is the expected type of behavior for this situation. The abrupt drops in power amplitude occur at the mode cutoff ranges where the outgoing energy associated with that mode is suddenly removed from the problem. In between mode cutoff ranges the power flow is constant indicating conservation of energy over regions having a constant number of modes.

The corrected coupled mode theory calculation (solid curve in Fig. V.2) which purports to conserve energy to order $\dot{H}$ should exhibit the same stair-step range dependence. At ranges greater than 4 km this type of behavior is present; however, at lesser ranges it is not evident. This departure from the expected behavior at short ranges is because of terms of order $\dot{H}^2$ and $\dot{H}^3$ that are introduced into the calculations through Eq. (5.25). The G_m functions of Eq. (5.25) satisfy Eq. (5.13) and contain terms of order zero and $\dot{H}$; therefore, since G_n occurs quadratically in (5.25), terms of order $\dot{H}^2$ and $\dot{H}^3$ are inadvertently retained. These higher order terms cause the departure from the expected behavior at the shorter ranges. This departure is more pronounced at the

shorter ranges because there are more modes present at these ranges
and more higher order terms introduced in the summation of Eq.
(5.25).

Notice the conventional coupled mode theory calcula-
tion (dotted line) in Fig. V.2. The nonconservation of energy is
immediately apparent with the observed rapid decrease of power flow
with range. Also notice the subtle differences between the
adiabatic and corrected calculations. The effects of the mode
conversion process are readily apparent. The corrected coupled
mode theory calculation shows an increased power flow compared to
the adiabatic calculation at the longer ranges. This increase is
due to energy cascaded from the higher modes to the lower modes.
The power amplitude of mode zero (region to the right of arrow 1)
for the corrected coupled mode theory calculation is significantly
larger than in the adiabatic case. The difference in levels is
entirely because of energy transferred into mode zero from the
higher modes.

In Fig. V.3 the same type of calculation as depicted
in Fig. V.2 for a bottom slope of 2.5° is shown. With the decrease
in bottom slope, the higher order terms inadvertently retained in
the calculation using (5.25) have a less pronounced effect as one
would expect. Once again, the mode cutoff ranges are denoted by
arrows.

Figures V.4 through V.6 are plots of the individual
mode power amplitude for modes 0 through 2. The solid curve was
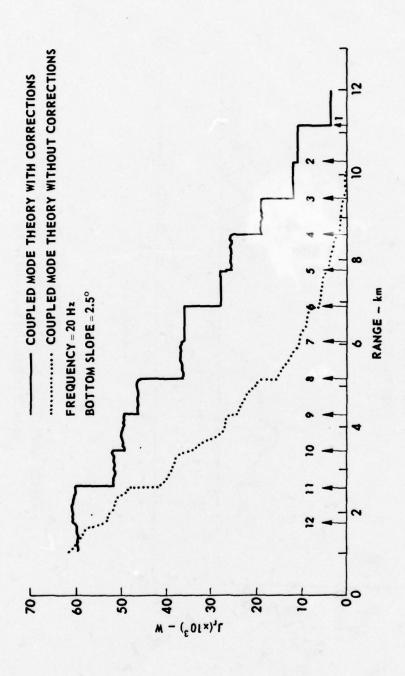
FIGURE V.3
TOTAL POWER AMPLITUDE versus RANGE
THE ARROWS DENOTE MODE CUTOFF RANGES
SOURCE DEPTH = 0.2 km, c = 1.5 km/sec
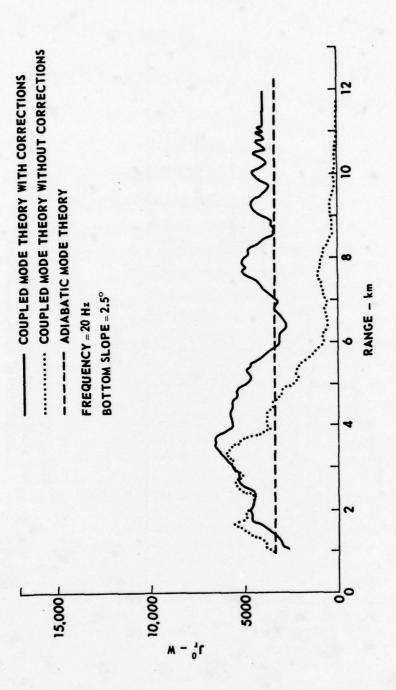
FIGURE Ⅴ.4

POWER AMPLITUDE OF MODE NUMBER 0 versus RANGE

SOURCE DEPTH = 0.2 km, c = 1.5 km/sec

161
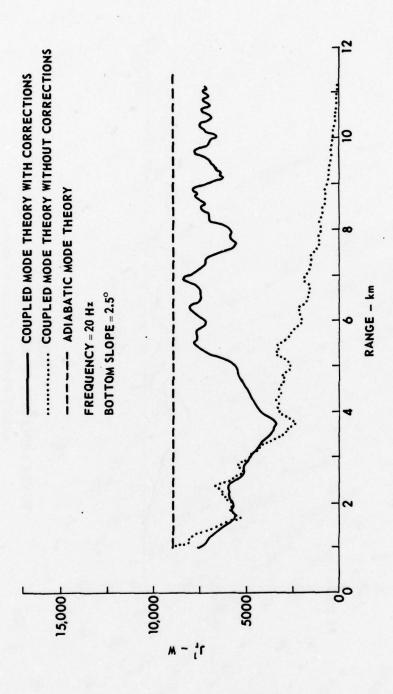
FIGURE V.5
POWER AMPLITUDE OF MODE NUMBER 1 versus RANGE
SOURCE DEPTH = 0.2 km, c = 1.5 km/sec

162
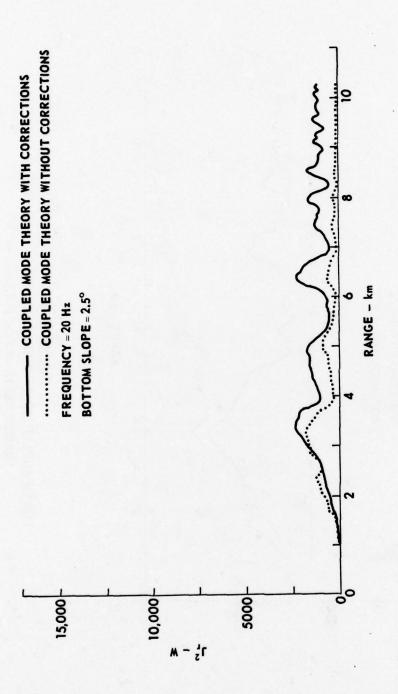
FIGURE V.6

POWER AMPLITUDE OF MODE NUMBER 2 versus RANGE

SOURCE DEPTH = 0.2 km, c = 1.5 km/sec

calculated from Eq. (5.25) and the dotted curve from Eq. (5.23). The dashed curve is the adiabatic power amplitude calculated from Eq. (3.16). The adiabatic calculation is missing from Fig. V.6 because a source depth of 0.2 km corresponds exactly to a null of the mode 2 depth function at the source; hence, mode 2 is not excited and has no power flow associated with it in the adiabatic approximation.

In Figs. V.4 through V.6, at ranges more than about 4 km there are large differences between the conventional and corrected theory calculations. Once again, this is a manifestation of nonconservation of energy caused by energy loss normal to the bottom boundary. The effect is quite pronounced, even for a slope of about 2.5°.

The departures of the solid curves in Figs. V.4-V.6 from a straight line are a consequence of the mode conversion process. The mode power amplitude rises when it is picking up energy from the other modes and drops when it is giving up energy to the other modes. Figure V.7 is a superposition of the solid curves in Figs. V.4-V.6. Note the approximate negative correlation between nearest neighbor modes. For example, the peaks in the curve for mode 0 are roughly correlated with the valleys of the curve for mode 1. The same type of behavior exists between modes 1 and 2 and all of the other neighboring modes. This tends to indicate that the coupling between modes is strongest for nearest neighbor modes.
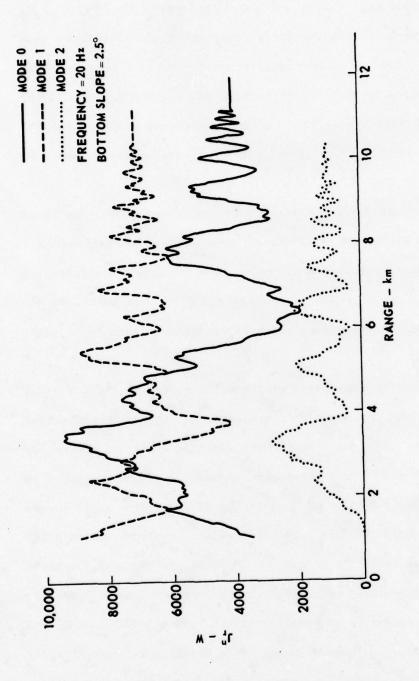
FIGURE V.7
POWER AMPLITUDES OF MODES 0, 1, AND 2 versus RANGE
SOURCE DEPTH = 0.2 km, c = 1.5 km/sec

164

Hence, mode 1 predominately feeds and receives power to and from modes 0 and 2. This is generally true for all the other modes also.

2. Radial Functions

Figures V.8-V.10 show the amplitude of the radial functions G_m computed from Eq. (5.13) for mode numbers 0 through 2. Also shown on Figs. V.8-V.9 is the adiabatic approximation to $|G_m|$. Note the differences between the adiabatic and coupled mode calculations that arise from the mode-mode interaction processes.

In Fig. V.10, no adiabatic amplitude is included because mode number 2 is not excited by the source; hence, in the adiabatic approximation, where no mode interaction occurs, the amplitude remains zero at all ranges. Notice how the mode coupling feeds amplitude to mode number 2. Mode number 2, which was initially unexcited at the source, is seen to build up significant amplitude as it propagates away from the source.

3. Corrections to the Depth Functions

In this subsection the results of the evaluation of the corrections to the mode depth functions $\delta\phi_n$ are presented. The differential equation for $\delta\phi_n$ is given by Eq. (4.76). If the WKB approximation for $\dot{R}_n/R_n$ is employed, Eq. (4.76) becomes

$$\left[\frac{\partial^2}{\partial z^2} + k^2 - k_n^2(r)\right]\delta\phi_n = -2ik_n B_{nn}\phi_n \quad . \tag{5.26}$$

The function ϕ_n is given by Eq. (5.9).
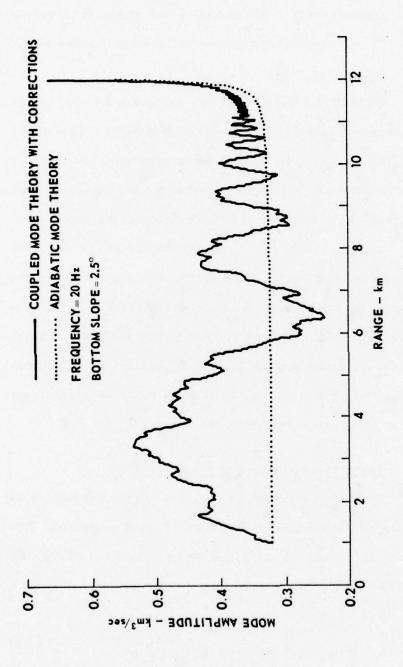
FIGURE V.8

RADIAL FUNCTIONS FOR MODE NUMBER 0 versus RANGE
WITH $1/\sqrt{r}$ RANGE DEPENDENCE REMOVED
SOURCE DEPTH = 0.2 km, c = 1.5 km/sec

COUPLED MODE THEORY WITH CORRECTIONS
ADIABATIC MODE THEORY

FREQUENCY = 20 Hz
BOTTOM SLOPE = 2.5°

RANGE – km

MODE AMPLITUDE – km³/sec
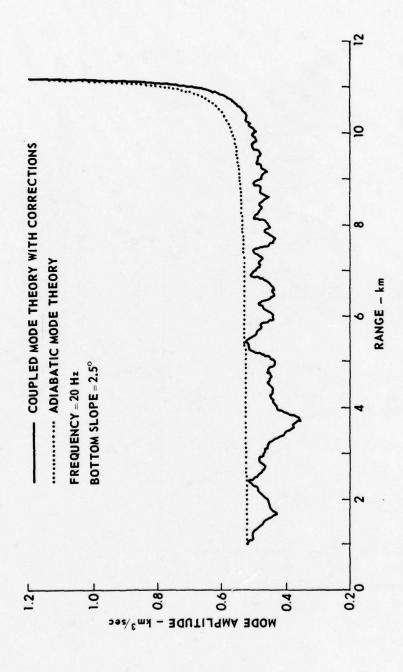
FIGURE Ⅴ.9

RADIAL FUNCTIONS FOR MODE NUMBER 1 versus RANGE
WITH 1/√r RANGE DEPENDENCE REMOVED

SOURCE DEPTH = 0.2 km, c = 1.5 km/sec
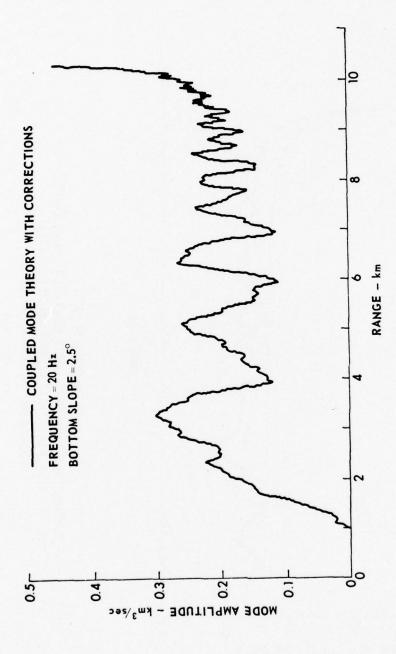
FIGURE $\overline{\text{V}}$.10
RADIAL FUNCTIONS FOR MODE NUMBER 2 versus RANGE
WITH 1/√r RANGE DEPENDENCE REMOVED
SOURCE DEPTH = 0.2 km, c = 1.5 km/sec

As determined in Chapter IV, the desired solution of (5.26) is the particular solution. The particular solution of Eq. (5.26) may be obtained analytically in this case from the two linearly independent solutions of the homogeneous form of Eq. (5.26). The particular solution of (5.26) is given by (see Ref. 5.7)

$$\delta\phi_n(z;r) = - 2ik_n(r)B_{nn}(r) \left\{ y_2(z;r) \int_0^z \frac{\phi_n(z';r)y_1(z';r)dz'}{\Delta(z')} \right.$$

$$\left. - y_1(z;r) \int_0^z \frac{\phi_n(z';r)y_2(z';r)dz'}{\Delta(z')} \right\} \quad . \tag{5.27}$$

In Eq. (5.27) y_1 and y_2 are any two linearly independent solutions of

$$\left[\frac{\partial^2}{\partial z^2} + k^2 - k_n^2(r) \right] \left\{ \begin{matrix} y_1 \\ y_2 \end{matrix} \right\} = 0 \quad , \tag{5.28}$$

and $\Delta(z)$ is the Wronskian given by

$$\Delta(z) = y_1 y_2' - y_1' y_2 \quad . \tag{5.29}$$

For the case considered here y_1, y_2, and Δ are given by

$$y_1(z;r) = \sin \kappa_n(r)z \qquad \Delta(z;r) = - \kappa_n(r) \tag{5.30}$$

$$y_2(z;r) = \cos \kappa_n(r)z \qquad \kappa_n(r) = \sqrt{k^2 - k_n^2(r)} = \frac{(n+1/2)\pi}{H(r)} \qquad .$$

Substituting Eqs. (5.9) and (5.30) in Eq. (5.27) one obtains

$$\delta\phi_n = i\sqrt{\frac{2}{H}} \frac{k_n(r)B_{nn}(r)}{\kappa_n(r)} \left\{ z \cos \kappa_n z - \frac{\sin \kappa_n z}{\kappa_n(r)} \right\} \tag{5.31}$$

The solution for $\delta\phi_n$ given in (5.31) is easily seen to satisfy the appropriate boundary conditions given in Chapter IV.

$$\delta\phi_n(z=0;r) = 0$$
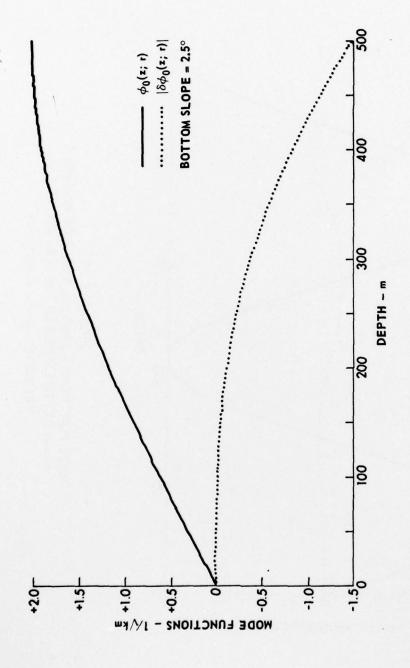
$$\frac{\partial}{\partial z} \delta\phi_n(z;r)\bigg|_{z=H(r)} = ik_n \dot{H} \, \phi_n(z;r)\bigg|_{z=H(r)} \qquad ,$$
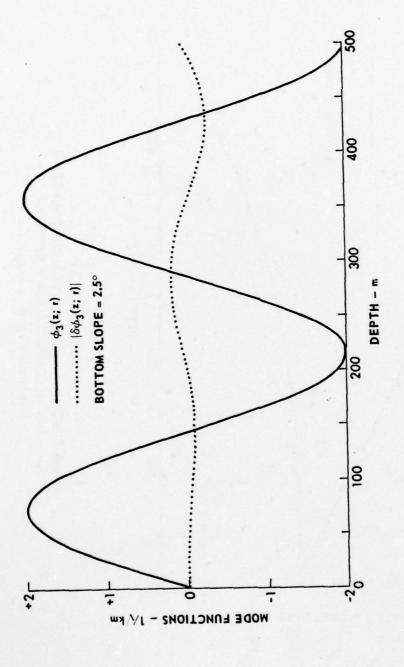
where B_{nn} is taken from (5.12)

$$B_{nn} = - \frac{\dot{H}}{H}$$
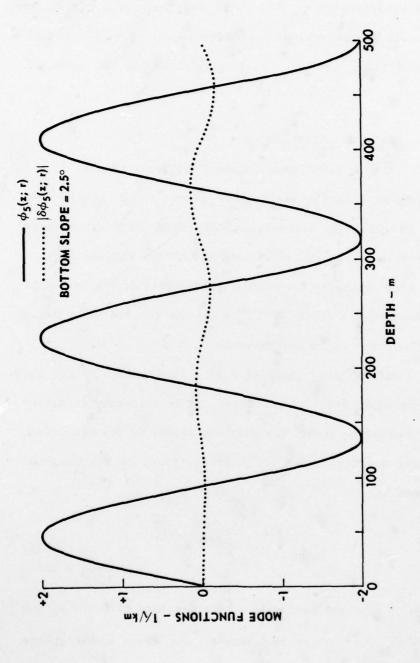
Figures V.11-V.13 depict $|\delta\phi_n|$ versus depth for mode numbers 0, 3, and 5 for a range of 1 km from the source. The bottom slope is 2.5 . Also shown on the plots is the mode depth function ϕ_n for comparison. Note that the magnitude of $\delta\phi_n$ is indeed small compared to the magnitude of ϕ_n.

171

FIGURE V.11

MODE FUNCTIONS ϕ_n AND $\delta\phi_n$ FOR MODE NUMBER 0
versus DEPTH COMPUTED FOR A RANGE OF 1 km
FREQUENCY = 20 Hz, c = 1.5 km/sec

FIGURE $\overline{\text{V}}$.12

MODE FUNCTIONS ϕ_n AND $\delta\phi_n$ FOR MODE NUMBER 3
versus DEPTH COMPUTED FOR A RANGE OF 1 km

FREQUENCY = 20 Hz, c = 1.5 km/sec

FIGURE Ⅴ.13

MODE FUNCTIONS ϕ_n AND $\delta\phi_n$ FOR MODE NUMBER 5
versus DEPTH COMPUTED FOR A RANGE OF 1 km
FREQUENCY = 20 Hz, c = 1.5 km/sec

At this point it should be emphasized that $\delta\phi_n$ may be determined analytically in this case, only because ϕ_n is known analytically. In a more realistic problem in which the ϕ_n must be computed numerically, the $\delta\phi_n$ will also have to be computed numerically.

4. Field Calculations

In this final subsection of Chapter V results of the calculation of the acoustic field ψ are given. When considering the acoustic field, it is customary to examine ψ as a function of range for specific source and receiver depths. The calculations to be presented here were made for the waveguide model of Fig. V.1 with the source located at a depth of 0.2 km and the receiver at a depth of 0.1 km. The slope angle was taken to be 5 .

Rather than examining ψ as a function of range, the absolute square of ψ, $\psi*\psi$, is considered, as is customary in underwater acoustic modeling work. The absolute square of the field is a more meaningful quantity since it is proportional to the measured intensity given by

$$I_{meas} = \frac{p_{rms}^2}{\rho_o c_o} \quad . \tag{5.32}$$

In Eq. (5.32), p_{rms} is the root mean square pressure measured at the receiver, and ρ_o and c_o are the density and sound speed at the receiver. The constant of proportionality linking I_{meas} and $\psi*\psi$ is $\omega^2 \rho_o / 2c_o$.

$$I_{meas} = \frac{\omega^2 \rho_o}{2c_o} \psi^*\psi \quad . \tag{5.33}$$

Figure V.14 shows $\psi^*\psi$ versus range for the indicated source-receiver depths. Two curves are presented in Fig. V.14, one for the adiabatic approximation of $\psi^*\psi$ and one for a coupled mode theory evaluation. Notice how the fine structure of $\psi^*\psi$ differs appreciably between the adiabatic and coupled mode calculations.

Figure V.15 shows the difference between the two curves of Fig. V.14 as a function of range. It is obvious from Fig. V.15 that some large differences exist between the adiabatic and the coupled mode calculations. If the curve in Fig. V.15 is averaged over range, one finds the mean to be +0.083 which is very close to zero. Hence, the range averaged difference between the adiabatic and coupled mode calculations is very slight. In many underwater acoustics applications, the fine structure of the field is not of interest. Many data analysis procedures involve a range averaging operation on the measured field. It seems plausible that, in situations such as these, an adiabatic calculation of the field might provide an adequate characterization of the medium, which would greatly simplify the computational requirements.

Figure V.16 shows the phase structure of the field used to generate Fig. V.14. The adiabatic and coupled mode theory calculations of the phase are both depicted. The reason for including this figure is to check the assertion made in Chapter III concerning the phase characteristics of the adiabatic solution. In
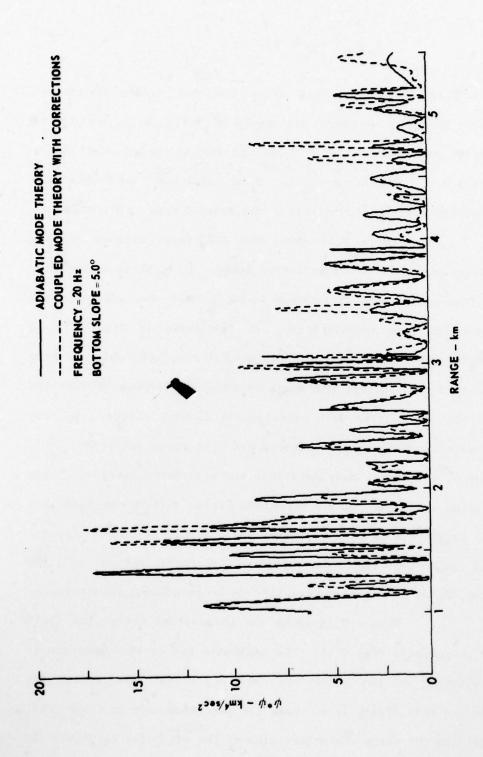
FIGURE V.14

$\psi^* \psi$ versus RANGE

SOURCE DEPTH = 0.2 km, RECEIVER DEPTH = 0.1 km, c = 1.5 km/sec
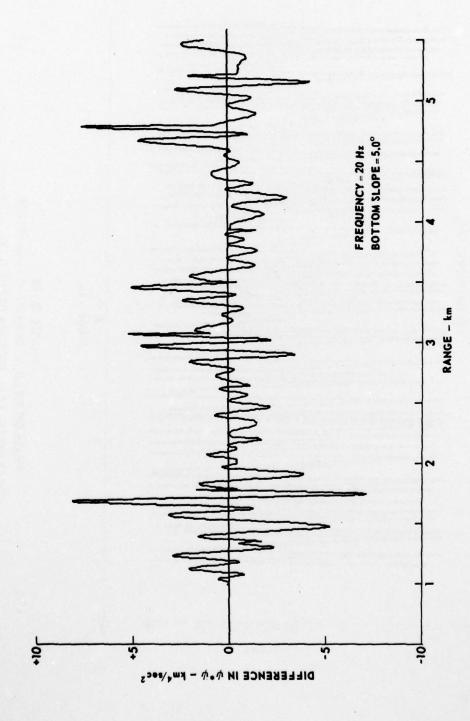
FIGURE Ⅴ.15

DIFFERENCE BETWEEN $\psi^*\psi$ COMPUTED BY COUPLED MODE THEORY AND ADIABATIC MODE THEORY versus RANGE

SOURCE DEPTH = 0.2 km, RECEIVER DEPTH = 0.1 km, c = 1.5 km/sec

FREQUENCY = 20 Hz
BOTTOM SLOPE = 5.0°
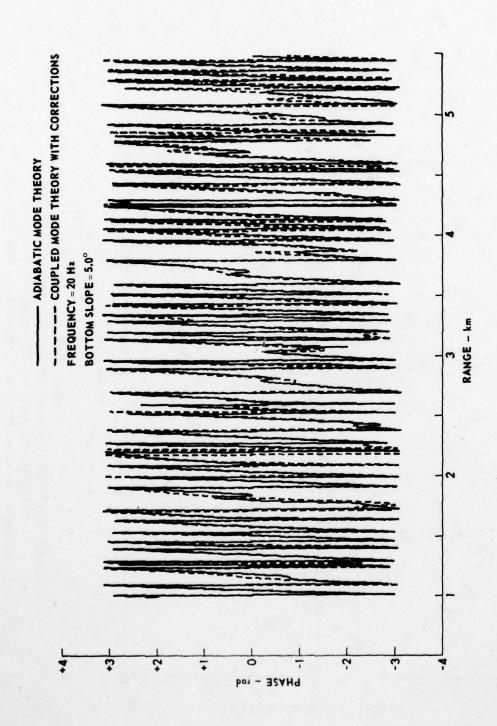
FIGURE V.16

PHASE OF FIELD, ψ, IN RADIANS versus RANGE

SOURCE DEPTH = 0.2 km, RECEIVER DEPTH = 0.1 km, c = 1.5 km/sec

Chapter III it was concluded that the adiabatic phase of the acoustic field should be a good approximation to the phase of the field computed using coupled mode theory with the mode-mode coupling effects primarily influencing the scalar distribution of amplitude among the modes. Figure V.16 supports this claim. The adiabatic phase tracks the coupled mode phase quite well. In fact, the agreement is better than indicated by Fig. V.16 since a good portion of the difference between the two curves is due to sampling effects and the resolution of the plotting hardware used to generate Fig. V.16. The finding that the adiabatic phase is a good approximation to the true phase of the field is important because in many applications, such as modeling array response, the phase of the field is of more importance than the amplitude information. Hence, it seems likely that, in cases such as this, an adiabatic characterization of the field would be adequate, again greatly simplifying the required computational effort.

CHAPTER VI

CONCLUSION

The purpose of this report has been to examine the
theory of sound propagation via coupled normal modes as applied to
acoustic propagation in a range dependent ocean environment. The
emphasis has been placed on low frequency propagation over range
variable ocean bottoms. Coupled mode theory and the adiabatic
approximation to coupled mode theory involve approximations
concerning the boundary conditions satisfied by the field and the
strength of the range dependence of the medium respectively.
Before the theory can be used as an acoustic propagation modeling
tool, the effect of the approximations involved in the theory must
be examined with regard to the types of range variability expected
to be encountered in realistic ocean media. This examination was
the main purpose of the work presented in this report.

In Chapter II the general framework of the theory, as
originally proposed, was described. In the derivations all
quantities which must be evaluated in the implementation of the
theory were given in a form suitable for numerical computation. The
methodology for implementing the theory in realistic problems was
also described.

Chapter III considered the adiabatic approximation to
coupled mode theory. Two aspects of the adiabatic approximation
were investigated: (1) its sensitivity, as a function of sediment

180
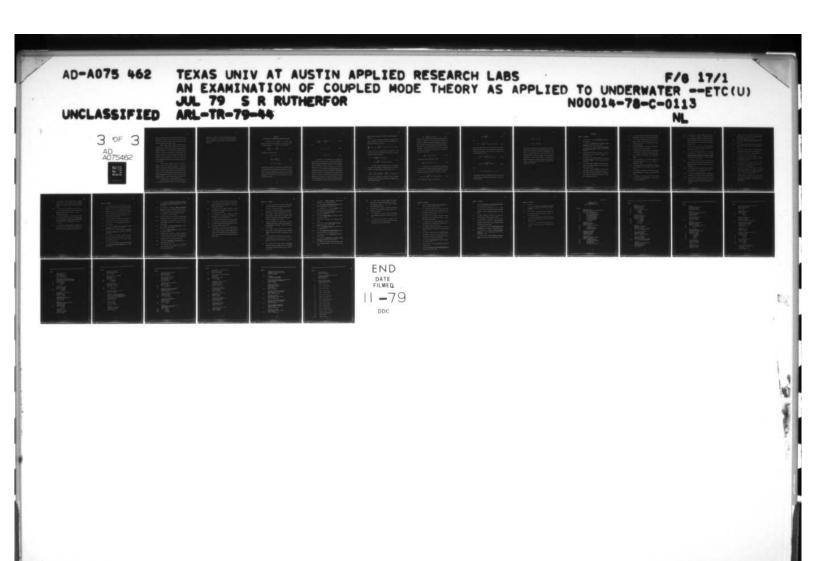
type, to radial sound speed derivative and water-sediment interface slope, and (2) whether the geometric (raypath) properties of the adiabatic field were given correctly. The adiabatic approximation was seen to be sensitive to bottom type with respect to lateral sound speed gradient and water-sediment interface slope, and the nature of the sensitivity was explained using ray theory arguments. The adiabatic solution was also seen to describe the raypath and phase structure of the field, even for quite large rates of radial change. This finding led to the conclusion that the mode-mode coupling effects neglected in the adiabatic approximation were primarily responsible for amplitude redistribution leaving the phase structure essentially unchanged.
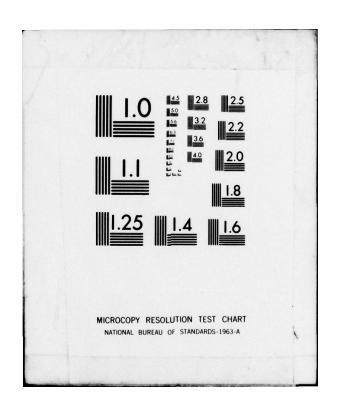
Chapter IV examined the boundary condition approximation inherent in coupled mode theory when applied to problems with range variable boundaries. Since nonhorizontal boundaries are present in almost all ocean propagation problems of interest, the work presented in this chapter is probably the most significant portion of the dissertation. In Chapter IV the consequence of the boundary condition approximation was explored. It was found that the order of the approximation on the boundary conditions was not consistent with the order of coupled mode theory. It was also shown that a consequence of this inconsistency was energy not being conserved within the original formulation of coupled mode theory. A consistent correction to coupled mode theory was then derived such that the field so obtained satisfied the proper boundary conditions

and conserved energy to first order in the local slopes of any nonhorizontal boundaries. The corrections to the theory were given in a form convenient for computational purposes. The results of Chapter IV have exposed the consequences of the inconsistent boundary condition approximation inherent in coupled mode theory, heretofore ignored, and have shown how to overcome the inconsistency.

Chapter V presents the results of numerical calculations that were performed for the purpose of illustrating and verifying the assertions and corrections proposed in Chapter IV. The numerical calculations given in this chapter were made for an isovelocity, wedge shaped waveguide having perfectly reflecting boundaries. Power flow calculations were presented to illustrate nonconservation of energy in the original formulation of the theory and to show that the proposed corrections produced the desired results. Calculations of the radial and depth functions as well as a calculation of the field were presented.

There are several possible extensions of the work presented in this report. One concerns the inclusion of solid properties of the medium. Coupled mode theory is based on the assumption of a fluid acoustic medium. In realistic oceanic waveguides the fluid assumption is valid for the water layer and is a good approximation for the unconsolidated sediments. However, the underlying basalt substrate which occurs at varying depths beneath the ocean bottom is known to exhibit significant solid properties.

MICROCOPY RESOLUTION TEST CHART
NATIONAL BUREAU OF STANDARDS-1963-A

Hence, one possible extension of the work given here would be a reworking of the theory to include the solid properties of the basalt. Such an extension, however, would likely make an already complicated formalism prohibitively complex.

Another possible extension concerns the importance of the nonconservation of energy effect compared with any realistic attenuation processes occurring in the medium. This comparison was suggested in Chapter IV. In the numerical calculations presented in Chapter V the effect of nonconservation of energy was seen to be severe. It might turn out that, in more realistic waveguides with attenuation included, the effect is negligible. If this were true in some cases the implementation of the theory could be considerably simplified because the corrections proposed in Chapter IV could be ignored.

A third possible extension concerns the finding of Chapter III that the true phase structure of the field is essentially given by the adiabatic approximation to coupled mode theory. A consequence of this finding is that in applications of the theory in which the phase structure of the field is the primary concern, e.g., array processing and field coherence studies, the adiabatic approximation is perhaps all that is required to obtain meaningful results. Since this would involve a great simplification of the calculations, it is worth examining further.

An obvious extension of the work presented in Chapter IV is to include second order corrections to the field and boundary

conditions and estimate, in terms of bottom slope, when their
inclusion is necessary. Such an extension, however, would probably
not be computationally feasible because of the added complexity it
would entail.

APPENDIX A

SOME PROPERTIES OF THE NORMAL MODE EIGENFUNCTION EXPANSION

The purpose of this appendix is to present a more detailed description of the properties of the normal mode depth function described by Eq. (2.12) which is reproduced below.

$$\left[\frac{d^2}{dz^2} + k^2(z) - k_n^2\right] \phi_n(z) = 0 \qquad . \qquad (A.1)$$

The boundary conditions on ϕ_n are

$$\phi_n(0) = \phi_n(\infty) = 0$$

$$\frac{\partial \phi_{i,n}}{\partial z} = \frac{\partial \phi_{i+1,n}}{\partial z}\bigg|_{H_i} \qquad (A.2)$$

$$\rho_i \, \phi_{i,n} = \rho_{i+1} \, \phi_{i+1,n}\bigg|_{H_i} \qquad .$$

The sound speed structure of a typical oceanic waveguide is such that the wave number, $k(z)$, attains some limiting value as z goes to infinity, k_{min}. The maximum value of $k(z)$ occurs in the water column at the sound speed minimum which defines the center of the sound channel. Call this value of k, k_{max}. Equation (A.1) may now be rewritten as follows.

185

$$\left[\frac{d^2}{dz^2} + \lambda_n - q(z)\right]\phi_n(z) = 0 \quad , \tag{A.3}$$

with

$$q(z) = k_{min}^2 - k^2(z) \tag{A.4}$$

$$\lambda_n = k_{min}^2 - k_n^2 \quad . \tag{A.5}$$

The function $q(z)$ as defined by (A.4) is negative and approaches zero as z goes to infinity. Equation (A.3) and boundary conditions define an eigenvalue problem whose properties have been widely investigated (see Refs. A.1 and A.2). The eigenvalue spectrum of Eq. (A.3) is known to be discrete for $\lambda_n < 0$ and continuous for $\lambda_n > 0$. For readers familiar with quantum mechanics, the problem defined by Eqs. (A.3)-(A.5) is analogous to the Schrodinger equation for a particle in a potential well where particles with energies less than zero occupy bound states with discrete energy eigenvalues and particles with positive energies can have a continuum of energy eigenvalues. Therefore, in the notation of Eq. (A.1) the eigenvalues k_n are discretely distributed for magnitudes

between k_{min} and k_{max} and are continuously distributed between 0 and k_{min}.

The mode functions ϕ_n including the continuum form a complete, closed set of functions on the depth interval $(0, \infty)$ having the following closure property.

$$\sum_{n=1}^{n} \rho(z) \phi_n(z) \phi_n(z') + \int_0^{k_{min}} \rho(z) \phi(\kappa, z) \phi(\kappa, z') d\kappa = \delta(z - z') \quad (A.6)$$

In (A.6) the $\phi(\kappa, z)$ is a continuum mode of eigenvalue κ. The equation for the field from a point source given in Eq. (2.21) with the inclusion of the continuum is

$$\psi(r, z) = i\pi\rho(z_0) \sum_n H_0^{(1)}(k_n r) \phi_n(z) \phi_n(z_0)$$

$$+ i\pi\rho(z_0) \int_0^{k_{min}} H_0^{(1)}(\kappa r) \phi(\kappa, z) \phi(\kappa, z_0) d\kappa \quad . \quad (A.7)$$

The depth functions satisfying Eq. (A.1) are orthogonal with respect to the density as a weighting function. To see this consider the following expression obtained from Eq. (A.1).

$$\phi_m \frac{d^2\phi_n}{dz^2} - \phi_n \frac{d^2\phi_m}{dz^2} = \frac{d}{dz}\left(\phi_m \frac{d\phi_n}{dz} - \phi_n \frac{d\phi_m}{dz}\right) = \left(k_n^2 - k_m^2\right)\phi_m\phi_n \quad (A.8)$$

If Eq. (A.8) is multiplied by the density which is piecewise continuous throughout the layers, and the result integrated over z the following is obtained,

$$\left(k_n^2 - k_m^2\right) \int_o^\infty \rho(z) \phi_m(z) \phi_n(z) dz = 0 \quad . \qquad \text{(A.9)}$$

The RHS of (A.9) is zero because of the boundary conditions given in Eq. (A.2). Equation (A.9) shows that the mode functions of different mode index are orthogonal to each other. The same arguments show that discrete and continuous modes are orthogonal to each other as are two continuous modes with different continuum eigenvalues. The density $\rho(z)$ plays the role of a weighting function in the orthogonality relationship. It is convenient to normalize the ϕ_n such that

$$\int_o^\infty \rho(z) \phi_n(z) \phi_m(z) dz = \delta_{n,m} \quad . \qquad \text{(A.10)}$$

The continuous modes are normalized as follows:

$$\int_o^\infty \rho(z) \phi(\kappa,z) \phi(\kappa',z) dz = \delta(\kappa - \kappa') \quad . \qquad \text{(A.11)}$$

In Chapter II it was stated that the contribution to the field from the continuum is negligible in many cases. To show that this is true, a proof given by Mitchell[A.3] is reproduced. Consider the continuum contribution to the field in Eq. (A.7).

$$\psi_{cont} = i\pi \rho(z_o) \int_o^{k_{min}} H_o^{(1)}(\kappa r) \phi(\kappa,z) \phi(\kappa,z_o) d\kappa \quad . \qquad \text{(A.12)}$$

Divide the interval $(0, k_{min})$ in such a way that

$$\psi_{\text{cont}} = \sum_{\ell} \psi(\ell) \tag{A.13}$$

with

$$\psi(\ell) = i\pi\rho(z_o) \int_{\kappa_\ell}^{\kappa_{\ell+1}} H_o^{(1)}(\kappa r)\phi(\kappa,z)\phi(\kappa,z_o)d\kappa \quad . \tag{A.14}$$

The intervals defining the $\psi(\ell)$ are chosen such that $H_o^{(1)}(\kappa r)$ vanishes at both end points and such that $\phi(\kappa,z)\phi(\kappa,z_o)$ has the same sign over the interval. With this choice of intervals one can set an upper bound on the $\psi(\ell)$,

$$\left| \psi(\ell) \right| \le \pi\overline{G}(\ell) \left| \int_{\kappa_\ell}^{\kappa_{\ell+1}} H_o^{(1)}(\kappa r) \, d\kappa \right| \quad , \tag{A.15}$$

$$\left| \psi(\ell) \right| \le \frac{\pi\overline{G}(\ell)}{r} \left| \int_{r\kappa_\ell}^{r\kappa_{\ell+1}} H_o^{(1)}(x)dx \right| \quad , \tag{A.16}$$

with

$$\overline{G}(\ell) = \max[\phi(\kappa,z)\phi(\kappa,z_o)]; \, \kappa_\ell < \kappa < \kappa_{\ell+1} \quad .$$

If the asymptotic form of the Hankel function, which is valid for ranges more than a few wavelengths from the source, is used in Eq. (A.16), one obtains

$$\left| \psi(\ell) \right| \leq \text{const} \frac{1}{r^{3/2}} \quad ,$$

$$\left| \psi_{\text{cont}} \right| \leq \text{const} \frac{1}{r^{3/2}} \quad .$$

The field from the continuous modes is therefore seen to fall off as $1/r^{3/2}$ for ranges more than a few wavelengths from the source. This falloff is $1/r$ times faster than the $1/\sqrt{r}$ range dependence of the discrete contribution to the field. Hence, one can see that the continuous mode contribution to the acoustic field is negligible in the farfield. At ranges in close proximity to the source and in problems involving only a few discrete modes, the continuum can be important. Papers by Stickler,[A.4] Williams,[A.5] and Tindle[A.6] have examined these situations.

BIBLIOGRAPHY

CHAPTER I - REFERENCES

1.1   I. Tolstoy and C. S. Clay, Ocean Acoustics (McGraw-Hill, New York, 1966).

1.2   C. B. Officer, Introduction to the Theory of Sound Transmission (McGraw-Hill, New York, 1958).

1.3   C. S. Clay and H. Medwin, Acoustical Oceanography: Principles and Applications (John Wiley and Sons, New York, 1977).

1.4   D. Ludwig, "Uniform asymptotic expansions at a caustic," Communications on Pure and Applied Mathematics, Vol. XIX, 215-250 (1966).

1.5   B. G. Roberts, Jr., "Horizontal-gradient acoustical ray-trace program TRIMAIN," U.S. Naval Res. Lab. Rep., NRL 7827 (1974).

1.6   J. J. Cornyn, "GRASS: A digital ray-tracing and transmission loss prediction system," Vol. I, U.S. Naval Res. Lab. Rep. 7621 (1973).

1.7   D. E. Weston, "Guided propagation in a slowly varying medium," Proc. Phys. Soc., London 73, 365-384 (1959).

1.8   D. E. Weston, "Horizontal refraction in a three dimensional medium of variable stratification," Proc. Phys. Soc., London 78, 46-52 (1960).

1.9   P. W. Smith, "Averaged sound transmission in range-depen-
       dent channels," J. Acoust. Soc. Am. <u>55</u>, 1197-1204 (1974).

1.10   C. H. Harrison, "Horizontal ray curvature effects in
       basins, troughs, and near seamounts by use of ray in-
       variants," NRL Report No. 8144, Naval Research Labora-
       tory, Washington, D.C.

1.11   R. Smith, "Propagation in slowly-varying waveguides,"
       SIAM J. Appl. Math. <u>33</u>, 39-50 (1977).

1.12   H. Weinberg and R. Burridge, "Horizontal ray theory for
       ocean acoustics," J. Acoust. Soc. Am. <u>55</u>, 63-79 (1974).

1.13   F. P. Bretherton, "Propagation in slowly varying wave-
       guides," Proc. R. Soc. London, Ser. A. <u>302</u>, 555-576
       (1968).

1.14   F. P. Bretherton and C. J. R. Garrett, "Wavetrains in
       inhomogeneous moving media," Proc. R. Soc. London, Ser. A
       <u>302</u>, 529-554 (1969).

1.15   S. T. McDaniel, "Parabolic approximations for underwater
       sound propagation," J. Acoust. Soc. Am. <u>58</u>, 1178-1185
       (1975).

1.16   S. T. McDaniel, "Propagation of normal mode in the para-
       bolic approximation," J. Acoust. Soc. Am. <u>57</u>, 307-311
       (1975).

1.17   J. A. DeSanto, J. S. Perkins, and R. N. Baer, "A correc-
       tion to the parabolic approximation," J. Acoust. Soc.
       Am. <u>64</u>, 1664-1666 (1978).

1.18   R. H. Hardin and F. D. Tappert, SIAM Rev. 15, 423 (1973).

1.19   C. W. Spofford, "A synopsis of the AESD workshop on acoustic propagation modeling by non-ray tracing techniques," AESD Tech. Note TN 73-05, Acoustic Environmental Support Detachment, Office of Naval Research, Arlington, Virginia, (1973).

1.20   F. Jensen and H. Krol, "The use of the parabolic equation method in sound propagation modeling: SACLANTCEN Memorandum SM-72, LaSpezia, Italy (1975).

1.21   F. D. Tappert, "Selected applications of the parabolic equation method in underwater acoustics," in _International Workshop on Low-Frequency Propagation of Noise_ Woods Hole, MA 15-19 October 1974, (U.S. GPO, Washington, D.C., 1977), Vol. 1, pp. 155-197.

1.22   J. S. Perkins and R. N. Baer, "A corrected parabolic equation program package for acoustic propagation," NRL Memorandum Report 3688 (Naval Research Laboratory, Washington, DC).

1.23   A. D. Pierce, "Extension of the method of normal modes to sound propagation in an almost-stratified medium," J. Acoust. Soc. Am. 37, 19-27 (1965).

1.24   D. M. Milder, "Ray and wave invariants for SOFAR channel propagation," J. Acoust. Soc. Am. 46, 1259-1263 (1969).

1.25   J. R. Wait and K. P. Spies, "On the calculation of mode conversion at a graded height change in the earth -- ionosphere waveguide at VLF," Radio Science 3, 787-791 (1968).

1.26   A. Wexler, "Solution of waveguide discontinuities by modal analysis," IEEE Transactions on Microwave Theory and Techniques MTT-15, 508-517 (1967).

1.27   H. G. Unger, Planar Optical Waveguides and Fibres (Oxford Press, 1977).

1.28   S. T. McDaniel, "Coupled power equations for cylindrically spreading waves," J. Acoust. Soc. Am. 60, 1285-1289 (1976).

1.29   S. T. McDaniel, "Mode conversion in shallow-water sound propagation," J. Acoust. Soc. Am. 62, 320-325 (1977).

1.30   S. T. McDaniel, "Calculation of mode conversion rates," J. Acoust. Soc. Am. 63, 1372-1374 (1978).

1.31   L. B. Dozier and F. D. Tappert, "Statistics of normal mode amplitudes in a random ocean. I. Theory," J. Acoust. Soc. Am. 63, 353-365 (1978).

1.32   L. B. Dozier and F. D. Tappert, "Statistics of normal mode amplitudes in a random ocean. II. Computations," J. Acoust. Soc. Am. 64, 533-547 (1978).

1.33   R. D. Graves, A. Nagl, H. Überall, and G. L. Zarur, "Range-dependent normal modes in underwater sound propagation: application to the wedge-shaped ocean," J. Acoust. Soc. Am. 58, 1171-1177 (1975).

1.34   A. Nagl, H. Überall, A. J. Haug, and G. L. Zarur, "Adiabatic mode theory of underwater sound propagation in a range-dependent environment," J. Acoust. Soc. Am. 63, 739-749 (1978).

1.35   R. D. Graves, A. Nagl, H. Überall, and G. L. Zarur,
        "Normal modes in a sound channel with range dependent
        parabolic sound speed profile," Acustica 39, 173-181
        (1978).

1.36   F. S. Chwieroth, A. Nagl, H. Überall, R. D. Graves, and
        G. L. Zarur, "Mode coupling in a sound channel with range-
        dependent parabolic velocity profile," J. Acoust. Soc.
        Am. 64, 1105-1112 (1978).

1.37   J. R. Wait, "An approach to the mode conversion problem
        in non-uniform acoustic waveguides," in Acoustic-Gravity
        Waves in the Atmosphere - Symposium Proceedings, edited
        by T. M. Georger (U.S. GPO, Washington, D.C., 1968)
        pp. 315-323.

1.38   M. K. MacPherson, "Range dependent sound propagation in
        shallow water," Master's Thesis, Physics Department, The
        University of Auckland, Auckland, New Zealand (1978).

CHAPTER II - REFERENCES

2.1   S. R. Rutherford and K. E. Hawker, "Effects of density
       gradients on bottom reflection loss for a class of marine
       sediments," J. Acoust. Soc. Am. 63, 750-757 (1978).

2.2   Stephen K. Mitchell, "An extension of Langer's asymptotic
       solution with applications to ocean acoustics," Ph.D.
       Dissertation, Physics Department, The University of Texas
       at Austin, Austin, Texas (1976).

2.3   C. L. Pekeris, "Theory of propagation of explosive sound
       in shallow water," Geol. Soc. Am., Mem. 27 (1948).

2.4   I. Tolstoy and C. S. Clay, Ocean Acoustics (McGraw-Hill,
       New York, 1966).

2.5   C. B. Officer, Introduction to the Theory of Sound
       Transmission (McGraw-Hill, New York, 1958).

2.6   C. S. Clay and H. Medwin, Acoustical Oceanography:
       Principles and Applications (John Wiley and Sons, New
       York, 1977).

2.7   J. F. Miller and F. Ingenito, "Normal mode Fortran
       programs for calculating sound propagation in the ocean,"
       NRL Memorandum Report No. 3071 (Naval Research
       Laboratory, Washington, DC).

2.8   E. C. Titchmarsh, Eigenfunction Expansions Associated
       with Second-Order Differential Equations, Part I (Oxford
       Press, 1962).

2.9   E. C. Titchmarsh, _Eigenfunction Expansions Associated with Second-Order Differential Equations_, Part II (Oxford Press, 1958).

2.10   P. M. Morse and H. Feshbach, _Methods of Theoretical Physics_, Parts I and II (McGraw-Hill, New York, 1953).

2.11   A. D. Pierce, "Extension of the method of normal modes to sound propagation in an almost-stratified medium," J. Acoust. Soc. Am. _37_, 19-27 (1965).

2.12   D. M. Milder, "Ray and wave invariants for SOFAR channel propagation," J. Acoust. Soc. Am. _46_, 1259-1263 (1969).

2.13   P. G. Bergmann, "The wave equation in a medium with a variable index of refraction," J. Acoust. Soc. Am. _17_, 329-333 (1946).

2.14   R. B. Leighton, _Principles of Modern Physics_, (McGraw-Hill, New York, 1959), Chapter 3.

2.15   L. I. Schiff, _Quantum Mechanics_, Third Edition (McGraw-Hill, New York, 1968).

2.16.   R. Gonzalez and K. E. Hawker, "A numerical approach to the calculation of acoustic normal modes," unpublished.

2.17   C. Froese, "Numerical solution of the Hartree-Fock equations," Can. J. Phys. _41_, 1895-1910 (1963).

2.18   J. C. Slater, _Quantum Theory of Atomic Structure_, Vol. I (McGraw-Hill, New York, 1960).

2.19   A. O. Williams, "Mode interactions in an isovelocity ocean of uniformly varying depth," J. Acoust. Soc. Am., to be published October 1979.

2.20   F. S. Chwieroth, A. Nagl, H. Überall, R. D. Groves, and G. L. Zarur, "Mode coupling in a sound channel with range-dependent parabolic velocity profile," J. Acoust. Soc. Am. 64, 1105-1112 (1978).

2.21   L. B. Dozier and F. D. Tappert, "Statistics of normal mode amplitudes in a random ocean, I. Theory," J. Acoust. Soc. Am. 63, 353-365 (1978).

2.22   L. B. Dozier and F. D. Tappert, "Statistics of normal mode amplitudes in a random ocean, II. Computations," J. Acoust. Soc. Am. 64, 533-547 (1978).

2.23   E. L. Hamilton, "Sound attenuation as a function of depth in the sea floor," J. Acoust. Soc. Am. 59, 528 (1976).

2.24   E. L. Hamilton, "Compressional-wave attenuation in marine sediments," Geophysics 37, 620 (1972).

2.25   K. E. Hawker, A. L. Anderson, K. C. Focke, and T. L. Foreman, "Initial phase of a study of bottom interaction of low frequency underwater sound," Applied Research Laboratories Technical Report No. 76-14 (ARL-TR-76-14), Applied Research Laboratories, The University of Texas at Austin (1976).

CHAPTER III - REFERENCES

3.1   A. D. Pierce, "Extension of the method of normal modes
       to sound propagation in an almost-stratified medium," J.
       Acoust. Soc. Am. 37, 19-27 (1965).

3.2   D. M. Milder, "Ray and wave invariants for SOFAR channel
       propagation," J. Acoust. Soc. Am. 46, 1259-1263 (1969).

3.3   R. D. Graves, A. Nagl, H. Überall, and G. L. Zarur,
       "Range-dependent normal modes in underwater sound
       propagation: application to the wedge-shaped ocean," J.
       Acoust. Soc. Am. 58, 1171-1177 (1975).

3.4   A. Nagl, H. Überall, A. J. Haug, and G. L. Zarur,
       "Adiabatic mode theory of underwater sound propagation in
       a range-dependent environment," J. Acoust. Soc. Am. 63,
       739-749 (1978).

3.5   R. D. Graves, A. Nagl, H. Überall, and G. L. Zarur,
       "Normal modes in a sound channel with range dependent
       parabolic sound speed profile," Acustica 39, 173-181
       (1978).

3.6   L. M. Brekhovskikh, "The possible role of acoustics in
       the exploration of the ocean," 1965 Proc. 5th Int.
       Congress on Acoustics, Liege, Belgium, Vol. II, pp. 19-
       39.

3.7   F. B. Jensen and M. C. Ferla, "SNAP: The SACLANTCEN
       normal-mode acoustic propagation model," SACLANTCEN
       Techical Report SACLANT ASW Research Centre, LaSpezia,
       Italy (1978).

3.8   H. Goldstein, _Classical Mechanics_ (Addison-Wesley Publishing Co., Inc., Reading, MA, 1950).

3.9   D. Ter Haar, _Elements of Hamiltonian Mechanics_, Second Edition (Pergamon Press, New York, 1964).

3.10   L. D. Landau and E. M. Lifshitz, _Mechanics_, Second Edition (Pergamon Press, New York, 1969).

3.11   J. D. Jackson, _Classical Electrodynamics_ (John Wiley and Sons, Inc., New York, 1962).

3.12   L. I. Schiff, _Quantum Mechanics_, Third Edition (McGraw-Hill, New York, 1968).

3.13   M. Born and J. R. Oppenheimer, Ann. Physik $\underline{84}$, 457-484 (1927).

3.14   M. Born and K. Huang, _Dynamical Theory of Crystal Lattices_ (Oxford Press, London, 1954).

3.15   F. Seitz, _Modern Theory of Solids_ (McGraw-Hill Book Co., Inc., New York, 1940).

3.16   B. A. Auld, _Acoustic Fields and Waves in Solids, Vol. I_, (John Wiley and Sons, Inc., New York, 1973).

3.17   I. Tolstoy and C. S. Clay, _Ocean Acoustics_ (McGraw-Hill, New York, 1966).

3.18   C. B. Officer, _Introduction to the Theory of Sound Transmission_ (McGraw-Hill, New York, 1958).

3.19   E. L. Hamilton, "Variations of density and porosity with depth in deep-sea sediments," J. Sed. Petrol. $\underline{46}$, 280-300 (1976).

3.20   J. F. Miller and F. Ingenito, "Normal mode Fortran programs for calculating sound propagation in the ocean," NRL Memorandum Report No. 3071 (Naval Research Laboratory, Washington, DC).

3.21   R. Gonzalez and K. E. Hawker, "A numerical integration approach to the calculation of acoustic normal modes," paper in preparation.

3.22   C. T. Tindle and K. M. Guthrie, "Rays as interfering modes in underwater acoustics," J. Sound Vib. 34, 291-295 (1974).

3.23   D. E. Weston, "Sound focusing and beaming in the interference field due to several shallow water modes," J. Acoust. Soc. Am. 44, 1706-1712 (1968).

CHAPTER IV - REFERENCES

4.1   B. A. Auld, _Acoustic Fields and Waves in Solids,_ Vol. I,
        (John Wiley and Sons, New York, 1973).

4.2   F. S. Chwieroth, A. Nagl, H. Uberall, R. D. Graves, and
        G. L. Zarur, "Mode coupling in a sound channel with
        range-dependent parabolic velocity profile," J. Acoust.
        Soc. Am. 64, 1105-1112 (1978).

4.3   L. B. Dozier and F. D. Tappert, "Statistics of normal
        mode amplitudes in a random ocean, I. Theory," J. Acoust.
        Soc. Am. 63, 353-365 (1978).

4.4   L. B. Dozier and F. D. Tappert, "Statistics of normal
        mode amplitude in a random ocean, II. Computations," J.
        Acoust. Soc. Am. 64, 533-547 (1978).

4.5   S. T. McDaniel, "Coupled power equations for cylindri-
        cally spreading waves," J. Acoust. Soc. Am. 60, 1285-1289
        (1976).

4.6   S. T. McDaniel, "Mode conversion in shallow-water sound
        propagation," J. Acoust. Soc. Am. 62, 320-325 (1977).

4.7   S. T. McDaniel, "Calculation of mode conversion rates,"
        J. Acoust. Soc. Am. 63, 1372-1374 (1978).

4.8   L. I. Schiff, _Quantum Mechanics_, Third Edition (McGraw-
        Hill, New York, 1968).

4.9   I. Tolstoy and C. S. Clay, _Ocean Acoustics_, (McGraw-Hill,
        New York, 1966).

4.10   C. B. Officer, _Introduction to the Theory of Sound Transmission_,
        (McGraw-Hill, New York, 1958).

CHAPTER V - REFERENCES

5.1   K. Smith, The Calculation of Atomic Collision Processes, (Wiley-Interscience, New York, 1971).

5.2   A. C. Allison, "The numerical solution of coupled differential equations arising from the Schrodinger equation," Journal of Computational Physics $\underline{6}$, 378-391 (1970).

5.3   C. Froese, "Numerical solution of the Hartree-Fock equations," Can. J. Phys. $\underline{41}$, 1895-1910 (1963).

5.4   S. R. Rutherford, "A comparative study of numerical techniques for the solution of integro-differential equations," Master's Thesis, Physics Department, Baylor University, Waco, Texas (1975).

5.5   L. F. Shampine and R. C. Allen, Numerical Computing: An Introduction, (W. B. Saunders Co., Philadelphia, 1973).

5.6   D. M. Young and R. T. Gregory, A Survey of Numerical Mathematics, Vol. II, (Addison-Wesley Publishing Co., Reading Mass., 1973).

5.7   P. M. Morse and H. Feshbach, Methods of Theoretical Physics, Parts I and II (McGraw-Hill, New York, 1953).

APPENDIX A - REFERENCES

A.1   See Ref. II.8.

A.2   B. Friedman, <u>Principles and Techniques of Applied Mathematics</u> (John Wiley and Sons, Inc., New York, 1956).

A.3   See Ref. II.2.

A.4   D. C. Stickler, "Normal-mode program with both the discrete and branch line contributions," J. Acoust. Soc. Am. <u>57</u>, 856-861 (1965).

A.5   A. O. Williams, "Pseudoresonances and virtual modes in underwater sound propagation," J. Acoust. Soc. Am. <u>64</u>, 1487-1491 (1978).

A.6   C. T. Tindle, "Virtual modes and mode amplitudes near cutoff," J. Acoust. Soc. Am., to be published, June 1979.

DISTRIBUTION LIST FOR
ARL-TR-79-44
UNDER CONTRACT N00014-78-C-0113

Copy No.

Commanding Officer
Naval Ocean Research and Development Activity
NSTL Station, MS 39529

1	Attn: CDR J. Paquin (Code 500)
2	R. D. Gaul (Code 600)
3	CDR T. McCloskey (Code 200)
4	S. W. Marshall (Code 340)
5	H. Eppert (Code 360)
6	A. L. Anderson (Code 320)
7	M. G. Lewis (Code 500)
8	J. Matthews (Code 360)
9	G. Morris (Code 340)
10	R. R. Goodman

Commanding Officer
Office of Naval Research
Arlington, VA 22217

11	Attn: J. B. Hersey (Code 102-OS)
12	A. Sykes
13	T. Pyle (Code 430)
14	H. Bezdek (Code 460)
15	M. McKisic (Code 486)

16   Office of Naval Research
Department of the Navy
Chicago Branch Office
536 South Clark Street
Chicago, IL 60605

Commanding Officer
Naval Electronic Systems Command
Washington, DC 20360

17	Attn: J. Sinsky (Code 320)
18	J. Cybulski (Code 320)
19	CDR D. Griffiths (Code 320)
20	Code PME 124-30
21	Code PME 124-62
22	E. Tunstall (Code 124TA)

Copy No.

Director
Naval Research Laboratory
Department of the Navy
Washington, DC 20375
23   Attn: R. H. Ferris
24   B. B. Adams (Code 8160)
25   Code 2627
26   O. Diachok
27   F. Ingenito
28   B. G. Hurdle

Commanding Officer
Naval Ocean Systems Center
Department of the Navy
San Diego, CA 92152
29 - 30   Attn: E. L. Hamilton
31   R. R. Gardner
32   M. A. Pederson
33   H. P. Bucker
34   D. Gordon
35   O. D. Grace

Commander
Naval Sea Systems Command
Department of the Navy
Washington, DC 20362
36   Attn: C. D. Smith (Code 06R163R)
37   A. P. Franceschetti

Chief of Naval Operations
Department of the Navy
Washington, DC 20350
38   Attn: R. S. Winokur (OP95E1)

Chief of Naval Material
Department of the Navy
Washington, DC 20360
39   Attn: G. R. Spalding (Code 08T24)
40   CDR E. Young (Code 08T24)

Commander
Naval Intelligence Support Center
Department of the Navy
4301 Suitland Road
Washington, DC 20390
41   Attn: Code 222

Copy No.

42 Commander
Naval Surface Weapons Center
White Oak Laboratory
Department of the Navy
Silver Spring, MD 20910

43 Commander
David W. Taylor Naval Ship Research and
  Development Center
Department of the Navy
Bethesda, MD 20034

Naval Oceanographic Office
Department of the Navy
Washington, DC 20373
44 - 45 Attn: W. H. Geddes

Commander
Naval Air Development Center
Department of the Navy
Warminister, PA 18974
46 Attn: P. Van Schuyler (Code 2052)
47   C. L. Bartberger
48   P. Haas

Officer in Charge
New London Laboratory
Naval Underwater Systems Center
Department of the Navy
New London, CT 06320
49 Attn: F. R. DiNapoli
50   R. Deavenport
51   J. Papadakis
52   R. Lauer
53   P. Herstein
54   R. Hasse

55 Assistant Director
Ocean Control DDR & E
Room 3D, 1048 Pentagon
Washington, DC 20301

OASN (R, E & S)
Room 4D, 745 Pentagon
Washington, DC 20301
56 Attn: G. A. Cann

Copy No.

            Defense Advanced Research Projects Agency
            Acoustic Research Center
            Moffett Field, CA 94035
57   Attn: E. Smith

            Superintendent
            Naval Postgraduate School
            Monterey, CA 93940
58   Attn: Library
59   H. Medwin
60   O. B. Wilson

            Commanding Officer
            Naval Air Systems Command
            Department of the Navy
            Washington, DC 20361
61   Attn: CDR J. Messegee (Code PMA-264)

62 - 63   Commanding Officer and Director
            Defense Documentation Center
            Cameron Station, Building 5
            5010 Duke Street
            Alexandria, VA 22314

            Arthur D. Little, Inc.
            15 Acorn Park
            Cambridge, MA 02140
64   Attn: G. Raisbeck

            Woods Hole Oceanographic Institution
            86-96 Water Street
            Woods Hole, MA 02543
65   Attn: E. E. Hays
66   G. Frisk
67   R. Spindel

            Science Applications, Inc.
            8400 Westpark Drive
            McLean, VA 22101
68   Attn: J. Hanna
69   C. Spofford
70   L. Dozier

            Applied Research Laboratory
            The Pennsylvania State University
            P.O. Box 30
            State College, PA 16801
71   Attn: S. McDaniel

Copy No.

              Underwater Systems, Inc.
              World Building
              8121 Georgia Avenue
              Silver Spring, MD 20910
    72   Attn: M. S. Weinstein

              Marine Physical Laboratory of
              The Scripps Institution of Oceanography
              The University of California, San Diego
              San Diego, CA 92132
    73   Attn: V. Anderson
    74   F. Fisher
    75   G. Shor

              Tracor, Inc.
              1601 Research Boulevard
              Rockville, MD 20850
    76   Attn: J. Gottwald
    77   A. Wittenborn
    78   R. J. Urick

              Bell Telephone Laboratories, Inc.
              Whippany Road
              Whippany, NJ 07961
    79   Attn: S. A. Kramer

              Planning Systems, Inc.
              7900 Westpark Drive, Suite 507
              McLean, VA 22101
    80   Attn: L. Solomon

              TRW, Inc.
              TRW Defense & Space Systems Group
              Washington Operations
              7600 Colshire Drive
              McLean, VA 22101
    81   Attn: R. T. Brown
    82   I. Gereben

              SUTRON Corporation
              Suite 700
              1925 North Lynn Street
              Arlington, VA 22209
    83   Attn: C. Dabney

<u>Copy No.</u>

Daubin Systems Corporation
104 Crandon Boulevard
Key Biscayne, FL 33149
84   Attn: S. Daubin

Defence Scientific Establishment
HMNZ Dockyard
Devonport, Auckland
NEW ZEALAND
85   Attn: K. M. Guthrie
86   R. N. Denham
87   R. Bannister

Physics Department
The University of Auckland
Private Bag, Auckland
NEW ZEALAND
88   Attn: A. C. Kibblewhite
89   G. Bold
90   C. T. Tindle

The Catholic University of America
Washington, DC 20064
91   Attn: H. M. Uberall

Department of Geology and Geophysics
Geophysical and Polar Research Center
Lewis G. Weeks Hall for Geological Sciences
The University of Wisconsin, Madison
1215 W. Dayton Street
Madison, WI 53706
92   Attn: C. S. Clay

93   Courant Institute
251 Mercer Street
New York, NY 10012
Attn: D. C. Stickler

Commander
Naval Coastal Systems Center
Department of the Navy
Panama City, FL 32407
94   Attn: G. McLeroy

Copy No.

```
       Bolt, Beranek, and Newman, Inc.
       50 Moulton Street
       Cambridge, MA 02138
  95   Attn:  P. W. Smith, Jr.

       Boeing Aerospace Corporation
       Advanced Projects
       P.O. Box 3999, M.S. 84-63
       Seattle, WA 98124
  96   Attn:  Bob Arnold

       The Institute of Acoustic Research
       615 SW 2nd Avenue
       Miami, FL 33130
  97   Attn:  M. Kronengold
  98          J. Clark

  99   Massachusetts Institute of Technology
       Department of Ocean Engineering
       Cambridge, MA 02139
       Attn:  Professor I. Dyer

       The Lamont-Doherty Geological Observatory
       Columbia University
       Palisades, NY 10964
 100   Attn:  R. D. Stoll
 101          H. A. Kutschale

       Hawaii Institute of Geophysics
       The University of Hawaii
       2525 Corres Road
       Honolulu, HI 96822
 102   Attn:  G. Sutton
 103          G. Fryer

       Director
       North Atlantic Treaty Organization
       SACLANT ASW Research Centre
       APO, NY 09019
 104   Attn:  T. Akal
 105          F. Jensen
 106          D. Ross
 107          W. Kuperman
```

Copy No.

Defence Research Establishment Pacific
CF Dockyard
Victoria, B.C., CANADA
108   Attn: G. R. Ebbeson

Defence Research Establishment Atlantic
9 Grove Street
P.O. Box 1012
Dartmouth, N.S., CANADA
109   Attn: I. Fraser
110   D. Chapman

Rosensteil School of Marine and
  Atmospheric Science
The University of Miami
10 Rickenbacker Causeway
Miami, FL 33149
111   Attn: Dr. H. DeFerrari

Applied Physics Laboratory
The Johns Hopkins University
Johns Hopkins Road
Laurel, MD 20810
112   Attn: L. H. Wallman

Bell Telephone Laboratories
Whippany Road
Whippany, NJ 07961
113   Attn: F. Labianca

Polar Research Laboratory, Inc.
123 Santa Barbara Street
Santa Barbara, CA 93101
114   Attn: B. M. Buck

The University of Miami
10 Rickenbacker Causeway
Miami, FL 33149
115   Attn: Dr. F. Tappert

The University of Rhode Island
Physics Department
Kingston, RI 02881
116   Attn: C. Kaufman

Copy No.

	Polytechnic Institute of New York
	Department of Electrical Engineering
	Farmingdale, NY 11735
117	Attn: L. B. Folsen
118	I. Tolstoy
	Knockvennie, Castle Douglas
	S.W. SCOTLAND, GREAT BRITAIN
	National Oceanic and Atmospheric Administration
	Environmental Research Laboratories
	Boulder, CO 80303
119	Attn: J. R. Wait
	Geophysics Laboratory
	Marine Science Institute
	The University of Texas
	700 The Strand
	Galveston, TX 77550
120	Attn: J. Worzel
	Department of Electrical Engineering
	The University of Texas at Austin
	Austin, TX 78712
121	Attn: Francis X. Bostick
	Department of Geology
	The University of Texas at Austin
	Austin, TX 78712
122	Attn: Dr. M. M. Backus
	Department of Electrical Engineering
	The University of Texas at Austin
	Austin, TX 78712
123	Attn: Dr. E. Hixon
	School of Mechanical Engineering
	Georgia Institute of Technology
	Atlanta, GA 30332
124	Attn: Dr. A. D. Pierce
	Department of Geology
	The University of Texas at Austin
	Austin, TX 78712
125	Attn: Dr. Clark Wilson

Copy No.

| | Brown University
Providence, RI 02912 |
| 126 | Attn: A. O. Williams, Jr. |

| | Defense Advanced Research Projects Agency
1400 Wilson Boulevard
Arlington, VA 22209 |
| 127 | Attn: T. Kooij |

| 128 | Office of Naval Research
Resident Representative
Room No. 582, Federal Bldg.
Austin, TX 78701 |

129	Glen E. Ellis, ARL:UT
130	Terry L. Foreman, ARL:UT
131	Ruth Gonzalez, ARL:UT
132	Loyd D. Hampton, ARL:UT
133	Kenneth E. Hawker, ARL:UT
134	John J. Lemmon, ARL:UT
135	Stephen K. Mitchell, ARL:UT
136	Susan G. Payne, ARL:UT
137	Steven R. Rutherford, ARL:UT
138	Jack A. Shooter, ARL:UT
139	Clark S. Penrod, ARL:UT
140	Dana S. Hougland, ARL:UT
141	Paul J. Vidmar, ARL:UT
142	Reuben H. Wallace, ARL:UT
143	Claude W. Horton, Sr., ARL:UT
144	Garland R. Barnard, ARL:UT
145	Library, ARL:UT
146-175	Reserve, ARL:UT